SOCRATES Technical Guide
Suite Of Community RAdiative Transfer codes based on Edwards and Slingo

James Manners, John M. Edwards, Peter Hill & Jean-Claude Thelen
Met Office, FitzRoy Rd, Exeter EX1 3PB [1]

April 12, 2026

Contents

Chapter 1

The Two-Stream Radiation Code

1.1 Overview

The purpose of the radiation code is to calculate radiative fluxes, from which heating rates and related quantities may be determined. In this radiation scheme these fluxes are determined by summing the results of a number of quasi-monochromatic calculations, each carried out using a two-stream approximation (in which the angular variation of the radiance field is represented simply by an upward and a downward diffuse flux, together with a direct solar flux in the shortwave region). The algorithm can perhaps most clearly be explained by describing first the spectral integration in broad terms, then the treatment of the quasi-monochromatic calculations in an atmospheric column composed of homogeneous layers, working backwards to the original physical inputs, before passing on to a discussion of the treatment of overlapping gaseous absorption and the treatment of fractional cloudiness.

Spectral data for the parametrizations used and the decomposition of each spectral region into bands are stored in a *spectral file*, generated by a pre-processing package (see section 3 for further discussion of spectral files). It is important to note that parametrizations which require spectrally dependent data may be selected only if such data are present in the spectral file, and therefore that parametrizations must be selected with due consideration to the spectral data available. Once created, a spectral file may be used with any subsequent version of the radiation code.

1.2 Spectral Integration

In this section F will denote any flux, whether direct, diffuse or net. The spectral region under consideration is divided into a number of spectral bands within which all quantities except the gaseous mass absorption coefficient are treated as independent of frequency. The total flux is then the sum over the partial fluxes, $F_j^{(b)}$, in each of the bands:

$$F = \sum_j F_j^{(b)} \tag{1.1}$$

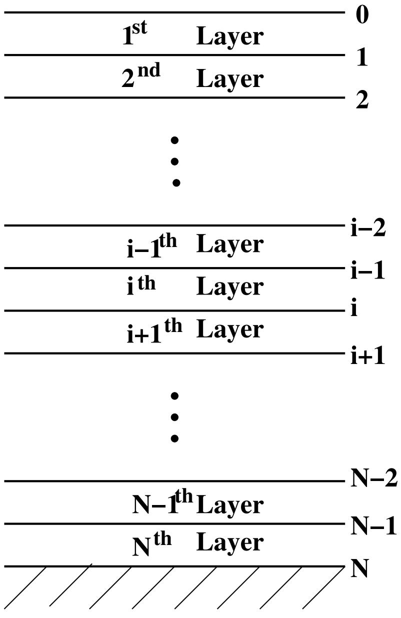

Figure 1.1: Vertical Resolution of Atmosphere

The flux in a band is calculated by dividing the band into a number of quasi-monochromatic regions in each of which the gaseous absorption coefficients for the active absorbing gases within the band have fixed values. A weight, w_k, is assigned to the k^{th} region, and the flux, taking the appropriate values of the gaseous absorption coefficients into account, is calculated for this region. The flux in the band is then a weighted sum of these quasi-monochromatic fluxes, $F_k^{(qm)}$

$$F_j^{(b)} = \sum_k w_k F_k^{(qm)} \tag{1.2}$$

The number of quasi-monochromatic calculations and the weights are determined by the method adopted for treating overlapping gaseous absorption and the data in the spectral file.

1.3 The Calculation of Monochromatic Fluxes

To calculate monochromatic fluxes the atmosphere is divided into N layers which are treated as homogeneous. The layers are numbered from 1 to N, starting at the top. The boundaries of these layers, referred to as levels, are numbered from 0 to N, again starting at the top; so that the i^{th} level marks the base of the i^{th} layer (see Fig.1.1). The layers match those adopted elsewhere in the model, with the interior boundaries corresponding to the ρ-levels $2, \ldots, N$, although inverted; the first ρ-level is omitted on the physics grid. Increments to the heating rates are applied on θ-levels. In order to minimize the execution time, it is convenient to choose the upward flux, U , the total downward (diffuse plus direct) flux, V, and the direct solar flux, Z , as the primary variables in the solar region (notice the non-standard choice of the total rather than the diffuse downward flux which allows a slight reduction of the operation count). In the infra-red it is convenient to use the upward and downward differential fluxes (the actual upward and downward fluxes less πB), which we here denote as U and V to achieve a unified description valid in both spectral regions. For applications where only heating rates or net fluxes are required, it is often convenient to work with the net flux $N = V - U$. The fluxes in a column consisting of homogeneous layers are then determined from the equations:

$$\begin{aligned} U_{i-1} &= T_i U_i + R_i V_{i-1} + S_i^+ \\ V_i &= T_i V_{i-1} + R_i U_i + S_i^- \\ Z_i &= T_{0i} Z_{i-1} \end{aligned} \tag{1.3}$$

T and R are the diffuse transmission and reflection coefficients and T_0 is the direct transmission coefficient. The subscripts on fluxes refer to levels and those on T, R , T_0 and S refer to layers. At the top of the atmosphere there is no incident diffuse flux, so the boundary condition for solar radiation is $V_0 = Z_0 = \Phi_0/\chi_0$ where Φ_0 is the solar irradiance in the band at the top of the atmosphere and χ_0 is the secant of the solar zenith angle. In the infra-red, the boundary condition is $V_0 = 0$. At the surface the appropriate boundary condition on the shortwave fluxes is

$$\begin{aligned} U_N &= (\alpha_s - \alpha_d) Z_N + \alpha_d V_N \\ &= \alpha_s Z_N + \alpha_D (V_N - Z_N) \end{aligned} \tag{1.4}$$

where α_s and α_d are the surface albedos for direct and diffuse radiation. In the infra-red

$$U_N = \alpha_d V_N + \epsilon_* \pi B_* \tag{1.5}$$

where ϵ_* is the emissivity of the surface and B_* is the corresponding Planckian function.

The source terms, $S^{\pm}$, are related to the direct solar flux (scattering of the direct beam into diffuse radiation) or to variations in the Planckian source function across the layer, as appropriate to the spectral region. In the solar spectrum,

$$S_i^+ = c_{1i} Z_{i-1} \quad \text{and} \quad S_i^- = c_{2i} Z_{i-1} \tag{1.6}$$

where the c_j depend on the properties of the layer and are considered below. In the infra-red

$$S_i^+ = c_{1i} \Delta_{1i} + c_{2i} \Delta_{2i} \quad \text{and} \quad S_i^- = -c_{1i} \Delta_{1i} + c_{2i} \Delta_{2i} \tag{1.7}$$

where Δ_1 and Δ_2 are related to the first and second differences of the Planck function across the layer, and terms involving Δ_2 are present only if the Planckian source function is assumed to vary quadratically across the layer. Explicitly,

$$\begin{aligned} \Delta_{1i} &= B_i - B_{i-1} \\ \Delta_{1i} &= 2(B_i + B_{i-1} - 2B_i^{(m)}) \end{aligned} \tag{1.8}$$

where B denotes the Planckian function integrated across the band at the appropriate level in the atmosphere and $B_i^{(m)}$ denotes the Planckian function at the middle of the i^{th} layer. B is given by a polynomial:

$$B = \sum_{k=0}^{n} \beta_k (\theta/\theta_R)^k \tag{1.9}$$

where the order of the polynomial, n, the coefficients β_k and the reference temperature, θ_R, are determined externally.

Note: In stand-alone radiation codes, it is usual to take the variation of the Planckian as linear across layer. In the Unified Model, because of the way in which temperatures are interpolated to the edges of layers and the weakness of non-radiative damping in the stratosphere, this led to the build up of two-grid-length waves on the timescale of about a month. The quadratic variation was introduced to allow these to be damped in climate integrations.

1.4 The Calculation of Fluxes

T, T_0, R and the c_j are related to the optical properties of the layer. Since each layer may be considered independently, the subscript i will be dropped in this section. The fundamental single scattering properties of a layer are the optical depth, τ, the albedo of single scattering, ω, and the asymmetry g . The precise way in which these determine the overall transmission and reflection coefficients depends on the actual two-stream approximation selected (there are several two-stream approximations: see, for example, Zdunkowski et al. [1980]). Here they determine two quantities s and d in the first instance. Usually the two-stream equations are expressed in terms of the diffuse fluxes, $F^{\pm}$ as

$$\frac{dF^+}{d\tau} = \alpha_1 F^+ - \alpha_2 F^- - Q^+ \tag{1.10}$$

$$\frac{dF^-}{d\tau} = \alpha_2 F^+ - \alpha_1 F^- - Q^- \tag{1.11}$$

where $Q^{\pm}$ are source terms: In terms of the variables used here, $s = \alpha_1 + \alpha_2$ and $d = \alpha_1 - \alpha_2$.

In the Eddington approximation,

$$\begin{aligned} s &= \frac{3}{2}(1 - \omega g) \\ d &= 2(1 - \omega) \end{aligned} \tag{1.12}$$

Using the approximation given by Zdunkowski and Korb [1985], which we denote as PIFM85,

$$\begin{aligned} s &= D - \frac{3}{2}\omega g \\ d &= D(1 - \omega) \end{aligned} \tag{1.13}$$

where D is the diffusivity factor, which is taken as 2 by these authors, though 1.66 is more commonly used in the infra-red to agree with Elsasser's value. The original version of the approximation given by Zdunkowski et al. [1980] is

$$\begin{aligned} s &= 2 - \frac{3}{2}\omega g - \frac{1}{2}\omega \\ d &= 2(1 - \omega) \end{aligned} \tag{1.14}$$

This approximation follows less naturally from the derivation, but agrees more closely with reference results in the solar region. Using discrete ordinates,

$$\begin{aligned} s &= \sqrt{3}(1 - \omega g) \\ d &= \sqrt{3}(1 - \omega) \end{aligned} \tag{1.15}$$

Under the Hemispheric mean approximation,

$$\begin{aligned} s &= 2(1-\omega g) \\ d &= 2(1-\omega) \end{aligned} \tag{1.16}$$

These quantities determine the diffuse transmission and reflection coefficients:

$$\begin{aligned} \lambda &= \sqrt{sd} \\ p &= e^{-\lambda\tau} \\ \Gamma &= \frac{s-\lambda}{s+\lambda} \\ T &= \frac{p(1-\Gamma^2)}{1-p^2\Gamma^2} \\ R &= \frac{\Gamma(1-p^2)}{1-p^2\Gamma^2} = \Gamma(1-pT) \end{aligned} \tag{1.17}$$

In the infra-red,

$$\begin{aligned} c_1 &= \frac{1-T+R}{s\tau} \\ c_2 &= -\frac{1}{s\tau}\left[1+R+T-2\frac{1-T-R}{\tau d}\right] \end{aligned} \tag{1.18}$$

It will be noticed that these expressions become indeterminate in the limit $\tau \to 0$. This indeterminacy is removed by adding a small tolerance (the square root of the precision of the machine) to the terms $s\tau$, $d\tau$, $1-T+R$, and $1+R+T$. However, when τ is very small we prefer to use the asymptotic form for the second term within square brackets in c_2 *viz.*:

$$2\frac{1-T-R}{\tau d} \approx 2-\tau d \tag{1.19}$$

To define the c_j in the solar region we introduce the quantity ξ_0, where

$$\xi_0 = \frac{3g}{2\chi_0} \tag{1.20}$$

for all the above two-stream approximations, except the discrete ordinate approximation, for which

$$\xi_0 = \frac{\sqrt{3}g}{\chi_0} \tag{1.21}$$

In this spectral region we now define

$$f = \omega\frac{\chi_0}{2} \tag{1.22}$$

$$\begin{aligned} \nu_+ &= f(s-\chi_0-\xi_0(d-\chi_0)) \\ \nu_- &= f(s+\chi_0+\xi_0(d+\chi_0)) \end{aligned} \tag{1.23}$$

Then,

$$\begin{aligned} c_1 &= (\nu_+ - R(1+\nu_-)) - \nu_+ T T_0 \\ c_2 &= T_0(1+\nu_- - R\nu_+) - (1+\nu_-)T \end{aligned} \tag{1.24}$$

1.5 Rescaling of the Single Scattering Properties

The rather crude representation of the angular variation of the radiance in the two-stream equations causes unacceptable inaccuracies in the representation of scattering. However, these errors can be substantially reduced by the δ-rescaling transformation (Joseph et al. [1976]) which allows for the strong forward scattering exhibited by most atmospheric scatterers. A forward scattering fraction, f, is defined, using the standard prescription $f = g^2$, and the single scattering properties are rescaled using the transformation

$$\begin{aligned} \tau &\rightarrow \tau(1-\omega f) \\ \omega &\rightarrow \omega(1-f)/(1-\omega f) \\ g &\rightarrow (g-f)/(1-f) \end{aligned} \tag{1.25}$$

However, the forward scattering fraction is too large for the determination of the direct solar beam radiation because the scattering contribution to the direct beam component is only confined within the circumsolar (aureole) area. The above transformation leads to substantial overestimation of the direct solar flux at the surface. Sun (Sun et al. [2018]) proposed a new forward scattering fraction f_{csr} based on an integration of a scattering phase function over a solid angle of the field of view (FOV) of an instrument,

$$\begin{aligned} f_{csr} &= \frac{1}{2}\{(1-\mu) + \sum_{l=1}^{n} g^l [P_{l-1}(\mu) - P_{l+1}(\mu)]\} \\ \mu &= cos(\alpha), \end{aligned} \tag{1.26}$$

where α is the half angle of FOV (usually 2.5°), g is asymmetry factor, P_l is the Legendre expansion polynomial of a scattering phase function. It is found that a stream number of $n = 32$ is sufficient for accurate calculation of the phase function. The 32 streams of the Legendre polynomial are precalculated for 20 half FOV angles between 0.25° and 5° with an increment of 0.25° so f_{csr} can be quickly determined for a given half angle α and asymmetry factor. Note that this forward scattering fraction is only used to scale the optical depth for the direct solar beam component when it is invoked by specifying a control parameter i_direct_tau=2.

1.6 The Calculation of the Single Scattering Properties

The single scattering properties most easily related to the physical sources are the mass extinction and scattering coefficients, $k^{(e)}$ and $k^{(s)}$, and the asymmetry g. When a number of optical processes are active in a region the contributions from each of them are combined in accordance with the formulae:

$$\begin{aligned} k^{(e)} &= \sum_j k_j^{(e)}, \\ k^{(s)} &= \sum_j k_j^{(s)}, \\ g &= \sum_j k_j^{(s)} g_j / \sum_j k_j^{(s)} \\ f &= \sum_j k_j^{(s)} f_j / \sum_j k_j^{(s)} \end{aligned} \tag{1.27}$$

where, for each process, indexed by j, $f_j = g_j^2$. The optical depth and single scattering albedo are then determined from the formulae:

$$\begin{aligned} \tau &= k^{(e)} \Delta m \\ \omega &= \frac{k^{(s)}}{k^{(e)}} \end{aligned} \tag{1.28}$$

where Δm is the column mass in the layer.

1.7 The Representation of Single Scattering Properties for Individual Processes

1.7.1 Gaseous Absorption

If there are M active absorbing gases, $j = 1, \ldots, M$ in a band, each will enter a single quasi-monochromatic calculation with mass extinction coefficients appropriate for the conditions of temperature and pressure at each layer of the atmosphere. The total contribution to the mass extinction coefficient is then

$$k^{(e,g)} = \sum_j^M K_j^{(g)} q_j f_j(p, \theta) \tag{1.29}$$

where $K_j^{(g)}$ is a mass extinction coefficient at reference pressure and temperature, q_j is the mixing ratio of the j^{th} gas and f_j is the scaling function, which allows for variations in the pressure, p, and the temperature, θ. The scaled extinction coefficients may be interpolated directly from a look-up table in the spectral file which is now the preferred method. Alternatively, scaling functions may be used of which two forms for f are allowed within the code:

$$f = \left(\frac{p + \Delta}{p_0 + \Delta}\right)^{\alpha} \left(\frac{\theta}{\theta_0}\right)^{\beta} \tag{1.30}$$

$$f = \left(\frac{p + \Delta}{p_0 + \Delta}\right)^{\alpha} \left[1 + A\left(\frac{\theta - \theta_0}{\theta_0}\right) + B\left(\frac{\theta - \theta_0}{\theta_0}\right)^2\right] \tag{1.31}$$

The second form is generally preferred as being more flexible and cheaper to compute. The free parameters α, β, Δ, A and B are determined by fitting to gaseous transmission data and are chosen such that if they are given values of 0 then $f = 1$. p_0 and θ_0 are the reference pressure and temperature. Δ represents the effects of Doppler broadening. A different scaling function may be used for each k-term, or one value may be used across the band; the latter is faster and originally was commonly used, but we now tend to use separate scaling for each term since this more accurate. All these choices are determined from the data in the spectral file.

1.7.2 Self-broadening of gases

If the mixing ratio of a gaseous absorber is close to unity, pressure broadening due to collisions between molecules of the same species will become important. The pressure-broadened width of a line will depend on the volume mixing ratio of the gas, which is in the code termed the gas fraction, and can be derived from the mass mixing ratios.

If dry mixing ratios are provided to the radiation code, then the gas fraction of species i is given by

$$\frac{n_i}{n_{\text{tot}}} = \frac{n_i}{n_{\text{tot, dry}} + n_{\text{H}_2\text{O}}} = \frac{\frac{n_i}{n_{\text{tot, dry}}}}{1 + \frac{n_{\text{H}_2\text{O}}}{n_{\text{tot, dry}}}} = \frac{\zeta_i \frac{m_{\text{air, dry}}}{m_i}}{1 + \zeta_{\text{H}_2\text{O}} \frac{m_{\text{air, dry}}}{m_{\text{H}_2\text{O}}}}, \tag{1.32}$$

where n_i is the number density of species i, n_{tot} and $n_{\text{tot, dry}}$ are the total air and dry air number density, respectively, ζ_i is the mass mixing ratio of species i, respectively, m_i is the molar weight of species i and $m_{\text{air, dry}}$ is the mean molar weight of dry air.

If mixing ratios include water vapour in the total density, then the gas fraction is given by

$$\frac{n_i}{n_{\text{tot}}} = \zeta_i \frac{m_{\text{air, wet}}}{m_i}, \tag{1.33}$$

where $m_{\text{air, wet}}$ is the mean molar weight of wet air. It is given by

$$m_{\text{air, wet}} = \frac{n_{\text{tot, dry}}}{n_{\text{tot}}} m_{\text{air, dry}} + \frac{n_{\text{H}_2\text{O}}}{n_{\text{tot}}} m_{\text{H}_2\text{O}} = \frac{m_{\text{air, dry}}}{1 + \left(\frac{m_{\text{air, dry}}}{m_{\text{H}_2\text{O}}} - 1\right) \zeta_{\text{H}_2\text{O}}}. \tag{1.34}$$

1.7.3 Continuum Absorption

Theoretical models of gaseous absorption agree well with observations at frequencies close to the centres of lines, but there remain some discrepancies far from the centres which are represented by a smoothly varying *continuum* in radiation codes. Continua are not significant for all gases and two continua are normally included in radiative calculations: the self and foreign-broadened continua of water vapour. Their contribution to the mass extinction coefficient is

$$k^{(e,c)} = K_f^{(c)} q_w f_f n_{bf} + K_s^{(c)} q_w f_s n_{bs} \tag{1.35}$$

where q_w is the mixing ratio of water vapour, f is the scaling function and n_b is the molar density of the appropriate broadening species; the subscripts f and s stand for the foreign and self-broadened continua respectively. The coefficients $K_f^{(c)}$ and $K_s^{(c)}$ are determined externally by fitting and the coefficients are read from the spectral file. For the self-broadened continuum, the broadening species is water vapour, and for the foreign-broadened continuum it comprises all other species except water vapour. The same functional forms for the scaling function that were used in the treatment of gaseous absorption are employed here. In the

Unified Model it is often convenient to combine the line data and the foreign continuum data, making use of the fact that in practice n_{bf} is almost exactly a function of the pressure and the temperature. k-terms are then determined for the combined transmission: this is discussed further in section 3.

There are a number of models for the continuum. The one used here is originally based on the CKD model of Clough et al. [1989], which has been developed as new observations to constrain it become available. The updating of this model is an issue in the generation of spectral files, rather than in the radiation code itself.

A more general continuum absorption parametrisation, which also supports collision-induced absorption (CIA), is also available. Continuum k-terms are derived in the same way as gaseous absorption k-terms. These are tabulated as a function temperature only in units of absorption per mass density of each of the two continuum gases [$\mathrm{m}^5/\mathrm{kg}^2$]. Overlapping absorption between different continua, and continua and gaseous absorption is treated as overlapping gaseous absorption, however, a continuum absorption spectrum can also be assumed to be perfectly correlated to that of a particular gas. The latter assumption is generally more accurate for the water vapour continua than random overlap. The overlap treatment for a particular continuum is specified in the spectral file, and defaults to that selected for gases.

1.7.4 Absorption and Scattering by Aerosols

The radiation code contains provision for treating aerosols. This section is concerned only with the description of the radiative treatment of aerosols within the code. The specification of mixing ratios and aerosol models is described in the UM documentation.

For each species of aerosol in each spectral band the contributions to the total and scattering extinctions are simply set proportional to the mass mixing ratio of the aerosol: the constants of proportionality and the asymmetry are determined externally and read from the spectral file. There is no allowance for variations in the shape of the size distribution within the model. Hence,

$$\begin{aligned} k^{(e,a)} &= \sum_j K_j^{(e,a)} q_j, \\ k^{(s,a)} &= \sum_j K_j^{(s,a)} q_j, \\ g^{(a)} &= \sum_j K_j^{(s,a)} q_j g_j / k^{(s,a)} \end{aligned} \tag{1.36}$$

where the sum is taken over all the species of aerosols present and the mixing ratios are denoted by q_j. Parametrizations of the influence of humidity on the optical properties hygroscopic aerosols are included by the use of a look-up table in the humidity. This look-up table is read from the spectral file.

1.7.5 Rayleigh Scattering

Rayleigh scattering is represented by adding to the scattering and total extinctions a constant value for each spectral band, again determined externally and read from the spectral file. The asymmetry for Rayleigh scattering is 0.

1.7.6 Absorption and Scattering by Water Droplets

The single scattering properties in a cloud clearly depend on the mass mixing ratio of water L and of ice I, but they also depend critically on the size of cloud particles, which can vary considerably. It is therefore important that the radiation code should include a treatment of the effect of particle size. A full scattering calculation for the whole size distribution is not possible, so a parametrization in terms of a radiatively appropriate size is used. For water droplets the effective radius is always used.

The properties of water droplets, then, are determined from the mass mixing ratio of liquid water, L, and the effective radius of the droplets, r_e, using an appropriate parametrization, which may take various different forms. With the parametrization of Slingo and Schrecker [1982],

$$\begin{aligned} k^{(e)} &= L(a + b/r_e) \\ k^{(s)} &= k^{(e)}(1 - c - dr_e) \\ g &= e + fr_e \end{aligned} \tag{1.37}$$

where the constants $a, \ldots, f$ are determined externally and vary with spectral band. An alternative is the parametrization of Ackerman and Stephens (Ackerman and Stephens [1987]) as extended by Hu and Stamnes [1993]:

$$\begin{aligned} k^{(e)} &= L(a_1 r_e^{b_2} + c_1) \\ k^{(s)} &= k^{(e)}(1 - a_2 r_e^{b_2} - c_2) \\ g &= a_3 r_e^{b_3} + c_3 \end{aligned} \tag{1.38}$$

Again, the a_j, b_j and the c_j are determined externally by fitting and are read from the spectral file. *Note: Whilst this parametrization is more flexible than that of Slingo and Schrecker [1982], we have not used in practice because of the expense of calculating exponentials.*

For fitting over a wide range of sizes, a parametrization with more free terms is required. A scheme based on the use of Padé approximants has therefore been introduced

$$\begin{aligned} k^{(e)} &= L\frac{p_1 + p_2 r_e + p_3 r_e^2}{1 + p_4 r_e + p_5 r_e^2 + p_6 r_e^3} \\ k^{(s)} &= k^{(e)}\left(1 - \frac{p_7 + p_8 r_e + p_9 r_e^2}{1 + p_{10} r_e + p_{11} r_e^2}\right) \\ g &= \frac{p_{12} + p_{13} r_e + p_{14} r_e^2}{1 + p_{15} r_e + p_{16} r_e^2} \end{aligned} \tag{1.39}$$

Section 3 should be consulted for information on the fits available in the spectral files.

1.7.7 Absorption and Scattering by Ice Crystals

Conceptually, the treatment of scattering by ice crystals is similar to that used for water vapour, but there are complexities because of the irregular shape of crystals. From the point of view of parametrizations, it is important to be aware that a number of different measures of crystal size are in use, and that different schemes are based on different measures. Thus, if the prediction of crystal size in the model is altered, it is important to be sure what is used by the radiation scheme.

The simplest scheme is to proceed by analogy with water clouds and to use a parametrization similar in form to that of Slingo and Schrecker [1982]:

$$\begin{aligned} k^{(e)} &= I(a + b/r_e) \\ k^{(s)} &= k^{(e)}(1 - c - dr_e) \\ g &= e + fr_e \end{aligned} \tag{1.40}$$

where the constants $a, \ldots, f$ are determined externally. We stress that this scheme is based on the use of r_e to measure the size. Schemes of this form were used in HadAM3.

A more elaborate and better scheme is based on the modified anomalous diffraction approximation (Mitchell et al. [1996]). In this scheme, the size of crystals is specified using the mean maximum dimension of the large mode, $\bar{D}_l$. $\bar{D}_l$ is not a natural measure of size for radiative purposes, but in this scheme, the underlying (bimodal) size distribution is characterized by a single free parameter, for which $\bar{D}_l$ is an acceptable choice, since once a particle shape is specified there is a bijective relationship between $\bar{D}_l$ and r_e. $\bar{D}_l$ varies by over two orders of magnitude in this scheme so a fairly elaborate fit is required. This has been done in two ways. The original form consists of two quartic polynomials for the small and large ranges of $\bar{D}_l$. We define $x = \log(\bar{D}_l/D_T)$ where D_T is a transitional dimension, supplied with the parametrization. Then,

$$\begin{aligned} k^{(e)} &= I \exp\left(\sum_{j=0}^{4} a_j^{\pm} x^j\right) \\ k^{(s)} &= k^{(e)}\left(1 - \sum_{j=0}^{4} b_j^{\pm} x^j\right) \\ g &= \sum_{j=0}^{4} c_j^{\pm} x^j \end{aligned} \tag{1.41}$$

where $a_j^{\pm}$, $b_j^{\pm}$ and $c_j^{\pm}$ are constants supplied with the parametrization, the sign being chosen according as $x > 0$ or $x < 0$.

For the published comparison of the scheme with runs in CCM3 (Kristjánsson et al. [1999], Kristjánsson et al. [2000]) a slightly different form based on tenth order polynomials in $\bar{D}_l$ was developed. This scheme represents the same data and, numerical differences in the fit aside, is identical to the matched quartic scheme.

Different crystal shapes may be represented within this same methodology, but data in the standard spectral files are based on planar polycrystals as these are the single most representative shape available amongst those to which Mitchell's scheme is applicable.

A number of parametrizations for the single scattering properties of ice crystals have been suggested by various authors, based on an effective dimension, D_e or D_{ge}, as the measure of size. These are proportional to the ratio of volume to projected area, and, for a sphere, D_e is equal to the diameter. A parametrization in D_e based on both the SW and LW parametrizations of Fu [1996] and Fu et al. [1998] has been developed:

$$\begin{aligned}
k^{(e)} &= I \sum_{j=0}^{2} a_j / D_e^j \\
k^{(s)} &= k^{(e)} \left(1 - \sum_{j=0}^{3} b_j D_e^j \right) \\
g &= \sum_{j=0}^{3} c_j D_e^j
\end{aligned} \tag{1.42}$$

To some extent, using D_e obviates the need to know the crystal shape (but see Mitchell [2002]); however, one may need to know the crystal shape to determine D_e.

The specification of crystal size is an important issue in these parametrizations. The size is supplied as an input field to the radiation code. In the Unified Model it is generally parametrized as a function of temperature only.

Baran et al. [2009] and Baran [2012] argue that ice crystal optical properties should be linked directly to GCM prognostic variables rather than indirect diagnosed quantities such as D_e. Three such parametrizations are available; the first relates the optical properties to ice water content and temperature as described by Baran et al. [2013]. The second depends on ice water content only as described by Baran et al. [2014]. The third is based on the same ensemble of ice crystals used by Baran et al. [2014], but reintroduces a temperature dependence.

Where a two moment microphysics scheme is used then both the ice water mass mixing ratio and the number concentration of ice crystals are available as prognostic variables. This provides the average mass per crystal directly to the radiation scheme, reducing the number of assumptions that are required. The remaining uncertainty is then the ice crystal habit and the shape of the size distribution. External calculations (using for example the Baran ensemble model) can provide ice crystal optical properties as a function of average crystal mass based on an assumed habit and size distribution. These are parametrised using the same Padé approximants used for cloud droplets. The effective radius in equation 1.39 is replaced by an *equivalent spherical radius* for the average ice crystal mass:

$$r_e = \left(\frac{3 I \rho_{air}}{4 \pi \rho_{ice} N} \right)^{\frac{1}{3}} \tag{1.43}$$

where I is the ice mass mixing ratio, N is the ice crystal number concentration, and the density of ice $\rho_{ice} = 917$ kg m^{-3}.

The spectral file may contain data for a number of types of ice crystal, and the types used may be selected at runtime. For a given type, the form of parametrization is determined by the spectral file. Further discussion of types in particular files is given in section 3.

1.8 The Treatment of Overlapping Gaseous Absorption

If several gases absorb in a spectral band which does not cover too large a range of frequencies, their spectral lines may be taken to overlap randomly. In representing this absorption using k-terms it is necessary to consider the overlap of each k-term for one gas with each k-term for every other gas active in the band. This full treatment of random overlap is available within the code, but it is computationally expensive, and computationally faster approximations to it are provided.

Equivalent extinction is an extension of the method of FESFT (Ritter and Geleyn [1992]) in which the effects of minor gases are represented by a single absorption coefficient within the band, but that coefficient is determined for the local atmospheric conditions by a subsidiary calculation. In the infra-red region, supposing a minor gas to have k-terms K_r, $r = 1, \ldots, n$ the net flux, N_r , including just absorption by the r^{th} k-term of the gas (and any non-cloudy grey absorption) is calculated. The equivalent extinction is then defined as

$$\bar{K} = \sum_r w_r K_r N_r / \sum_r w_r N_r \tag{1.44}$$

where the w_r are the corresponding weights. A practical point concerning the numerical implementation of this approximation is that fluxes are calculated on levels, whereas the extinction coefficient must be a representative value in a layer. The equivalent extinction is therefore calculated using the mean net flux in the layer, which is taken as a simple average of the values at the boundaries. This is described more fully in Edwards [1996].

Two further variations of this method are available: the modulus (absolute value) of the layer incident fluxes may be used in place of the net fluxes in equation 1.44. This should lead to increased accuracy around temperature inversions where the net flux may change sign. Where each k-term has different scaling characteristics a correction to the method is also required so that the scaled values are used before the meaning is done (this method also uses the modulus of the incident fluxes to weight the k-terms in the LW).

In the solar region it is less easy to define an equivalent extinction, since the character of downwelling radiation may be quite different from that of upwelling radiation, and the scheme adopted is provisional. For each minor gas the direct transmission through any atmospheric layer may be calculated and these transmissions are multiplicative, so the direct flux may be calculated precisely and efficiently at all atmospheric levels. The calculation of diffuse fluxes is less straightforward, but also much less critical, given the particular spectral characteristics of the SW overlaps. It is assumed that the absorption by the minor gas falls into weak and strong parts, so that radiation which is scattered into the diffuse beam will be effectively denuded in parts of the band where absorption is strong. If the remaining absorption is weak it may be treated as grey. The equivalent extinction for diffuse radiation is therefore taken to have a uniform value

$$\bar{K} = \sum_r w_r K_r Z_{*r} / \sum_r w_r Z_{*r} \tag{1.45}$$

where Z_{*r} is the direct flux at the surface for the rth k-term. One further approximation is necessary to fit in with the calculation of cloudy transmission and reflection coefficients: in the calculation of source terms across a cloudy layer the direct flux is taken to vary from its true value at the top of the layer with the effect of minor gases being represented by the direct transmission calculated using the equivalent extinction.

1.9 The Treatment of Clouds

Two schemes are available for the treatment of cloud. In the original scheme, a fairly general prescription is adopted where fluxes are solved for a single column with fraction cloud cover. Within any atmospheric layer, i, a fractional cloud cover, W_i, may be specified. This cloud is divided into N_T *types*, each constituting a fraction, ϕ_j , of the total amount of cloud. Each of these sub-clouds is made up of mixtures of various *components*. The rule which determines how the components are partitioned between the types of cloud is termed a *representation*. For use in the Unified Model three representations are provided, depending on the treatment of ice and water clouds. Clouds consist of four components: stratiform water and ice and convective water and ice. Mixed-phase clouds may be represented as homogeneous, in which case there are two types, stratiform and convective, with homogeneous mixtures of water and ice in each; as segregated, in which case there are four types of clouds, each consisting of a different component; or as segregated for a single cloud type in which case we have two types, ice and liquid.

A second scheme involves the sampling of a generated field of cloudy sub-columns. The Monte Carlo Independent Column Approximation (McICA) Pincus et al. [2003] is used to sample a different cloud profile for each spectral integration point. Both these options are described in more detail below.

1.9.1 Single Column Approach

The geometry of the clouds affects the radiative fluxes. In this code there is no allowance for three-dimensional effects since clouds are treated as plane parallel. Geometrical considerations are therefore restricted to the overlapping of clouds in the vertical. The overlapping algorithm is a generalization of that described by Geleyn and Hollingsworth [1979] and Zdunkowski et al. [1982]. For reasons of numerical efficiency we do not consider the overlap between each individual type of cloud in a layer, but aggregate them into regions. Within each region the fluxes are considered to be horizontally uniform and at the boundaries between layers the fluxes are transferred from one region to another in accordance with a rule determined by the assumption regarding overlaps. There are two methods of decomposing the layer into regions at present. All cloud may be aggregated into one region (the original scheme), thus splitting the layer into clear and cloudy parts, or the convective and stratiform clouds may be aggregated into separate regions, thus giving three regions in the layer and maintaining the vertical coherence of convective cloud. (From the algorithmic point of view, this aggregation is performed implicitly in the original scheme, but explicitly in the new scheme).

The overlapping is represented by the coefficients used to couple fluxes at the boundaries of layers. For the upward flux we write:

$$\hat{U}^{+}_{i,j} = \sum_{k} u_{i,j,k} \check{U}^{+}_{i,k} \tag{1.46}$$

where U_{ij} denotes the upward flux in the j^{th} region at the i^{th} level, with the circumflex denoting a value just above the boundary and the háček a value just below it. Similarly, for the downward flux we write

$$\hat{V}_{i,j} = \sum_k v_{i,j,k} \check{V}_{i,k} \tag{1.47}$$

with an identical equation for Z. Let $X_{i,j}$ denote the area within the i^{th} layer covered by the j^{th} region and $Y_{i,j,k}$ denote the area on the i^{th} level where the j^{th} region overlies the k^{th}. Then, generally, we have

$$u_{i,j,k} = Y_{i,j,k}/X_{i+1,k} \tag{1.48}$$

and

$$v_{i,j,k} = Y_{i,j,k}/X_{i,k} \tag{1.49}$$

In the case where $X_{i,j} = 0$, $u_{i,j,k}$ is undefined, and its value does not affect the radiative fluxes, but it is necessary to assign a legitimate value for the execution of the subsequent algorithm. In such cases we set $u_{i,j,k}$ to 1 if $j = k$ and 0 otherwise; a similar rule is applied to $v_{i,j,k}$.

The assumption regarding the overlap determines the $Y_{i,j,k}$. If random overlap is assumed

$$Y_{i,j,k} = X_{i,j} X_{i+1,k} \tag{1.50}$$

If maximum-random overlap is assumed, similar regions are maximally overlapped, but dissimilar ones are randomly overlapped, so we take

$$Y_{i,j,j} = \min(X_{i,j}, X_{i+1,j}) \tag{1.51}$$

and if $k \neq j$

$$Y_{i,j,k} = \frac{(X_{i,j} - Y_{i,j,j})(X_{i+1,k} - Y_{i,k,k})}{1.0 - \sum_k Y_{i,k,k}} \tag{1.52}$$

A third option is exponential-random overlap Hogan and Illingworth [2000]. Here random and maximum-random overlap are combined linearly so that

$$Y_{i,j,j} = \alpha \min(X_{i,j}, X_{i+1,j}) + (1 - \alpha) X_{i,j} X_{i+1,j} \tag{1.53}$$

while if $k \neq j$, $Y_{i,j,k}$ is given by equation 1.52. α is called the overlap coefficient and is given by

$$\alpha = EXP\left(\frac{-\delta p}{p_0}\right) \tag{1.54}$$

where δp is the distance between the layers and p_0 is a constant called the decorrelation length. This is set separately for stratiform and convective cloud.

The radiative effect of sub-grid scale water content variability can be included by multiplying the water content by a constant value, known as a scaling factor, which may be set separately for each cloud type.

1.9.2 Monte Carlo Independent Column Approximation

The main purpose of McICA is to allow the radiative effects of sub-grid scale cloud water content variability to be represented. However it also has the advantage of separating the description of cloud from the radiation scheme, which makes coding and development easier.

McICA is a efficient approximation to the full independent column approximation (ICA) calculation Barker et al. [1999]. Each atmospheric column is represented by a field of sub-columns. Each layer in each sub-column is either overcast or cloud-free (i.e. sub-columns cannot be partially cloudy) and when the sub-columns are averaged together they have the same properties as the original atmospheric column. In a full ICA calculation the radiative profile is calculated by performing the calculation for each sub-column and then averaging the results together. In MCICA, a different randomly chosen sub-column is used for each spectral integration point. Thus the resulting radiative profile is unbiased with respect to the full calculation but includes noise.

The sub-columns required for McICA are provided by a stochastic cloud generator based on Räisänen et al. [2004]. The water content in each layer in each sub-column is a random sample from a gamma distribution with mean equal to the mean cloud water content and standard deviation determined by the fractional standard deviation (standard deviation divided by the mean), which may be set to a constant global value or parametrized from resolution and other cloud properties (e.g. Hill et al. [2012], Boutle et al. [2013]).

Hill et al. [2011] describes the implementation of McICA in Edwards-Slingo and describes the effect of the associated noise and methods for reducing this noise that have been applied. McICA is currently only available when the cloud representation is segregated by phase, but not by type (i.e. no convection).

1.10 Algorithmic Details

The foregoing sections describe the scientific basis of the scheme, but do not touch on questions of computational efficiency. Here we are concerned with the principal issues of efficiency.

1.10.1 Overview of the algorithm

On entry into the radiation code, a number of spectrally independent calculations are carried out, addressing such considerations as cloud overlap and the properties of moist aerosols. The fluxes in each spectral band are then calculated in turn and the broad-band fluxes are incremented. Within each band, the single scattering properties of radiatively active species other than gases are calculated first, since they are uniform across the band. Gaseous scaling functions may be calculated if they are independent of the k-term. A separate routine is called for each option for treating overlapping gaseous absorption; these routines are focused on generating a set of pseudo-monochromatic calculations, where the branches of the code come together again. In each such calculation, the final single scattering properties, including gaseous contributions are assembled and the code branches again, depending on the treatment of cloud overlaps. At this level, the linear two-stream equations are assembled and solved.

1.10.2 The Solution of the two-stream equations

The two-stream equations generate a set of linear simultaneous equations which may be solved by any standard algorithm of linear algebra. Whilst the method of solution of these equations is not strictly part of the physical basis of the scheme, it is useful to comment on the efficiency of the method of solution adopted. Coding the equations for the fluxes generates a banded matrix containing a significant proportion of zeros even along those diagonals in which every element is not zero. It therefore turns out that the most efficient and accurate method to solve these equations numerically is not to generate a full banded matrix and employ a standard algorithm directly, but rather to construct a set of algebraic recurrences which follow the pattern of Gaussian elimination, but take full account of the position of zero entries in the matrix, thus reducing the operation count to a minimum.

The first stage of this reduction is to generate a set of relations between the upward flux just above the boundary of a layer and the downward fluxes just below it. Using the notation of the earlier section on cloud properties we write

$$\hat{U}_{ij} = \sum_k \alpha_{i+1,jk} \check{V}_{ik} + G^+_{i+1}, j \tag{1.55}$$

where α is a generalized albedo and G^+ is independent of U and V . The boundary condition at the surface is of this form with G^+ including the solar term. It is convenient to work with $\hat{U}$ and $\check{V}$, so the diacritical marks on the fluxes may now be dropped. To form the recurrence we take the preceding equation and substitute for V, thus obtaining

$$U_{ij} = \sum_k \alpha_{i+1,jk} \big[\sum_l v_{ikl} (T_{il} V_{i-1,l} + R_{il} U_{il} + S^-_{ik}) \big] + G^+_{i+1,j} \tag{1.56}$$

We define

$$\theta_{ijl} = \sum_k \alpha_{i+1,jk} v_{ikl} \tag{1.57}$$

so that

$$\sum_l (\delta_{jl} - \theta_{ijl} R_{il}) U_{il} = \sum_l \theta_{ijl} T_{il} V_{i-1,k} + \sum_l \theta_{ijl} S^-_{il} G^+_{i+1,j} \tag{1.58}$$

which is of the form

$$\sum_l \beta_{ijl} U_{il} = \sum_l \gamma_{ijl} V_{i-1,l} + H^+_{ij} \tag{1.59}$$

and by taking linear combinations of these equations as necessary we can ensure that $\beta_{ijl} = 0$ whenever $l > j$. We now take the equation for the upward fluxes

$$U_{i-1,j} = \sum_k u_{i-1,jk} (T_{ik} U_{ik} + R_{ik} V_{i-1,k} + S^+_{ik}) \tag{1.60}$$

and observe that this is of the form

$$U_{i-1,j} = \sum_k \zeta_{ijk} U_{ik} + \sum_k \alpha_{ijk} V_{i-1,k} + G^+_{ij} \tag{1.61}$$

By using the previous equation but one U may be eliminated from the right to give us an equation of the original form with i replaced by $i-1$. In layers above clouds this scheme can be simplified for efficiency.

Back substitution proceeds easily. Suppose that at the ith level we know the downward fluxes just above the boundary, $\hat{V}_{ij}$, then we may calculate the downward fluxes just below the boundary using the coefficients v_{ijk}. The upward fluxes just below the boundary may be determined from

$$\sum_l \beta_{ijl} U_{il} = \sum_k \gamma_{ijl} V_{i-1,l} + H^+_{ij} \tag{1.62}$$

The downward fluxes at the base of the layer may now be determined from the equations of transfer, thus completing the recurrence.

Technical Note: No pivoting is done. Given that ω is perturbed away from 1 to avoid singularity on rescaling and that elimination proceeds from the ground upwards, starting with an albedo that is less than 1, pivoting should not be necessary.

1.10.3 Approximate Scattering in the Longwave Region

This scheme may be applied in both spectral regions, but in the longwave region scattering is not so important as in the shortwave region and its effects may be treated approximately. The transmission and reflection coefficients of the layers are calculated including the effects of scattering, but the equations of transfer are solved using the first two stages of an iterative scheme. Recall that the code is formulated in terms of differential fluxes in this spectral region. Thus if we assume that the upward flux at a level in the atmosphere is Planckian at the local temperature we may calculate the downward differential flux setting the upward differential flux to 0 and therefore these fluxes may be calculated by transmitting them down from the top of the atmosphere. Knowing the downward differential fluxes at each level we may then work upwards through the atmosphere calculating the upward fluxes. This procedure includes the effect of scattering in reducing the upward radiation from the top of clouds by reducing the emissivity, but it does not represent the increased downward emission from the base of a cloud through the direct reflection of radiation when it overlies a warmer surface. However, the former effect is the main result of including scattering and for most purposes it will be found preferable to approximate scattering in the longwave in order to reduce the execution time of the code.

1.10.4 Other Fast Algorithms

LW scattering may be ignored entirely, which enables faster calculation of the single scattering properties and the use of a faster procedure to calculate the fluxes, for if scattering is neglected, the equations for the fluxes reduce to problems of transmission. This is not recommended where clouds and aerosols such as dust can cause significant scattering in the LW. A hybrid scattering method is also available which allows a different treatment of scattering for each monochromatic calculation (i.e. per k-term). The specified methods are read from the spectral file and so require a compatible spectral file to be used. This restricts the expensive scattering calculations to those wavelengths where the atmosphere is optically thin and scattering is important, resulting in a significant decrease in computation time for only a small increase in bias.

1.10.5 The Magnification Factor

The radiation arriving at a point on the Earth's surface from the Sun has travelled along a straight path through the atmosphere. Allowing for the curvature of the Earth, the local zenith angle at any point in the atmosphere increases as one traces the ray back towards the Sun. Thus, to calculate the total column absorption, the local zenith angle should be used, or alternatively, the zenith angle at the surface point should be scaled by a *magnification factor* to represent this effect. However, in a GCM one requires not only the surface flux, but also a profile of radiative heating rates, and this extends vertically from the surface point. Yet, as one moves up vertically, the local zenith angle does not change. Without proper treatment of the spherical geometry (see next section), a consistent treatment of the effects of curvature is not possible. Whilst some radiation codes do include a magnification factor, the view taken here is that errors in local heating rates high in the atmosphere are more undesirable than errors in surface fluxes, so the magnification factor is omitted.

1.11 Treatment of Spherical Geometry

There is now an option to treat the direct flux using spherical geometry. This uses the so called 'pseudo-spherical approximation' whereby scattering and absorption from the direct beam are treated using the slant path through the spherical atmosphere to each point, while the resulting diffuse fluxes are still treated under the plane-parallel approximation.

Under the plane-parallel approximation a single calculation may be done tracing the transmission of the direct beam through each layer of the atmosphere, where the direct flux arriving at the top of each layer is equal to the direct flux leaving the bottom of the layer above.

Here, instead, the plane-parallel atmosphere is replaced by a set of spherical shells. Where the local zenith angle is greater than zero, the direct flux arriving at each layer will take a different path through these shells. A separate calculation for the direct beam is then required for each layer.

Figure 1.2 displays the geometry considered. The impact parameter for a given layer b_l is calculated for the path arriving at the centre of the layer (at radius r_l) as follows:

$$b_l = r_l \sqrt{1 - \cos^2 \zeta} \tag{1.63}$$

A layer is considered to be lit if the impact parameter is above the horizon in the direction of the solar azimuth (currently implemented as just the planet radius).

For the beam arriving at this layer, the element of the slant path within each layer i is then:

$$\begin{aligned} ds_i &= \left(\sqrt{r_{i-1}^2 - b^2} - \sqrt{r_i^2 - b^2}\right) \quad && [r_i > b] \\ ds_i &= 2\sqrt{r_{i-1}^2 - b^2} && [r_{i-1} > b,\ r_i < b] \\ ds_i &= 0 && [r_{i-1} < b] \end{aligned} \tag{1.64}$$

Note that the beam may pass through a layer twice if the solar zenith angle is greater than 90 degrees.

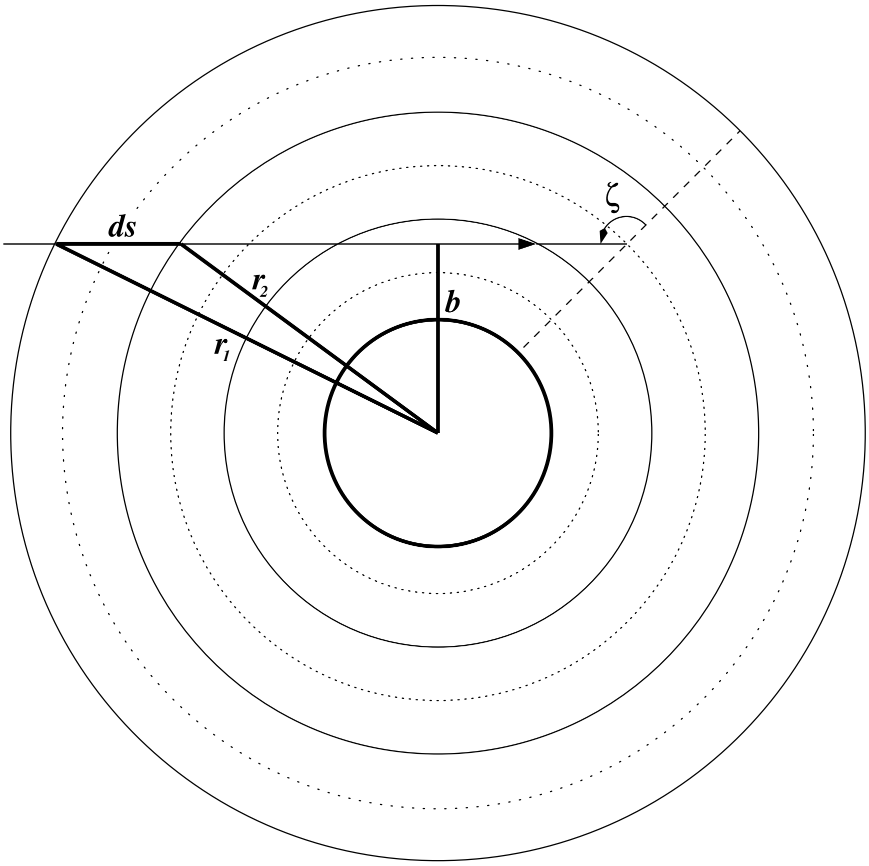

Figure 1.2: Spherical shell geometry. Layer centres are denoted by dotted lines and layer edges by solid lines. Parameters are shown for the slant path to a particular layer for a model column located in the position of the dashed line. ζ denotes the local solar zenith angle (which may be greater than 90 degrees), b the impact parameter, and ds the path length element for the layer bounded by radii r_1 and r_2.

Once the beam arrives at the layer where the source function is to be calculated we need to consider the path length through the column element for extinction of the direct beam. This path length should represent the range in paths that a beam would pass through before arriving at each part of the vertical column element. For zenith angles less than 90 degrees this should range from zero at the top of the column element to the slant path to the bottom of the layer for the bottom of the column element. Given that we only have a single incoming beam calculated as the path to the middle of the layer, we approximate this range by scaling the slant path to the middle of the layer by the vertical depth down to the middle of the layer. A similar scaling is done for beams arriving from below using the slant path from the bottom of the layer to the mid-point. A pragmatic treatment is then required for beams that arrive from above, pass down to an impact parameter within the layer and then back up to the mid-point. One limit for this case is where the impact parameter coincides with the bottom of the layer. For impact parameters fractionally smaller than this the beam will already have passed through the current layer on the way down, then passed through a tiny part of the layer below before arriving at the bottom of the current layer. For impact parameters fractionally higher than the bottom of the layer we maintain continuity by considering the start of the column element to be located at this point. The path down from the top of the layer is included with the path taken before arriving at the column element. As the impact parameter increases, the path through the column element can then be interpolated to its known value at the limit where the zenith angle is 90 degrees and the impact parameter coincides with the mid-point of the layer.

The slant path elements described here are calculated in the routine `spherical_path.F90` before the loop over bands. The path within each layer is scaled by the vertical depth of the layer (dr_i) so that it may be later used to scale the optical depths.

Within the loop over bands and k-terms, the total optical depth along the slant path for a given frequency ν is then calculated within the routine `spherical_trans_coeff.F90` as follows:

$$\tau(\nu) = \sum_{i=1}^{n} \frac{ds_i \kappa_i(\nu) dm_i}{dr_i} \tag{1.65}$$

where the sum is over the number of model layers (n), κ_i is the mass extinction coefficient (m^2kg^{-1}) for layer i and dm_i is the mass per square metre of the layer.

1.11.1 Determination of the diffuse source function

With the transmission of the direct beam to each layer so defined above it is then necessary to determine the absorbed flux for radiative heating of the model layer and also the diffuse source terms in the vertical up and down directions.

Now that the direct flux is treated separately we must recast the calculation of the diffuse fluxes in terms of just the up, U, and down, D diffuse flux rather than the total downward flux, V. This can be done by combining equations 1.4, 1.6 and 1.24:

$$\begin{aligned} V_i &= T_i V_{i-1} + R_i U_i + S_i^- \\ D_i + Z_i &= T_i D_{i-1} + T_i Z_{i-1} + R_i U_i + c_{2i} Z_{i-1} \\ D_i &= T_i D_{i-1} + R_i U_i + Z_{i-1}[T_{0i}(\nu_{-i} - R_i \nu_{+i}) - T_i \nu_{-i}] \\ &= T_i D_{i-1} + R_i U_i + S_i^{'-} \end{aligned} \tag{1.66}$$

$$\begin{aligned} U_{i-1} &= T_i U_i + R_i V_{i-1} + S_i^+ \\ &= T_i U_i + R_i D_{i-1} + R_i Z_{i-1} + c_{1i} Z_{i-1} \\ &= T_i U_i + R_i D_{i-1} + Z_{i-1}[\nu_{+i}(1 - T_i T_{0i}) - R_i \nu_{-i}] \\ &= T_i U_i + R_i D_{i-1} + S_i^{'+} \end{aligned} \tag{1.67}$$

where

$$S_i^{'+} = c_{1i}^{'} Z_{i-1} \text{ and } S_i^{'-} = c_{2i}^{'} Z_{i-1} \tag{1.68}$$

and

$$\begin{aligned} c_1^{'} &= \nu_+(1 - TT_0) - R\nu_- \\ c_2^{'} &= T_0(\nu_- - R\nu_+) - T\nu_- \end{aligned} \tag{1.69}$$

This new formulation of the source coefficients is used in place of equation 1.24 in the routine `trans_source_coeff.F90`.

We take the column element for the layer to be at an effective solar zenith angle, ζ', where the scaling factor for the path length is equal to $\sec\zeta'$. We can then solve for the direct flux extinction and the up and down source terms in the normal way. The divergence of the direct flux over the layer is saved directly at this point to be used later for the heating rate calculation.

The source terms, however, have been calculated using ζ' and need to be converted to sources in the vertical. We assume the scattered flux in the forward and backwards directions along the slant path are isotropic across the respective hemispheres. The source terms in the up and down directions can then be calculated as follows:

$$\begin{aligned} S_{up} &= \frac{1}{2}[(1+\cos\zeta\sec\zeta')S'^{+} + (1-\cos\zeta\sec\zeta')S'^{-}] \\ S_{down} &= \frac{1}{2}[(1+\cos\zeta\sec\zeta')S'^{-} + (1-\cos\zeta\sec\zeta')S'^{+}] \end{aligned} \tag{1.70}$$

This is done in the routine `spherical_solar_source.F90`

The plane-parallel calculation for the diffuse fluxes can then proceed as before with a slight alteration of the boundary conditions to account for the fact we are only including the diffuse component in the downward flux:

$$\begin{aligned} U_0 &= 0 \\ U_N &= \alpha_s Z_N + \alpha_d D_N \end{aligned} \tag{1.71}$$

1.11.2 Determination of heating rates

Finally, it should be noted that to diagnose the flux absorbed in each layer we must now take account of both the direct and diffuse flux divergence across the layer. The diffuse flux divergence is simply the difference of the net diffuse fluxes at the top and bottom of the layer as before. The direct flux divergence has been calculated separately and is held in the additional output variable `flux_direct_div`. Only the sum of these two quantities has any physical meaning and should be used in the calculation of heating rates.

1.12 Calculation of photolysis rates

A comprehensive and flexible scheme is available for the calculation of photolysis and photoionisation rates along with an adjustment of the direct radiative heating for the energy used in the photolysis reactions.

The components of the scheme are described below.

1.12.1 Correlated-*k* mapping technique

In order to maintain accuracy whilst reducing computational cost a novel wavelength mapping technique is implemented as part of the correlated-k method. Spectral absorption lines can vary dramatically over very small wavelength intervals. The correlated-k method essentially just reorders the wavelengths within a spectral band in order of increasing strength of absorption and then bins up wavelengths with similar absorption coefficients. Radiative transfer calculations are only done for each absorption bin, or *k-term*. The novel technique here is to retain the information on the wavelengths that each k-term represents. Once the radiative transfer calculations have been done, the calculated fluxes for each k-term are mapped back to spectral *sub-bands* at these wavelengths. The high resolution fluxes are then convolved with the solar spectrum, photo-absorption cross-sections and branching ratios (or quantum yields) in order to derive accurate photolysis rates for any given photolysis pathway. An added benefit to this mapping technique is that spectra can be diagnosed at high-resolution, effectively providing line-by-line resolution for the cost of a broad-band calculation.

Treatment of overlapping gaseous absorption

For this mapping technique to work, careful consideration must be given to the treatment of how different gas absorption spectra overlap in wavelength. The Socrates correlated-k scheme treats the discretisation of k-terms in wavelength space separately for each gas in the band. Therefore the k-terms of each gas will map to different wavelengths. For band-averaged fluxes it is assumed that the absorption coefficients for different gases are uncorrelated so that the k-terms can be randomly overlapped. Here, we introduce a more accurate method to calculate fluxes for each of the mapped sub-bands. This new overlap method is termed *exact-major overlap*. A major gas is defined for the band that is assumed to have the most significant absorption in the atmospheric column. The k-terms of this gas are used to define the mapping to sub-bands for the new technique. For each sub-band the fractional contribution of each minor gas k-term (i.e. the k-term weight) is determined from the wavelength mapping of the minor gas. The fluxes calculated for each sub-band will then use the correct proportion of minor gas absorption, although the minor gas k-terms are still randomly overlapped with each other.

The *exact-major overlap* method can be used for bands where there is more than one significant absorber. For other bands the cheaper *equivalent-extinction* method can be used. When using equivalent-extinction, the fractional contribution of the minor gas absorption to each sub-band is assumed to be the same as for the band as a whole. In either case, once the flux for the mapped sub-band has been determined, the solar spectrum (including any time-variation), photo-absorption cross-sections and quantum yields are always convolved at the full sub-band wavelength resolution.

1.12.2 Calculation of actinic flux

The actinic flux (or more correctly, the *actinic radiation field*), A, is the integrated radiative intensity (I) over all directions (ω):

$$A = \int_{4\pi} I d\omega \tag{1.72}$$

It can be thought of as the radiative energy incident upon a sphere, or molecule, at a given level in the atmosphere. We determine a representative actinic flux for a given model layer from the available two-stream fluxes, that is the up (U) and down (D) hemispheric diffuse fluxes and the direct intensity of the solar beam (S). These are available at the layer boundaries and would be attenuated across the layer, so in order to obtain a representative value of A for the layer it is best to use the total flux divergence (ΔF):

$$\begin{aligned}
\frac{dI}{d\tau} &= -I \qquad (1.73)\\
\int_{4\pi} \frac{dI\cos\theta}{d\tau_{vert}} d\omega &= \int_{4\pi} -I d\omega \qquad (1.74)\\
\frac{-\Delta F}{\Delta\tau_{vert}} &= A \qquad (1.75)
\end{aligned}$$

where we start from the Beer-Lambert law for the change in intensity with optical depth to absorption along the slant path (τ), and convert to flux absorbed over a layer with optical depth to absorption in the vertical of $\Delta\tau_{vert}$. Here, θ is the angle between the slant path and the vertical.

Using equation 1.75 to calculate the actinic flux is particularly beneficial as the flux divergence is also used to calculate the radiative heating rates. This ensures the energy used for photolysis and radiative heating are calculated in a consistent way. Equation 1.75 becomes numerically unstable when the optical depth for absorption in the layer ($\Delta\tau_{vert}$) is small. In this case, we fall back to a calculation using the fluxes at the layer boundaries:

$$\begin{aligned}
A &= \int_{4\pi} I d\omega\\
&= S + 2\pi I^{+} + 2\pi I^{-}\\
&= S + 2U + 2D \qquad (1.76)
\end{aligned}$$

The actinic flux is calculated in `calc_actinic_flux` per k-term in units of W m^{-2}. It is later mapped to spectral sub-bands where it is converted to units of photons m^{-2} s^{-1} by dividing by the energy of a photon at the mid-point wavenumber for the sub-band (see eqn 1.78).

1.12.3 Calculation of photolysis and photoionisation rates

The rate of photolysis or photoionisation (J in units of s^{-1}) for a given molecule that results in a particular set of products is:

$$J = \int \sigma Q A d\lambda \qquad (1.77)$$

where σ is the absorption cross-section of the molecule (in m^2), Q is the quantum yield (or branching ratio) for photolysis resulting in a particular set of products, A is the actinic flux (in photons m^{-2} s^{-1}) and the integral is over all wavelengths (λ). We perform this calculation for each mapped sub-band in the `augment_radiance.F90` routine, with operations broken down into those necessary at each level of looping. Starting from the variables in the units in which they are available in the code, mass absorption coefficient for the photolysing species k_{layer}

($\text{m}^2\text{kg}_{air}^{-1}$), and actinic flux F_A (W m^{-2}), the equation becomes:

$$J = \sum_{\text{sub-bands}} k_{layer} \frac{m}{\zeta N_A} Q F_A \frac{\lambda}{hc} w \tag{1.78}$$

$$= \frac{m}{\zeta N_A hc} \sum_{\text{k-terms}} F_A \sum_{\text{sub-bands}} k_{layer} Q \lambda w \tag{1.79}$$

where m is the molecular weight of the absorbing species (kg_{gas} mol^{-1}), ζ is the mass mixing ratio ($\text{kg}_{gas}/\text{kg}_{air}$) of the species, N_A is Avagadro's number (mol^{-1}), h is Planck's constant (J s), c is the speed of light (m s^{-1}), and w is the sub-band weight (i.e. fraction of the actinic flux in this sub-band). The sum over sub-bands is done in the internal routine `calc_photolysis_incr` while the rest of the calculation is done in `finalise_photol_incr` for each k-term outside of the loop over the sub-bands for that k-term.

The quantum yield (Q) is parametrised at arbitrary wavelength resolution and is read in as part of the standard configuration file (or *spectral file*). The list of photolysis reactions required can be simply added to the spectral file specifying the gas absorber to be photolysed and the threshold wavelength beyond which photolysis can occur. In the case of highly energetic photons causing photoionisation it is possible for the photoelectron to cause further dissociation/ionisation events. This can be parametrised by providing scaled quantum yields that may exceed 1. The summation over sub-bands is done by weighting each sub-band by the incoming solar spectrum. The solar spectrum may be specified at arbitrary time resolution (year, month, day, second) in an extended spectral file.

1.12.4 Calculation of residual heating

The radiative heating rate is determined from the flux divergence across the layer divided by the heat capacity of the layer. Where photolysis occurs some of the flux absorbed in the layer would be used to dissociate or ionise the molecules. This fraction of the energy is therefore not (immediately) available to increase the temperature of the gas and should instead be handled by the chemistry scheme for possible release in exothermic reactions after advection of the product species. The proportion of the flux used for photolysis is determined at the same time as the photolysis rates within each sub-band:

$$\Delta F_J = Q \frac{E_J}{E_{photon}} \frac{\Delta\tau_J}{\Delta\tau_{total}} \Delta F \tag{1.80}$$

$$= Q \frac{\lambda}{\lambda_t} \Delta\tau_J F_A \tag{1.81}$$

$$= Q \frac{\lambda}{\lambda_t} \Delta M k_{layer} F_A \tag{1.82}$$

where ΔM is the mass of air per unit area in the layer and the energy required for a photolysis event (E_J) is determined by the energy of a photon at the threshold wavelength (λ_t) for the reaction.

The flux divergence used for photolysis is then summed over sub-bands in the same way as the photolysis rates, reusing the terms already calculated in `finalise_photol_incr` (compare with eqn 1.79):

$$\Delta F_J = \frac{\Delta M}{\lambda_t} \sum_{\text{k-terms}} F_A \sum_{\text{sub-bands}} k_{layer} Q \lambda w \tag{1.83}$$

Once summed over all photolysis pathways, the residual heating is determined by subtracting this from the total flux divergence.

Where the energy needed for photolysis is expected to be released immediately to heat the atmosphere then it is not necessary to include it in the flux divergence used for photolysis. This can be specified per photolysis reaction so that the chemistry scheme need only include those exothermic reactions where the species involved have a lifetime that is long compared to the advection. The spectral file includes a thermalisation indicator per reaction to flag the reactions for which the energy should be immediately thermalised.

1.12.5 Configuration for the far-UV and extreme-UV

The scheme developed here has been designed to be applicable over the entire spectral range from X-ray to near-infrared wavelengths. This is entirely configurable within the *spectral file* which contains all the information on the wavelength breakdown, the gas absorbers present, gas absorption coefficients, photolysis pathways and quantum yields, the solar spectrum (optionally time varying), Rayleigh scattering coefficients, and cloud and aerosol absorption and scattering parameters.

Two initial spectral file configurations have been developed in the `example/sp_uv` Socrates directory: a high-resolution reference configuration covering the wavelengths 0.5nm-320.5nm with 320 bands and 6867 sub-bands; and a broadband configuration for use in general circulation models (GCMs) covering the wavelengths 0.4nm-10μm with 26 bands and 2401 sub-bands (this includes 21 bands and 2391 sub-bands between 0.4-320nm).

Both configurations use the same base data for absorption cross-sections, quantum yields etc. At UV and shorter wavelengths we include absorption, photolysis and photoionisation involving the species O_3, O_2, N_2, O, N and H_2O. Following Solomon and Qian [2005] we have used absorption cross-sections and quantum yields from Fennelly and Torr [1992] for the extreme-UV, and Henke et al. [1993] for the X-ray, for the species O_2, N_2, O and N. Shortward of 65nm the photoelectron enhancement factors derived by Solomon and Qian [2005] are used to enhance the quantum yields. In the far-UV, gas absorption coefficients are derived from the recommendations in the JPL report 15-10 Burkholder et al. [2015]. Quantum yields for the important region around the solar H Lyman-α line (121.6nm) are taken from Lacoursière et al. [1999]. O_2 absorption dominates throughout the far-UV with complex absorption spectra over particular wavelength ranges such as the Schumann-Runge bands at 175-205nm. The k-term mapping technique automatically concentrates sub-bands in these complex parts of the spectrum.

The broadband configuration extends into the near-IR by including the visible and near-IR bands used for the Global Atmosphere 7 (GA7) configuration Walters et al. [2019]. The new 26-band configuration can then be used to entirely replace the GA7 configuration in the GCM providing heating rates for total solar absorption throughout the atmosphere. The 26-band configuration uses a total of 92 major gas k-terms compared to 41 in the 6-band GA7 configuration with the computational cost of radiation calculations scaling approximately linearly with the number of k-terms.

Non-LTE effects may be accounted for in the extreme-UV by applying a heating efficiency of 0.05. In the broadband configuration this is achieved by setting the thermalisation indicator to true for all photolysis reactions that occur in the extreme-UV, and then applying a non-LTE correction reducing the heating rates to 5% of their initial value for wavelengths shortward of 98.6nm. At these wavelengths absorption leads to photoionisation and the kinetic energy of the released photoelectrons is only partially transferred to atmospheric heating. This treatment follows Roble et al. [1987] and is similar to the treatment of extreme-UV heating in WACCM.

Solar spectral variations have been parametrised for the 2401 sub-bands in the broadband configuration using the monthly variations recommended by Matthes et al. [2017]. The scheme therefore provides heating, photolysis and photoionisation rates for the mesosphere and lower thermosphere region directly linked to observed solar activity.

Chapter 2

The Spherical-Harmonic Radiance Code

2.1 Fundamentals of Solving for Radiances

The monochromatic equation of transfer is used in the form

$$\begin{aligned}(\mathbf{n}.\nabla)I(\mathbf{x},\mathbf{n}) &= -(k^{(s)}+k^{(a)})I(\mathbf{x},\mathbf{n}) \\ &+ \frac{k^{(s)}}{4\pi}\int_{\Omega} I(\mathbf{x},\mathbf{n}')P(\mathbf{n}',\mathbf{n})\,d\omega_{\mathbf{n}'} + j(\mathbf{x},\mathbf{n})\end{aligned} \tag{2.1}$$

The phase function can be rescaled using the standard prescription

$$k^{(s)} \to (1-f)k^{(s)}, \tag{2.2}$$

$$P(\mathbf{n}',\mathbf{n}) \to \frac{P(\mathbf{n}',\mathbf{n}) - 4\pi f\delta(\mathbf{n}'-\mathbf{n})}{1-f} \tag{2.3}$$

i. e.

$$P(\mathbf{n}',\mathbf{n}) - 4\pi\delta(\mathbf{n}'-\mathbf{n}) \to \frac{P(\mathbf{n}',\mathbf{n}) - 4\pi\delta(\mathbf{n}'-\mathbf{n})}{1-f}. \tag{2.4}$$

Since this does not alter the functional form of the equation no further reference to rescaling wil be made here.

The phase function may be expanded in Legendre polynomials:

$$P(\mathbf{n}',\mathbf{n}) = \sum_{l=0}^{\infty}(2l+1)g_l P_l(\mathbf{n}'.\mathbf{n}) \tag{2.5}$$

We make use of the standard results

$$P_l(\mathbf{n}'.\mathbf{n}) = \frac{4\pi}{2l+1} \sum_{m=-l}^{l} Y_l^m(\mathbf{n}) Y_l^{m*}(\mathbf{n}') \tag{2.6}$$

$$\delta(\mathbf{n}' - \mathbf{n}) = \sum_{l=0}^{\infty} \sum_{m=-l}^{l} Y_l^m(\mathbf{n}) Y_l^{m*}(\mathbf{n}') \tag{2.7}$$

It is useful to keep the direct solar beam separate, so we write:

$$I(\mathbf{x}, \mathbf{n}) = \sum_{l=0}^{\infty} \sum_{m=-l}^{l} I_{lm}(\mathbf{x}) Y_l^m(\mathbf{n}) + I_\odot \delta(\mathbf{n}' - \mathbf{n}_\odot) \tag{2.8}$$

It now follows that

$$\begin{aligned} \sum_{lm} Y_l^m(\mathbf{n})(\mathbf{n}.\nabla) I_{lm}(\mathbf{x}) &+ (\mathbf{n}.\nabla) I_\odot(\mathbf{x}) \delta(\mathbf{n}' - \mathbf{n}_\odot) \\ &= -(k^{(s)} + k^{(a)}) \Big(I_\odot(\mathbf{x}) \delta(\mathbf{n}' - \mathbf{n}_\odot) \\ &+ \sum_{lm} I_{lm}(\mathbf{x}) Y_l^m(\mathbf{n}) \Big) + \sum_{lm} j_{lm}(\mathbf{x}) Y_l^m(\mathbf{n}) \\ &+ k^{(s)} \int_\Omega \left\{ \sum_{lm} I_{lm}(\mathbf{x}) Y_l^m(\mathbf{n}') + I_\odot(\mathbf{x}) \delta(\mathbf{n}' - \mathbf{n}_\odot) \right\} \\ &\qquad \left\{ \sum_{l'm'} g_{l'} Y_{l'}^{m'*}(\mathbf{n}') Y_{l'}^{m'}(\mathbf{n}) \right\} d\omega_{\mathbf{n}'} \end{aligned} \tag{2.9}$$

We separate the singular terms involving exposed δ-functions to get

$$(\mathbf{n}.\nabla) I_\odot(\mathbf{x}) = -(k^{(s)} + k^{(a)}) I_\odot(\mathbf{x}). \tag{2.10}$$

which may be integrated directly.

Making the assumption that the atmosphere is plane-parallel,

$$(\mathbf{n}.\nabla) I(\mathbf{x}) = n_0 \, dI_{lm}/dz, \tag{2.11}$$

where $n_0 (= n_z)$ is the zeroth component of $\mathbf{n}$ in the spherical basis (the others are $n_\pm = \mp(n_x \pm i n_y)/\sqrt{2}$, so that $\mathbf{n} = \sum_{j=-1}^{1} n_j \boldsymbol{\epsilon}_j^*$ where $\boldsymbol{\epsilon}_{\pm 1} = \mp(\mathbf{e}_x \pm i \mathbf{e}_y)/\sqrt{2}$). Hence, using the orthogonality of the Y_l^m,

$$\begin{aligned} \sum_{lm} n_0 Y_l^m(\mathbf{n}) \frac{dI_{lm}(z)}{dz} &= -(k^{(s)} + k^{(a)}) \sum_{lm} I_{lm}(z) Y_l^m(\mathbf{n}) + \sum_{lm} j_{lm} Y_l^m(\mathbf{n}) \\ &+ k^{(s)} \Big\{ \sum_{lm} I_{lm}(z) g_l Y_l^m(\mathbf{n}) \\ &+ I_\odot(z) \sum_{lm} g_l Y_l^{m*}(\mathbf{n}_\odot) Y_l^m(\mathbf{n}) \Big\} \end{aligned} \tag{2.12}$$

The left-hand side of this equation can be expressed as a pure function of spherical harmonics using the recurrence

$$n_0 Y_l^m(\mathbf{n}) = c_{lm}^+ Y_{l+1}^m(\mathbf{n}) + c_{lm}^- Y_{l-1}^m(\mathbf{n}) \tag{2.13}$$

where

$$c_{lm}^+ = \sqrt{\frac{(l+1-m)(l+1+m)}{(2l+1)(2l+3)}} \tag{2.14}$$

and

(2.15)

$$c_{lm}^- = \sqrt{\frac{(l-m)(l+m)}{(2l-1)(2l+1)}} \tag{2.16}$$

are the Clebsch-Gordan coefficients, $\langle l+1, m|1, 0, l, m\rangle$ and $\langle l-1, m|1, 0, l, m\rangle$

By forming the inner product of this equation with Y_l^m the individual spherical harmonics may be separated. At the same time we introduce the optical depth, τ, and the albedo of single-scattering, ω:

$$d\tau = -(k^{(s)} + k^{(a)})\, dz \tag{2.17}$$

and

(2.18)

$$\omega = k^{(s)}/(k^{(s)} + k^{(a)}). \tag{2.19}$$

For a Planckian source $j_{lm}(\mathbf{x}, \mathbf{n}) = k^{(a)}\sqrt{4\pi}B(\mathbf{x})\delta_{l0}\delta_{m0}$ where $B(\mathbf{x})$ is isotropic. The equation therefore becomes:

$$\begin{aligned} c_{l-1,m}^+ \frac{dI_{l-1,m}(\tau)}{d\tau} + c_{l+1,m}^- \frac{dI_{l+1,m}(\tau)}{d\tau} = \\ s_l I_{lm}(\tau) - s_0\sqrt{4\pi}B(\tau)\delta_{l0}\delta_{m0} \\ - \omega g_l Y_l^{m*}(\mathbf{n}_\odot) I_\odot(\tau) \end{aligned} \tag{2.20}$$

where $s_l = 1 - \omega g_l$. For conservative scattering $s_0 = 0$, which case will require some special treatment. To solve these equations we divide the atmosphere into N homogeneous layers with optical thicknesses $\tau_i, i = 1, \ldots, N$ and boundaries at optical depths $\Delta_i, i = 0, \ldots, N$ in each of which the optical properties are constant: τ will be used as a local optical depth when considering a single layer. As these equations are linear the solution is the sum of a particular integral and a complementary function.

2.1.1 The Complementary Function

Since the equation is linear the complementary function will consist of a sum of exponentials of the form $H_{lm}(\mu)e^{\tau/\mu}$ for $\mu \in \mathbb{R}$. For any value of μ and a fixed value of m, a recurrence relation may be established for the coefficients H_{lm}, starting from H_{mm}. The expansion of the radiance in spherical harmonics is truncated at an odd order L, so this recurrence must terminate with $H_{L'+1,m} = 0$ where $L' = L$ if m is even and $L' = L + 1$ if m is odd (the reason for this is explained below). This imposes a constraint on the permissible values of μ and defines an eigenvalue problem.

$$c^{-}_{m+1,m} H_{m+1,m} = s_m \mu H_{mm}, \tag{2.21}$$

$$c^{+}_{l-1,m} H_{l-1,m} + c^{-}_{l+1,m} H_{l+1,m} = s_l \mu H_{lm}, \quad m < l < L', \tag{2.22}$$

and

$$c^{+}_{L'-1,m} H_{L'-1,m} = s_{L'} \mu H_{L'm} \tag{2.23}$$

This may be cast in a more usual form by defining $K_{lm} = \sqrt{s_l} H_{lm}$ so that

$$\sum_{l=m}^{L} C_{ql} K_{lm} = \mu K_{lm}, \quad m \leqslant q \leqslant L', \tag{2.24}$$

where the non-zero entries in the matrix C are given by:

$$C_{l-1,l} = c^{+}_{l-1,m} / \sqrt{s_l s_{l-1}} \quad \text{and} \quad C_{l,l+1} = c^{-}_{l+1,m} / \sqrt{s_l s_{l+1}}, \tag{2.25}$$

where $m \leqslant l \leqslant L'$. In fact, since $c^{+}_{lm} = c^{-}_{l+1,m}$ the matrix C is symmetrical. As it is also tridiagonal, the eigenvalues could be found directly using the QR-algorithm, though it is possible to reduce the size of the problem as discussed below. Once the eigenvalues have been determined the recurrence relation may be used to determine the K_{lm}.

Care is needed with the recurrence. As $l \to \infty$ $c^{\pm}_{l,m} \sim 1/2$ and $s_l \sim 1$. Hence, the recurrence approaches the form

$$H_{l-1,m} + H_{l+1,m} = 2\mu H_{lm}, \tag{2.26}$$

When $|\mu| > 1$ this has growing solutions, which will be triggered by rounding errors in numerical practice. Physically, we seek a solution which decays as $l \to \infty$, so the recurrence must be used in the direction of decreasing l, in which direction the desired solution grows and will swamp the error. When $|\mu| < 1$ recurrence in the upward or downward direction is stable, so for algorithmic convenience downward recurrence is used consistently. (Note that Benassi et al. [1984] use upward recurrence in this case, but it is not necessary to do so). One further refinement is required in practice. When scattering is almost conservative, one eigenvalue is very large and traversing the sequence in the downward direction terms increase by a factor of about 2μ at each stage. When the order of truncation is large enough this can lead to numerical overflows. The recurrence itself is therefore recast in the quantities $H'_{lm} = \sigma^{-l} H_{lm}$, where $\sigma = 1/\max(1, 2\mu - 1)$, to separate the overflowing behaviour while not affecting behaviour for small values of μ.

(*Note:* For comparison with the program we can define

$$E_j = c^{+}_{m-2+j,m} / \sqrt{s_{m-1+j} s_{m-2+j}} \quad 2 \leqslant j \leqslant L + 1 - m \tag{2.27}$$

as the subdiagonal element on the jth row of the matrix. Because the optical properties of the layer do not depend on direction we might expect that if $e^{\tau/\mu}$ is an eigensolution, $e^{-\tau/\mu}$ should also be. This is seen to be so by observing that if μ is an eigenvalue with an eigenvector $K_{lm}(\mu)$, a vector for which every other element of $K_{lm}(\mu)$ is changed in sign will be an eigenvector for an eigenvalue $-\mu$ as $C_{ij} = 0$ unless $|i - j| = 1$. This explains why odd and even orders are truncated separately: if the eigenproblem is of an odd size $\mu = 0$ will be an eigenvalue, causing numerical overflows in evaluating the exponential. Writing the eigenvector for the eigenvalue μ as $\mathbf{K}_e + \mathbf{K}_o$, where the first term contains the even entries and the second the odd entries, it follows that

$$C(\mathbf{K}_e + \mathbf{K}_o) = \mu(\mathbf{K}_e + \mathbf{K}_o) \tag{2.28}$$

and

$$C(\mathbf{K}_e - \mathbf{K}_o) = -\mu(\mathbf{K}_e - \mathbf{K}_o) \tag{2.29}$$

from which

$$C\mathbf{K}_e = \mu\mathbf{K}_o \tag{2.30}$$

and

$$C\mathbf{K}_o = \mu\mathbf{K}_e \tag{2.31}$$

so that

$$C^2\mathbf{K}_o = \mu^2\mathbf{K}_o \tag{2.32}$$

By direct calculation the $(C^2)_{ij} = 0$ if $i - j$ is odd. This means that even rows and columns can be deleted from C^2 to halve the size of the eigenproblem. Indexing the rows of *this* matrix with j and denoting the main diagonal elements by d_j and the sub-diagonal elements by e_j,

$$d_j = E_{2j-1}^2 + E_{2j}^2 \tag{2.33}$$

and

$$e_j = E_{2j-2}E_{2j-1} \tag{2.34}$$

for $1 \leqslant j \leqslant (L' + 1 - m)/2$: here $E_1 = 0$)

The eigenvalues are of the form $\pm\mu_k$, $k = 1, \ldots (L' + 1 - m)/2$, so the complementary function may be written as

$$I_{lm}(\tau) = \sum_k H_{lmk}^- e^{-\tau/\mu_k} + \sum_k H_{lmk}^+ e^{-(\tau_i - \tau)/\mu_k} \tag{2.35}$$

where we follow Stamnes et al. in using only negative exponentials so as to avoid overflows when τ_i is large. The coefficients $H_{lmk}^{\pm}$ are determined by the eigenvectors, $\mathbf{K}_k$ of the matrix C. In fact,

$$H_{lmk}^{\pm} = u_{mk}^{\pm} s_l^{-1/2} (\pm 1)^{(m+l)} K_{klm} \tag{2.36}$$

It is now convenient to define $\mathbf{V}_k$ so that $V_{klm} = K_{klm}/\sqrt{s_l}$.

Conservative scattering poses a certain difficulty. As $\omega \to 1$, the matrix $\mathbf{C}$ becomes singular in the case where $m = 0$. Then, $\mathbf{C}$ has two eigenvalues of $O((1 - \omega)^{-1/2})$ with eigenvalues $\mathbf{K} = (1, \pm 1, 0, \ldots, 0) + O((1 - \omega)^{-1/2})$ and eigenvalues of $O(1)$ with eigenvectors $\mathbf{K} = (O((1 - \omega)^{-1/2}), O((1 - \omega)^{-1/2}), O(1), \ldots, O(1))$. When $\omega = 1$ a solution linear in τ must be sought. Since we may want to solve for a number of atmospheric columns simultaneously it is desirable to avoid special pleading for singular cases, so for the present we artificially reduce ω to avoid ill-conditioning: this seems to preform well enough in practice, but it may be undesirable in extremely optically thick conservative layers.

2.1.2 The Particular Integral for Thermal Radiation

In the infra-red region is is most convenient to reformulate the equation of transfer in terms of differential radiances. We write

$$I = I' + B \tag{2.37}$$

so that the equation of transfer becomes

$$\begin{aligned}(\mathbf{n}.\nabla)I'(\mathbf{x},\mathbf{n}) &= -(k^{(s)}+k^{(a)})I'(\mathbf{x},\mathbf{n}) \\ &\quad + \frac{k^{(s)}}{4\pi}\int_\Omega I'(\mathbf{x},\mathbf{n}')P(\mathbf{n}',\mathbf{n})\,d\omega_{\mathbf{n}'} - (\mathbf{n}.\nabla)B(\mathbf{x}).\end{aligned} \tag{2.38}$$

Introducing the optical depth, τ

$$n_0\frac{dI'(\tau,\mathbf{n})}{d\tau} = I'(\tau,\mathbf{n}) - \frac{\omega}{4\pi}\int_\Omega I'(\mathbf{x},\mathbf{n}')P(\mathbf{n}',\mathbf{n})\,d\omega_{\mathbf{n}'} - n_0\frac{dB(\tau)}{d\tau} \tag{2.39}$$

Now, $n_0 = \sqrt{4\pi/3}.Y_1^0(\mathbf{n})$, so on expanding this in spherical harmonics,

$$\begin{aligned}\sum_{lm} n_0 Y_l^m(\mathbf{n})\frac{dI'_{lm}(\tau)}{d\tau} &= \sum_{lm} I'_{lm}(z)Y_l^m(\mathbf{n}) \\ &\quad - \omega\sum_{lm} I'_{lm}(z)g_l Y_l^m(\mathbf{n}) \\ &\quad - \sqrt{4\pi/3}\delta_{l1}\delta_{m0}Y_l^m(\mathbf{n})\frac{dB(\tau)}{d\tau}\end{aligned} \tag{2.40}$$

Proceeding as before,

$$\begin{aligned}c^+_{l-1,m}\frac{dI_{l-1,m}(\tau)}{d\tau} + c^-_{l+1,m}\frac{dI_{l+1,m}(\tau)}{d\tau} &= \\ s_l I_{lm}(\tau) - \sqrt{4\pi/3}\delta_{l1}\delta_{m0}\frac{dB(\tau)}{d\tau}.\end{aligned} \tag{2.41}$$

The simplest case to consider is that when B is linear in τ. The particular integral then becomes

$$I_{i,lm} = \frac{1}{s_{1i}}\sqrt{\frac{4\pi}{3}}\frac{\Delta B_i}{\tau_i}\delta_{l1}\delta_{m0} \tag{2.42}$$

where ΔB_i is the difference in the Planckian across the ith layer in the direction of increasing τ.

We also consider the case where the variation of the Planckian is quadratic across the layer. In this case we have

$$I_{i,10} = \frac{1}{s_{1i}}\sqrt{\frac{4\pi}{3}}\frac{\Delta B_i}{\tau_i} - \frac{2}{s_{1i}}\sqrt{\frac{4\pi}{3}}\frac{\Delta^2 B_i}{\tau_i^2}\tau \tag{2.43}$$

$$I_{i,00} = -\frac{2c^-_{1,0}}{s_{0i}s_{1i}}\sqrt{\frac{4\pi}{3}}\frac{\Delta^2 B_i}{\tau_i^2} \tag{2.44}$$

and

$$I_{i,20} = -\frac{2c^{+}_{1,0}}{s_{2i}s_{1i}}\sqrt{\frac{4\pi}{3}}\frac{\Delta^2 B_i}{\tau_i^2} \tag{2.45}$$

with $I_{i,lm} = 0$ otherwise.

Small Optical Depths

The solutions will clearly fail in the case when $\tau = 0$, but even when τ is not quite 0 ill-conditioning will arise; this could theoretically be overcome by increasing τ to some mimimum value, but in practice such a value would be unacceptably large. Conditioning is therefore restored by adding to the particular integral a solution of the homogeneous system which exhibits the same singularity as $\tau \to 0$. We consider only the case of linear variations in τ for now. Restricting ourselevs to the relevant case $m = 0$ the foregoing particular integral can be written as

$$I_{l0} = q_0\delta_{l1}, \tag{2.46}$$

where q_0 is a constant. As the optical depth tends to 0, the homogeneous solution becomes

$$I_{l0} = \sum_k \left\{u_k^{+}V_{kl} + u_k^{-}(-1)^l V_{kl}\right\} + O(\tau/\mu_k). \tag{2.47}$$

Since C is real and symmetric its eigenvectors, $\mathbf{K}_k$, are orthogonal and may be normalized. We therefore have

$$\sum_l V_{kl}V_{k'l}s_l = \delta_{kk'} \tag{2.48}$$

and

$$\sum_l V_{kl}V_{k'l}(-1)^l s_l = 0 \tag{2.49}$$

We immediately find that

$$u_k^{+} = -q_0 s_1 V_{k1} \tag{2.50}$$

and

$$u_k^{-} = q_0 s_1 V_{k1} \tag{2.51}$$

so the homogeneous solution to restore conditioning becomes

$$I_{l0} = q_0 s_1 \sum_k V_{kl}V_{k1}\left\{(-1)^l e^{-\tau/\mu_k} - e^{-(\tau_i-\tau)/\mu_k}\right\}. \tag{2.52}$$

2.1.3 The Solar Particular Integral

Using the standard notation $\mu_0 = -\cos\theta_\odot$ the direct solar beam in a layer may be written as

$$I_{\odot i}(\tau) = I_\odot(\Delta_{i-1})e^{-\tau/\mu_0} \tag{2.53}$$

Provided that $\mu_0 \neq \mu_k$ for any eigenvalue μ_k a particular integral of the form $I_{ilm}(\tau) = Z_{ilm}e^{-\tau/\mu_0}$ may be sought. This gives

$$c^{+}_{l-1,m}Z_{i,l-1,m} + c^{-}_{l+1,m}Z_{i,l+1,m} = -\mu_0 s_{li}Z_{ilm} + \mu_0 I_\odot(\Delta_{i-1})\omega_i g_{li}Y_l^{m*}(\mathbf{n}_\odot). \tag{2.54}$$

A truncation is imposed by setting $Z_{i,L'+1,m} = 0$. Noting that $\omega g_l = 1 - s_l$ and that $\mu_0 = -(\mathbf{n}_\odot)_0$, it follows on using the recurrence relation that

$$\begin{aligned} & c^+_{l-1,m}(Z_{i,l-1,m} + I_\odot(\Delta_{i-1})Y^{m*}_{l-1}(\mathbf{n}_\odot)) \\ & + c^-_{l+1,m}(Z_{i,l+1,m} + I_\odot(\Delta_{i-1})Y^{m*}_{l+1}(\mathbf{n}_\odot)) \\ & = -\mu_0 s_{li}(Z_{ilm} + I_\odot(\Delta_{i-1})Y^{m*}_{l}(\mathbf{n}_\odot)) \end{aligned} \tag{2.55}$$

This admits a solution

$$Z_{ilm} = -I_\odot(\Delta_{i-1})Y^{m*}_l(\mathbf{n}_\odot) + \gamma\mathcal{V}_{ilm}(\mu_0) \tag{2.56}$$

with

$$\gamma = I_\odot(\Delta_{i-1})Y^{m*}_{L'+1}(\mathbf{n}_\odot)/\mathcal{V}_{i,L'+1,m}(\mu_0) \tag{2.57}$$

where $\mathcal{V}(\mu_0)$ is defined by the recurrence

$$c^+_{l-1,m}\mathcal{V}_{i,l-1,m} + c^-_{l+1,m}\mathcal{V}_{i,l+1,m} = -\mu_0 s_l \mathcal{V}_{ilm} \tag{2.58}$$

starting from $\mathcal{V}_{imm} = 1$.

The issue of ill-conditioning must be addressed here. If μ_0 is close to one of the eigenvalues of the linear system ill-conditioning will arise, with a singularity in the case when equality obtains. This can be removed by finding the eigenvalue closest to μ_0 and subtracting from the particular integral a multiple of the coressponding eigensolution which cancels the singularity in the limit. Instead of implementing this using an `IF`-test, it is applied using a weighting involving the separation of μ_0 and the eigenvalue and so removes ill-conditioning at nearby values.

2.1.4 Interior Boundary Conditions

On interior boundaries we must apply the conditions

$$I_{ilm}(\tau_i) = I_{i+1,lm}(0), \quad 1 \leqslant i \leqslant N, \forall l, m. \tag{2.59}$$

We write the particular integral in the ith layer as $\hat{G}_{ilm}$ at the top and as $\check{G}_{ilm}$ at the bottom. Then,

$$\begin{aligned} 0 = \sum_k \Big\{ & u^-_{mik}(-1)^{l+m}V_{lmik}\vartheta_{ik} + u^+_{mik}V_{lmik} + \check{G}_{lmi} \\ & - u^-_{m,i+1,k}(-1)^{l+m}V_{lm,i+1,k} - u^+_{m,i+1,k}V_{lm,i+1,k}\vartheta_{i+1,k} - \hat{G}_{lm,i+1}\Big\} \end{aligned} \tag{2.60}$$

for $l = m, \ldots, L'$.

2.1.5 The Upper boundary Condition

At the top boundary of the atmosphere the radiance must be specified in downward directions. Typically, the indicent radiation will comprise only the direct solar beam, but we shall formulate the boundary condition more generally to allow for possiblities such as the use of differential radiances in the infra-red. The condition is then

$$I(\mathbf{n}) = I^{(0)}(\mathbf{n}), \qquad \mathbf{n} \in \Omega_-. \tag{2.61}$$

where $I^{(0)} = \sum_{lm} I^{(0)}_{lm} Y^m_l(\mathbf{n})$. As $I^{(0)}$ is specified only on Ω_-, the coeffieicnts $I^{(0)}_{lm}$ are not uniquely defined, but they can be made so by making $I^{(0)}$ symmetric or antisymmetric.

In a truncated system it is not possible to impose the boundary condition for every $\mathbf{n} \in \Omega_-$. The simplest possibility is to specify that $I(\mathbf{n}) = I^{(0)}(\mathbf{n})$ for a finite number of $\mathbf{n}$, but most authors prefer Marshak's conditions

$$\int_{\Omega_-} (I(\mathbf{n}) - I^{(0)}(\mathbf{n})) Y^{m'*}_{l'}(\mathbf{n})\, d\omega_{\mathbf{n}} = 0 \tag{2.62}$$

for those $Y^{m'}_{l'}$ with odd parity. The equation becomes trivial if $m' \neq m$, so considering a fixed value of m, this restricts us to $l' = m+1, \ldots, L'$. The boundary conditions are therefore

$$\sum_l \kappa_{ll'm}(I_{lm} - I^{(0)}_{lm}) = 0 \tag{2.63}$$

for the given l', where,

$$\kappa_{ll'm} = \int_{\Omega_-} Y^m_l(\mathbf{n}) Y^{m*}_{l'}(\mathbf{n})\, d\omega_{\mathbf{n}}. \tag{2.64}$$

Substituting the expression for I_{lm} we obtain the equation

$$\begin{aligned} \sum_l \kappa_{ll'm}(I^{(0)}_{lm} - \hat{G}_{lm1}) = \sum_k \Bigg\{ & u^-_{m1k} \left(\sum_l \kappa_{ll'm} V_{lm1k} (-1)^{l+m} \right) \\ & + u^+_{m1k} \left(\sum_l \kappa_{ll'm} V_{lm1k} \right) \vartheta_{1k} \Bigg\} \end{aligned} \tag{2.65}$$

Turning to the calculation of $\kappa_{ll'm}$ note that

$$\begin{aligned} \int_{\Omega_-} Y^m_l(\mathbf{n}) Y^{m'*}_{l'}(\mathbf{n})\, d\omega_{\mathbf{n}} &= \int_{\Omega_+} Y^m_l(-\mathbf{n}) Y^{m'*}_{l'}(-\mathbf{n})\, d\omega_{\mathbf{n}} \\ &= (-1)^{l+m+l'+m'} \int_{\Omega_+} Y^m_l(\mathbf{n}) Y^{m'*}_{l'}(\mathbf{n})\, d\omega_{\mathbf{n}} \end{aligned} \tag{2.66}$$

A number of simplifications may now be made. If $l + l'$ is even, the integrand is even and will have the same value on Ω_+, so extending the integral and applying orthogonality,

$$\kappa_{ll'm} = 1/2\ \delta_{ll'} \tag{2.67}$$

if $l + l'$ is even.

If $l + l'$ is odd, the evaluation of $\kappa_{ll'm}$ is not so trivial. Dave (1974) give results for the case $m = 0$. To derive the more general results required here, it seems easiest to follow the procedure given in Copson for Legendre polynomials and proceed from the basic differential equation. Defining

$$Y^m_l \equiv \Upsilon^m_l e^{im\phi} \equiv \Xi^m_l P^m_l e^{im\phi}, \tag{2.68}$$

it follows that

$$\int_{\Omega_+} Y_l^m Y_{l'}^{m*}\, d\omega_{\mathbf{n}} = 2\pi\, \Xi_l^m \Xi_{l'}^m \int_0^1 P_l^m(x) P_{l'}^m(x)\, dx \tag{2.69}$$

By definition,

$$\frac{d}{dx}\left[(1-x^2)\frac{dP_l^m}{dx}\right] + \left[l(l+1) - \frac{m^2}{1-x^2}\right] P_l^m = 0. \tag{2.70}$$

Multiplying by $P_{l'}^m$, subtracting P_l^m multiplied by the corresponding differential equation for $P_{l'}^m$, and integrating by parts,

$$\begin{aligned}(l-l')(l+l'+1)P_l^m P_{l'}^m = {} & \frac{d}{dx}\left[P_l^m(1-x^2)\frac{dP_{l'}^m}{dx}\right] - (1-x^2)\frac{dP_l^m}{dx}\frac{dP_{l'}^m}{dx} \\ & - \frac{d}{dx}\left[P_{l'}^m(1-x^2)\frac{dP_l^m}{dx}\right] + (1-x^2)\frac{dP_{l'}^m}{dx}\frac{dP_l^m}{dx}.\end{aligned} \tag{2.71}$$

Hence,

$$\int_0^1 P_l^m P_{l'}^m\, dx = \frac{(1-x^2)\left\{P_l^m \frac{dP_{l'}^m}{dx} - P_{l'}^m \frac{dP_l^m}{dx}\right\}\Big|_0^1}{(l-l')(l+l'+1)} \tag{2.72}$$

Only the lower limit gives a contribution. To evalaute this note that when x is small

$$P_l^m(x) \sim \frac{(-1)^{m+l}}{2^l l!}\left[1 - \frac{m}{2}x^2 + \ldots\right] \frac{d^{l+m}}{dx^{l+m}} \sum_{r=0}^{l} \binom{l}{r} (-1)^r x^{2r} \tag{2.73}$$

When $x = 0$ the only contribution arises from the term of the final series with $2r = l + m$, so $l + m$ must be even.

$$\therefore \qquad P_l^m(0) = \frac{(-1)^{\frac{m+l}{2}}}{2^l l!} \frac{(l+m)!}{\left(\frac{l+m}{2}\right)!\left(\frac{l-m}{2}\right)!}. \tag{2.74}$$

Similarly, the only contribution to dP_l^m/dx arises from the term with $2r = l+m+1$, so $l+m$ must be odd.

$$\therefore \qquad \frac{dP_l^m(0)}{dx} = \frac{(-1)^{\frac{m+l-1}{2}}}{2^l l!} \frac{(l+m+1)!}{\left(\frac{l+m+1}{2}\right)!\left(\frac{l-m-1}{2}\right)!}. \tag{2.75}$$

From a numerical point of view, these are easiest to evaluate using recurrences:

$$P_l^m(0) = -\frac{l+m-1}{l-m} P_{l-2}^m(0) \tag{2.76}$$

with $P_m^m(0) = (-1)^m/2^m.(2m)!/m!$ when $l+m$ is even and

$$\frac{dP_l^m(0)}{dx} = -\frac{l+m}{l-m-1} \frac{dP_{l-2}^m(0)}{dx} \tag{2.77}$$

with $P_{m+1}^m(0) = (-1)^m/2^{m+1}.(2(m+1))!/(m+1)!$ when $l+m$ is odd. Finally, it is useful to express these in terms of Υ_l^m to keep terms closer to 1:

$$\Upsilon_l^m(0) = -\sqrt{\frac{(2l+1)}{(2l-3)}.\frac{(l+m-1)}{(l+m)}.\frac{(l-m-1)}{(l-m)}}\, \Upsilon_{l-2}^m(0) \tag{2.78}$$

with $\Upsilon_m^m(0) = (-1)^m/2^m \cdot 1/m! \cdot \sqrt{(2m+1)!/4\pi}$ when $l+m$ is even and

$$\frac{d\Upsilon_l^m(0)}{dx} = -\sqrt{\frac{(2l+1)}{(2l-3)}.\frac{(l-m)}{(l-m-1)}.\frac{(l+m)}{(l+m-1)}}\,\frac{d\Upsilon_{l-2}^m(0)}{dx} \tag{2.79}$$

with $\Upsilon_{m+1}^m(0) = (-1)^m/2^m.1/m!.\sqrt{(2m+3).(2m+1)!/4\pi}$ when $l+m$ is odd.

Finally, therefore,

$$\begin{aligned}\kappa_{ll'm} &= \int_{\Omega_-} Y_l^m(\mathbf{n})Y_{l'}^{m'*}(\mathbf{n})\,d\omega_{\mathbf{n}} = (-1)^{l+l'}\delta_{mm'}\int_{\Omega_+} \Upsilon_l^m(\mathbf{n})\Upsilon_{l'}^m(\mathbf{n})\,d\omega_{\mathbf{n}} \\ &= 2\pi(-1)^{(l+l'+1)}\frac{\Upsilon_l^m(0)d\Upsilon_{l'}^m(0)/dx - \Upsilon_{l'}^m(0)d\Upsilon_l^m(0)/dx}{(l-l')(l+l'+1)}\end{aligned} \tag{2.80}$$

(*Note:* For comparison with the program $\Upsilon_l^m(0) = 0$ if $d\Upsilon_l^m(0)/dx \neq 0$, so only one array is required to hold both quantities. Also, only one term in the numerator of the preceeding equation can be non-zero.)

2.2 Boundary Conditions at the Surface

To define the surface characteristics we must use a bidirectional reflectance, function γ_r, so that the reflected ray in the direction $\mathbf{n} \in \Omega_+$, is given by

$$I(\mathbf{n}) = \int_{\Omega_-} \gamma_r(\mathbf{n},\mathbf{n}')I(\mathbf{n}')(\mathbf{n}'.-\mathbf{e}_z)\,d\omega_{\mathbf{n}'} \tag{2.81}$$

where the geometrical factor $\mathbf{n}'.-\mathbf{e}_z$ accounts for the projected area of the horizontal surface seen by the incident beam. In the case of a Lambertian surface γ_r is a constant and may be related to the albedo of the surface by $\gamma_r = \alpha/\pi$, which follows directly from the definition. (For scattering into finite solid angles a biconical reflectance is defined as

$$R(\mathbf{n},\mathbf{n}') = \frac{\int_{\Omega_r}\int_{\Omega_i} \gamma_r(\mathbf{n},\mathbf{n}')I(\mathbf{n}')(\mathbf{n}'.-\mathbf{e}_z)(\mathbf{n}.\mathbf{e}_z)\,d\omega_{\mathbf{n}'}d\omega_{\mathbf{n}}}{\int_{\Omega_r}\int_{\Omega_i} \frac{1}{\pi}I(\mathbf{n}')(\mathbf{n}'.-\mathbf{e}_z)(\mathbf{n}.\mathbf{e}_z)\,d\omega_{\mathbf{n}'}d\omega_{\mathbf{n}}} \tag{2.82}$$

where the factor of $1/\pi$ in the denominator represents the BRDF of a white Lambertian surface.)

For use in a spherical harmonic procdure, the BRDF may be expanded in a double spherical harmonic series:

$$\gamma_r(\mathbf{n},\mathbf{n}') = \sum_{l,m}\sum_{l',m'} \Gamma_{lml'm'}Y_l^m(\mathbf{n})Y_{l'}^{m'*}(\mathbf{n}') \tag{2.83}$$

where the use of complex conjugates in the second sum is for convenience. Various constraints on the coefficients $\Gamma_{lml'm'}$ must be imposed, limiting the number of free coefficients. Firstly,

$\gamma_r \in \mathbb{R}$ so

$$\begin{aligned}\sum_{l,m}\sum_{l',m'}\Gamma_{lml'm'}Y_l^m(\mathbf{n})Y_{l'}^{m'*}(\mathbf{n}') &= \sum_{l,m}\sum_{l',m'}\Gamma^*_{lml'm'}Y_l^{m*}(\mathbf{n})Y_{l'}^{m'}(\mathbf{n}')\\ &= \sum_{l,m}\sum_{l',m'}\Gamma^*_{lml'm'}(-1)^m Y_l^{-m}(\mathbf{n})(-1)^{m'}Y_{l'}^{-m'*}(\mathbf{n}')\\ &= \sum_{l,m}\sum_{l',m'}\Gamma^*_{l,-m,l',-m'}(-1)^{(m+m')}Y_l^m(\mathbf{n})Y_{l'}^{m'*}(\mathbf{n}')\end{aligned}\tag{2.84}$$

Hence,

$$\Gamma_{l,-m,l',-m'} = (-1)^{(m+m')}\Gamma^*_{lml'm'}.\tag{2.85}$$

Helmholtz's principal of reciprocity imposes a requirement that

$$\gamma_r(\mathbf{n},\mathbf{n}') = \gamma_r(\mathbf{n}',\mathbf{n});\tag{2.86}$$

hence,

$$\begin{aligned}\sum_{l,m}\sum_{l',m'}\Gamma_{lml'm'}Y_l^m(\mathbf{n})Y_{l'}^{m'*}(\mathbf{n}') &= \sum_{l,m}\sum_{l',m'}\Gamma_{lml'm'}Y_l^m(\mathbf{n}')Y_{l'}^{m'*}(\mathbf{n})\\ &= \sum_{l',m'}\sum_{l,m}\Gamma_{l'm'lm}Y_{l'}^{m'}(\mathbf{n}')Y_l^{m*}(\mathbf{n})\\ &= \sum_{l',m'}\sum_{l,m}\Gamma_{l'm'lm}(-1)^{(m+m')}Y_l^{-m}(\mathbf{n})Y_{l'}^{-m'*}(\mathbf{n}')\\ &= \sum_{l',m'}\sum_{l,m}\Gamma_{l',-m',l,-m}(-1)^{(m+m')}Y_l^m(\mathbf{n})Y_{l'}^{m'*}(\mathbf{n}')\end{aligned}\tag{2.87}$$

whence,

$$\Gamma_{l',-m,l,-m'} = (-1)^{(m+m')}\Gamma_{lml'm'}.\tag{2.88}$$

In addition to these general properties we impose the specific constraints of rotational and reflectional symmetry:

$$\gamma_r(\mathcal{R}(\mathbf{n}),\mathcal{R}(\mathbf{n}')) = \gamma_r(\mathbf{n}',\mathbf{n})\tag{2.89}$$

and

$$\gamma_r(\mathcal{I}(\mathbf{n}),\mathcal{I}(\mathbf{n}')) = \gamma_r(\mathbf{n}',\mathbf{n})\tag{2.90}$$

$$\tag{2.91}$$

for any rotation $\mathcal{R}$ about a vertical axis and any inversion $\mathcal{I}$ in a vertical plane. Since

$$Y_l^m(\mathcal{R}(\mathbf{n})) = e^{im\phi_{\mathcal{R}}}Y_l^m(\mathbf{n}),\tag{2.92}$$

we have,

$$\begin{aligned}\gamma_r(\mathcal{R}(\mathbf{n}),\mathcal{R}(\mathbf{n}')) &= \sum_{l,m}\sum_{l',m'}\Gamma_{lml'm'}Y_l^m(\mathcal{R}(\mathbf{n}))Y_{l'}^{m'*}(\mathcal{R}(\mathbf{n}'))\\ &= \sum_{l,m}\sum_{l',m'}\Gamma_{lml'm'}e^{im\phi_{\mathcal{R}}}Y_l^m(\mathbf{n})e^{-im'\phi_{\mathcal{R}}}Y_{l'}^{m'*}(\mathbf{n})\\ &= \sum_{l,m}\sum_{l',m'}\Gamma_{lml'm'}Y_l^m(\mathbf{n})Y_l^{m*}(\mathbf{n}')\end{aligned}\tag{2.93}$$

which can be true only if

$$\Gamma_{lml'm'} = \Psi_{ll'm}\delta_{mm'} \tag{2.94}$$

for suitable Ψ. Now, to impose reflectional symmetry, it suffices to consider inversion in the plane $\phi = 0$:

$$\begin{aligned} \gamma_r(\mathcal{I}(\mathbf{n}), \mathcal{I}(\mathbf{n}')) &= \sum_{l,m}\sum_{l',m'} \Gamma_{lml'm'} Y_l^m(\mathcal{I}(\mathbf{n})) Y_{l'}^{m'*}(\mathcal{I}(\mathbf{n}')) \\ &= \sum_{l,m}\sum_{l',m'} \Gamma_{lml'm'} Y_l^{m*}(\mathbf{n}) Y_{l'}^{m'}(\mathbf{n}') \\ &= \sum_{l,m}\sum_{l',m'} \Gamma_{l,-m,l',-m'} (-1)^{(m+m')} Y_l^m(\mathbf{n}) Y_{l'}^{m'*}(\mathbf{n}') \end{aligned} \tag{2.95}$$

from which it follows that

$$\Gamma_{l,-m,l',-m'} = (-1)^{(m+m')}\Gamma_{lml'm'}. \tag{2.96}$$

Together with the condition the imposed by $\gamma_r \in \mathbb{R}$, this shows that $\Gamma_{lml'm'} \in \mathbb{R}$.

Collecting these results, we find that

$$\Psi_{ll'm} \in \mathbb{R}; \tag{2.97}$$

$$\Psi_{l'lm} = \Psi_{ll'm} \tag{2.98}$$

and

$$\Psi_{ll'-m} = \Psi_{ll'm} \tag{2.99}$$

Since the BRDF is defined only for $\mathbf{n} \in \Omega_+$ and $\mathbf{n}' \in \Omega_-$ the $\Psi ll'm$ are not uniquely defined. We can, hwoever, coplete the specification by demanding that $\Psi_{ll'm} = 0$ if $l = m$ or $l' + m$ is odd. This is the natural choice since a Lambertian surface is then characterized by one value of Ψ: namely that with $l = l' = m = 0$.

2.2.1 The Relation between the BRDF and the Albedo

In some instances it is useful to know the relationship between the BRDF and the albedo for isotropic incident radiation. This may be derived as follows.

$$\begin{aligned} \alpha_i &= \frac{1}{\pi}\int_{\Omega_+}\int_{\Omega_-} \gamma(\mathbf{n}', \mathbf{n})(-\mathbf{n}'.\hat{\mathbf{e}}_z)(\mathbf{n}.\hat{\mathbf{e}}_z)\, d\omega\mathbf{n}\, d\omega\mathbf{n}' \\ &= \frac{1}{\pi}\sum_{ll'm} \Psi_{ll'm} \int_{\Omega_+}\int_{\Omega_-} Y_{l'}^m(\mathbf{n}') Y_l^m(\mathbf{n})(-\mathbf{n}'.\hat{\mathbf{e}}_z)(\mathbf{n}.\hat{\mathbf{e}}_z)\, d\omega\mathbf{n}'\, d\omega\mathbf{n} \\ &= \frac{1}{\pi}\sum_{ll'm} \Psi_{ll'm} \int_{\Omega_+} Y_l^m(\mathbf{n})(\mathbf{n}.\hat{\mathbf{e}}_z)\, d\omega\mathbf{n}.(-1) \int_{\Omega_-} Y_{l'}^m(\mathbf{n}')(\mathbf{n}'.\hat{\mathbf{e}}_z)\, d\omega\mathbf{n}' \\ &= \frac{1}{\pi}\sum_{ll'm} \Psi_{ll'm}(-1)^{l+m} \int_{\Omega_+} Y_l^m(\mathbf{n})\sqrt{\frac{4\pi}{3}}Y_1^0(\mathbf{n})\, d\omega\mathbf{n} \int_{\Omega_-} Y_{l'}^m(\mathbf{n}')\sqrt{\frac{4\pi}{3}}Y_1^0(\mathbf{n}')\, d\omega\mathbf{n}' \\ &= \frac{4}{3}\sum_{ll'}(-1)^l \Psi_{ll'}\kappa_{l10}\kappa_{l'10}. \end{aligned} \tag{2.100}$$

2.2.2 Specification of Real BRDFs

Various analytic expressions for BRDFs have been proposed. These typically represnt a blend of physical reasoning and fitting to experimental data. An example is provided by Roujean et al. [1992] who considers the effect of geometric irregularities on the surface which produce shadowing effects and of radiative transfer in the medium below the surface which is treated by solving the equation of transfer with a highly truncated phase function. The model gives a BRDF of the form

$$\gamma_r(\theta_s, \theta_v, \phi) = k_0 + k_1 f_1(\theta_s, \theta_v, \phi) + k_2 f_2(\theta_s, \theta_v, \phi) \tag{2.101}$$

where $k_0, \ldots k_2$ are fitted constants, f_1 and f_2 are prescribed functions and θ_s and θ_v are the polar angle of incident radiation and the viewing angle. f_1 and f_2 have the following forms:

$$\begin{aligned} f_1(\theta_s, \theta_v, \phi) = \frac{1}{2\pi}\left[(\pi - \phi)\cos\phi + \sin\phi\right]\tan\theta_s \tan\theta_v - \frac{1}{\pi}\Big(\tan\theta_s \\ + \tan\theta_v + \sqrt{\{\tan^2\theta_s + \tan^2\theta_v - 2\tan\theta_s\tan\theta_v\cos\phi\}}\Big). \end{aligned} \tag{2.102}$$

and

$$f_2(\theta_s, \theta_v, \phi) = \frac{3}{4\pi}\frac{1}{\cos\theta_s + \cos\theta_v}\left[\left(\frac{\pi}{2} - \xi\right)\cos\xi + \sin\xi\right] - \frac{1}{3} \tag{2.103}$$

where

$$\cos\xi = \cos\theta_s\cos\theta_v + \sin\theta_s\sin\theta_v\cos\phi \tag{2.104}$$

Legendre expansions for f_1 and f_2 can be precalculated, so this model is fairly easy to implement: Roujean *et al.*'s paper gives coefficients for some land surfaces. This has a convenient functional form consisting of a linear combination of angularly dependent functions. To simplify the treatment of the surface it will be assumed that the BRDF may be expanded in the form

$$\gamma_r(\mathbf{n}, \mathbf{n}') = \sum_j \rho_j f_j(\mathbf{n}, \mathbf{n}') \tag{2.105}$$

where the ρ_j are functions of the surface type and the functions f_j (not necessarily equal to those above are known). It is then possible to precalculate the expansion of each f_j in spherical harmonics:

$$f_j(\mathbf{n}, \mathbf{n}') = \sum_{ll'm} F_{jll'm} Y_l^m(\mathbf{n}) Y_{l'}^{m*}(\mathbf{n}') \tag{2.106}$$

so that

$$\Psi_{ll'm} = \sum_j \rho_j F_{jll'm}. \tag{2.107}$$

2.2.3 The Optical Properties of the Ocean Surface

Perhaps frustratingly, there is apparently no directly applicable reference which provides a BRDF of the ocean surface. To provide such an entity the radiance code itself can be used to calculate the radiatiance in the ocean, with special upper boundary conditions to deal with refraction at the surface. In order to implement such a capability the optical properties of the ocean must be specified; these are greatly influenced by particulate matter – indeed, this is the basis of ocean colour sensing – and very considerable variations occur. An extremely useful review of this field is provided by Mobley [1994]: a very brief discussion of ocean optics for use in the present version of the code, based on this book, is now presented.

The Optical Properties of Oceanic Waters

Rayleigh scattering occurs in the oceans just as it does in the atmosphere and is described by a phase function

$$P_w(\theta) = \frac{3}{4\pi(3+p)}(1 + p\cos^2\theta) \tag{2.108}$$

where p is the polarization factor, which is taken as 0.835. The scattering coefficient (m^{-1}) has the wavelength dependence

$$k_w^{(s)}(\lambda) = K_R(\lambda_0/\lambda)^{4.32} \tag{2.109}$$

where $\lambda_0 = 550\mathrm{nm}$ and $K_R = 0.93$ for pure water and $K_R = 1.21$ for sea water. The dependence on wavelength is steeper than λ^{-4} because of the effect of dissolved ions on the refractive index. (Note: the values given in Table 3.8 of Mobley [1994] do not exactly follow this realationship, which is presumably only applicable locally in frequency space).

Scattering by particulate matter is much more important than Rayleigh scattering in almost all waters. Petzold [1972] has investigated the phase function in various waters: to some extent, particulate scattering can be represented by a Henyey-Greenstein phase function with an asymmetry factor of 0.924, though this does not capture the full forward peak. The scattering coefficient (m^{-1}) of particulates is often related to the concentration of chlorophyll, C (mgm^{-3}) using the fitted formula:

$$k_P^{(s)} = \left(\frac{550}{\lambda[\mathrm{nm}]}\right) 0.3C^{0.62} \tag{2.110}$$

In the UM oceanic waters are assumed to be of type IB in Jerlov's classification for radiative purposes; it would seem sensible to assume the same here and thus to take $C \approx 0.1$ mgm^{-3}.

Absorption by oceanic waters is complicated by the presence of various dissolved organic compounds which can give the water a yellow tinge and are therefore often referred to as *yellow matter*. By making the questionable assumption the concentration of yellow matter is correlated with that of phytoplankton Prieur and Sathyendranath [1981] produced an expression for the absorption coefficient (m^{-1}) of oceanic water that was simplified by Morel [1991] to give

$$k^{(a)} = \left(k_w^{(a)}(\lambda) + 0.66a_c^{*\prime}(\lambda)C^{0.65}\right)\left[1 + 0.2\exp(-0.014(\lambda[\mathrm{nm}] - 440))\right]. \tag{2.111}$$

Here, $k_w^{(a)}$ is the absorption coefficient of pure water and $a_c^{*\prime}$ is the dimensionless absorption coefficient of chlorophyll.

Conditions at the Oceanic Surface

A discussion of conditions at the oceanic surface is presented by Mobley [1994] who discusses level surfaces and also explains how waves can be treated. The influence of waves on the BRDF is not negligible, but we do not currently include a representation of waves in the specification of the albedo in the UM and inclusion of such effects is by no means simple. Moreover, most current published work on reflection from the ocean surface (Morel and Gentili [1993], Morel et al. [1995] and Yang and Gordon [1997]) does not include such effects.

Transfer across the surface into the ocean is governed by Snell's Law:

$$\sin\theta_i = n\sin\theta_t \tag{2.112}$$

where n is the real part of the refractive index and is quite close to 1.34 for oceanic waters at frequencies of interest. For unpolarized light Fresnel's formulae may be combined to give an overall reflection coefficient:

$$r_{aw} = \frac{1}{2}\left\{\left[\frac{\sin(\theta_i-\theta_t)}{\sin(\theta_i+\theta_t)}\right]^2 + \left[\frac{\tan(\theta_i-\theta_t)}{\tan(\theta_i+\theta_t)}\right]^2\right\}. \tag{2.113}$$

The radiance of the transmitted ray is then obtained from the fundamental theorem of radiometry as

$$I_t = n^2(1-r)I_i. \tag{2.114}$$

For rays travelling upward in the ocean similar considerations apply, but with n replaced by $1/n$. Principally, however, we are concerned with the reflection coefficient in the water r_{wa}: for glancing incidence total internal reflection occurs and $r_{wa}=1$, but generally it is given by Fresnal's formula. The appropriate boundary condition is

$$I(\mathbf{n}) = r_{wa}I(\mathbf{n}_r) + (1-r_{aw})n^2 I_a(\mathbf{n}_a), \qquad \mathbf{n}\in\Omega_-. \tag{2.115}$$

where $\mathbf{n}_r$ is the direction which is reflected to $\mathbf{n}$ in the water and $\mathbf{n}_a$ is the direction in the air which is refrected to $\mathbf{n}$. For the purposes of determining a BRDF, we need consider only

$$I_a(\mathbf{n}) = \delta(\mathbf{n}-\mathbf{n}_0). \tag{2.116}$$

The effect of reflection is to cahnge the polar angle θ to $\pi-\theta$, so since

$$I = \sum_{lm} I_{lm}Y_l^m(\mathbf{n}), \tag{2.117}$$

we have

$$I(\mathbf{n}_r) = \sum_{lm} I_{lm}Y_l^m(\mathbf{n}_r) = \sum_{lm} I_{lm}(-1)^{l+m}Y_l^m(\mathbf{n}) \tag{2.118}$$

Fresnel's coefficient r_{wa} is axially symmetric so it may be written as

$$r_{wa} = \sum_{\lambda}\rho_\lambda Y_\lambda^0(\mathbf{n}). \tag{2.119}$$

Since the boundary condition applies only on Ω_-, we must apply Marshak's procedure and form the inner product with Y_L^M for those spherical harmonics with odd parity. This leads to the condition

$$\sum_l \kappa_{LlM}I_{lM} = \sum_{l\lambda} r_\lambda I_{lM}C^{LM}_{lM\lambda0} + \left[1-r_{aw}(\mathbf{n}_0)\right]n^2 Y_L^{M*}(\mathbf{n}_0'). \tag{2.120}$$

where $\mathbf{n}_0'$ is the direction into which $\mathbf{n}$ is refracted on entering the ocean and $C^{LM}_{lM\lambda0}$ is the Clebsch-Gordan coefficient. Note here the general expression for the Clebsch-Gordan coefficient (Brink and Satchler [1968])

$$\begin{aligned} C^{c\gamma}_{a\alpha b\beta} &= \delta(\alpha+\beta,\gamma)\Delta(a,b,c) \\ &\quad\times\left[(2c+1)(a+\alpha)!(a-\alpha)!(b+\beta)!(b-\beta)!(c+\gamma)!(c-\gamma)!\right]^{1/2} \\ &\quad\times\sum_\nu(-1)^\nu\big[(a-\alpha-\nu)!(c-b+\alpha+\nu)!(b+\beta-\nu)! \\ &\qquad\qquad(c-a-\beta+\nu)!\nu!(a+b-c-\nu)!\big]^{-1} \end{aligned} \tag{2.121}$$

where the sum is taken over values of ν which lead to non-negative factorials and

$$\Delta(a,b,c) = \left[\frac{(a+b-c)!(b+c-a)!(c+a-b)!}{(a+b+c+1)!}\right]^{1/2} \tag{2.122}$$

2.2.4 Implementation of BRDFs

Including the source term of the surface the condition to be applied is

$$I(\mathbf{n}) = \int_{\Omega_-} \gamma_r(\mathbf{n},\mathbf{n}')(I(\mathbf{n}') + I_\odot\delta(\mathbf{n}'-\mathbf{n}_\odot) - B_*)(\mathbf{n}'.{-\mathbf{e}_z})\, d\omega_{\mathbf{n}'} + B_* \tag{2.123}$$

for $\mathbf{n} \in \Omega_+$. Here, B_* is the isotropic Planckian radiance that is emitted by a blackbody at the surface temperature. The form of the surface emission term is a direct consequence of Kirchoff's law.

Expanding this equation in spherical harmonics,

$$\begin{aligned}\sum_{lm} I_{lm}Y_l^m(\mathbf{n}) = \int_{\Omega_-} &\sum_{lm}\sum_{l'm'} \Gamma_{lml'm'}Y_l^m(\mathbf{n})Y_{l'}^{m'*}(\mathbf{n}')(\mathbf{n}'.{-\mathbf{e}_z}) \\ &\left[I_\odot\delta(\mathbf{n}'-\mathbf{n}_\odot) + \sum_{\lambda\mu} I_{\lambda\mu}Y_\lambda^\mu(\mathbf{n}') - B_*\right] d\omega_{\mathbf{n}'} + B_*\end{aligned} \tag{2.124}$$

As this covers only the upper hemisphere Marshak's procedure should be applied, so inner products with $\int_{\Omega_+} Y_L^{M*} \dots d\omega_{\mathbf{n}}$ are formed. It is easiest to consider each term separately, so noting the symmetries of $\kappa_{ll'm}$ as defined above,

$$\int_{\Omega_+} Y_L^{M*}(\mathbf{n}) \sum_{lm} I_{lm}Y_l^m(\mathbf{n})\, d\omega_{\mathbf{n}} = \sum_l I_{lM}(-1)^{L+l}\kappa_{LlM} \tag{2.125}$$

For the solar term,

$$\begin{aligned}&\int_{\Omega_+} Y_L^{M*}(\mathbf{n}) \int_{\Omega_-} \sum_{lm}\sum_{l'm'} \Gamma_{lml'm'}Y_l^m(\mathbf{n})Y_{l'}^{m'*}(\mathbf{n}')(-\mathbf{n}'.\mathbf{e}_z)\, I_\odot\delta(\mathbf{n}'-\mathbf{n}_\odot)\, d\omega_{\mathbf{n}'}\, d\omega_{\mathbf{n}} \\ &\qquad = I_\odot(-\mathbf{n}_\odot.\mathbf{e}_z)\sum_{lm}\sum_{l'm'}\Gamma_{lml'm'}Y_{l'}^{m'*}(\mathbf{n}_\odot)\int_{\Omega_+} Y_L^{M*}(\mathbf{n})Y_l^m(\mathbf{n})\, d\omega_{\mathbf{n}} \\ &\qquad = I_\odot\mu_\odot \sum_l\sum_{l'} Y_{l'}^{m'*}(\mathbf{n}_\odot)\Psi_{ll'M}(-1)^{L+l}\kappa_{LlM}.\end{aligned} \tag{2.126}$$

For reflected diffuse radiation

$$\begin{aligned}
&\int_{\Omega_+} Y_L^{M*}(\mathbf{n}) \int_{\Omega_-} \sum_{lm}\sum_{l'm'} \Gamma_{lml'm'} Y_l^m(\mathbf{n}) Y_{l'}^{m'*}(\mathbf{n}')(-\mathbf{n}'.\mathbf{e}_z) \sum_{\lambda\mu} I_{\lambda\mu} Y_\lambda^\mu(\mathbf{n}')\, d\omega_{\mathbf{n}'}\, d\omega_{\mathbf{n}} \\
&\quad = \sum_{lm}\sum_{l'm'}\sum_{\lambda\mu} \Gamma_{lml'm'} I_{\lambda\mu} \cdot \int_{\Omega_+} Y_L^{M*}(\mathbf{n}) Y_l^m(\mathbf{n})\, d\omega_{\mathbf{n}} \\
&\quad \cdot \int_{\Omega_-} (-\mathbf{n}'.\mathbf{e}_z) Y_{l'}^{m'*}(\mathbf{n}') Y_\lambda^\mu(\mathbf{n}')\, d\omega_{\mathbf{n}'} \\
&\quad = \sum_{l}\sum_{l'}\sum_{\lambda} \Psi_{ll'M} I_{\lambda M} (-1)^{L+l} \kappa_{LlM} \\
&\quad \cdot \int_{\Omega_-} Y_\lambda^M(\mathbf{n}')(-1) \left[c^+_{l'M} Y^{M*}_{l'+1}(\mathbf{n}') + c^-_{l'M} Y^{M*}_{l'-1}(\mathbf{n}')\right] d\omega_{\mathbf{n}'} \\
&\quad = \sum_{\lambda} I_{\lambda M} \sum_{l}\sum_{l'} \Psi_{ll'M} (-1)^{L+l+1} \kappa_{LlM} \left[c^+_{l'M}\kappa_{l'+1,\lambda,M} + c^-_{l'M}\kappa_{l'-1,\lambda,M}\right].
\end{aligned} \tag{2.127}$$

For the Planckian term coupled to the BRDF,

$$\begin{aligned}
&\int_{\Omega_+} Y_L^{M*}(\mathbf{n}) \int_{\Omega_-} \sum_{lm}\sum_{l'm'} \Gamma_{lml'm'} Y_l^m(\mathbf{n}) Y_{l'}^{m'*}(\mathbf{n}')(-\mathbf{n}'.\mathbf{e}_z) B_*\, d\omega_{\mathbf{n}'}\, d\omega_{\mathbf{n}} \\
&\quad = B_* \sum_{lm}\sum_{l'm'} \Gamma_{lml'm'} \cdot \int_{\Omega_+} Y_L^{M*}(\mathbf{n}) Y_l^m(\mathbf{n})\, d\omega_{\mathbf{n}} \cdot \\
&\sqrt{\frac{4\pi}{3}} \int_{\Omega_-} -Y_1^0(\mathbf{n}') Y_{l'}^{m'*}(\mathbf{n}')\, d\omega_{\mathbf{n}'} \\
&\quad = \sqrt{\frac{4\pi}{3}} B_* \sum_{l}\sum_{l'} \Psi_{ll'M} (-1)^{L+l+1} \kappa_{LlM} \kappa_{l'10} \delta_{M0}.
\end{aligned} \tag{2.128}$$

Finally, the black-body term gives

$$\int_{\Omega_+} Y_L^{M*}(\mathbf{n}) B_*\, d\omega_{\mathbf{n}} = \sqrt{4\pi} B_* \kappa_{L00} \delta_{0M} (-1)^L. \tag{2.129}$$

Now note that $c^-_{l,m} = c^+_{l-1,m}$, that $\Psi_{ll'm} = \sum_j \rho_j F_{jll'm}$, and that each term contains a factor of $(-1)^L$, which may be cancelled, so collecting terms,

$$\begin{aligned}
&\sum_{\lambda} I_{\lambda M} \Bigg\{ (-1)^{\lambda} \kappa_{L\lambda M} + \sum_j \rho_j \sum_l \sum_{l'} (-1)^l F_{jll'M} \kappa_{LlM} \\
&\quad \cdot \left[c^+_{l',M} \kappa_{l'+1,\lambda,M} + c^+_{l'-1,M} \kappa_{l'-1,\lambda,M} \right] \Bigg\} \\
&\quad = I_\odot \mu_\odot \sum_j \rho_j \sum_{l'} Y_L^{M*}(\mathbf{n}_\odot) \left[\sum_l (-1)^l \kappa_{LlM} F_{jll'M} \right] \\
&\quad = B_* \delta_{0M} \left[\sqrt{4\pi} \kappa_{L00} + \sqrt{\frac{4\pi}{3}} \sum_j \rho_j \sum_{l'} \kappa_{l'10} \sum_l (-1)^l \kappa_{LlM} F_{jll'M} \right].
\end{aligned} \tag{2.130}$$

We define,

$$\Xi_{jLl'M} = \sum_{l} (-1)^{l} \kappa_{LlM} F_{jll'M} \tag{2.131}$$

$$\Phi_{jL\lambda M} = \sum_{l'} \Xi_{jLl'M} \left[c^{+}_{l',M} \kappa_{l'+1,\lambda,M} + c^{+}_{l'-1,M} \kappa_{l'-1,\lambda,M} \right] \tag{2.132}$$

and

$$\tag{2.133}$$

$$\Lambda_{jL} = \sqrt{\frac{4\pi}{3}} \sum_{l'} \kappa_{l'10} \Xi_{jLl'0}. \tag{2.134}$$

Hence,

$$\begin{aligned} \sum_{l} I_{lM} \left\{ (-1)^{l} \kappa_{LlM} + \sum_{j} \rho_j \Phi_{jLlM} \right\} &= I_{\odot} \mu_{\odot} \sum_{j} \rho_j \sum_{l'} Y^{M*}_{l'}(\mathbf{n}_{\odot}) \Xi_{jLl'M} \\ &+ B_{*} \delta_{0M} \left\{ \sqrt{4\pi} \kappa_{L00} + \sum_{j} \rho_j \Lambda_{jL} \right\} \end{aligned} \tag{2.135}$$

When multiple calculations are performed within the same band (so that the constants ρ_j remain fixed) it is useful to simplify a little further by writing the equation as

$$\sum_{l} I_{lM} M^{(1)}_{LlM} = I_{\odot} M^{(2)}_{LM} + B_{*} \delta_{0M} M^{(3)}_{L} \tag{2.136}$$

where $M^{(1,2,3)}$ are defined by the obvious identifications.

Now, the components of the spherical harmonics at the bottom of the lowest layer will be given by

$$I_{Nlm}(\tau_N) = \sum_{k} \left\{ u^{-}_{mNk} (-1)^{l+m} V_{lmNk} \vartheta_{Nk} + u^{+}_{mNk} V_{lmNk} \right\} + \check{G}_{lmN} \tag{2.137}$$

Substituting into the boundary condition and replacing M by m and L by l' to match the normal notation used at the top boundary,

$$\begin{aligned} \sum_{k} u^{-}_{mNk} \left[\vartheta_{Nk} \sum_{l} M^{(1)}_{l'lm} (-1)^{(l+m)} V_{lmNk} \right] + u^{+}_{mNk} \left[\sum_{l} M^{(1)}_{l'lm} V_{lmNk} \right] \\ = I_{\odot} M^{(2)}_{l'm} + B_{*} \delta_{0m} M^{(3)}_{l'} - \sum_{l} M^{(1)}_{l'lm} \check{G}_{lmN} \end{aligned} \tag{2.138}$$

2.3 Numerical Implementation

In principle, the coefficients I_{lm} must be calculated for the range $0 \le l \le L$ and $-l \le m \le l$; moreover, these coefficients are complex. In practice, the storage required can be reduced by making use of the various symmetries of the coefficients.

First note that $I \in \mathbb{R}$, so that $I = I^*$ and

$$\sum I_{lm} Y_l^m = \sum I_{lm}^* Y_l^{m*} = \sum I_{lm}^* (-1)^m Y_l^{-m} = \sum I_{l,-m}^* (-1)^{-m} Y_l^m \tag{2.139}$$

whence

$$I_{l,-m} = (-1)^m I_{lm}^*, \tag{2.140}$$

so coefficients with $m < 0$ may be found by symmetry.

The complex nature of Y_l^m appears only through the factor $e^{im\phi}$, so we may define $Y_l^m = \Upsilon_l^m e^{im\phi}$ where $\Upsilon_l^m \in \mathbb{R}$. With the restrictions imposed on the BRDF above which forbid the coupling of harmonics with different azimuthal orders, the complex nature of I_{lm} appears only through a factor $e^{-im\phi_\odot}$, so we write $I_{lm} = C_{lm} e^{-im\phi_\odot}$ (in the case of IR radiation where the radiance is azimuthally symmetric the value of $\phi_\odot$ is immaterial). Hence, if $m > 0$

$$\begin{aligned} I_{lm} Y_l^m + I_{l,-m} Y_l^{-m} &= C_{lm} e^{-im\phi_\odot} \Upsilon_l^m e^{im\phi} \\ &\quad + (-1)^m C_{lm} e^{im\phi_\odot} \Upsilon_l^m (-1)^m e^{-im\phi} \\ &= 2 C_{lm} \Upsilon_l^m \cos m(\phi - \phi_\odot) \end{aligned} \tag{2.141}$$

2.4 Increasing the Speed of Computation

So far, we have described the method of calculating the amplitudes of the spherical harmonics. This is perfectly adequate to calculate fluxes, but it converges very slowly when calculating radiances. The source function technique, due originally to Kourganoff (1955), can be used to circumvent this problem. In this technique, the radiance is calculated by integrating along a ray, using the direct solution by spherical harmonics to represent the scattered radiation (the term in the equation of transfer involving an integral over the phase function): this can be looked upon as a kind of iterated solution of the problem. This technique has many points in common with a technique for reducing the number of harmonics required to obtain a given accuracy, as described next.

When the equation of transfer is solved using spherical harmonics, a high order of truncation may be required to represent the radiance field. These higher orders are principally required to represent singly scattered radiation; but singly scattered radiances can be calculated more simply than the multiply scattered radiances, so it is sensible to examine ways of separating the singly scattered component of the radiance so that a rather lower order of truncation can be used to calculate the multiply scattered radiances. Nakajima and Tanaka [1988] have considered various approximations of this form, particularly for the case of optically thin layers. They eventually derived a method they refer to as IMS, but this is insufficiently general for optically thick layers because it exhibits an instability, and is therefore inappropriate for use in a code that will be used in a GCM. We will therefore adopt the method which they refer to as TMS, which performs almost as well as IMS except very close to the forward direction. They present only a very sketchy derivation of the method and no justification, so it is useful to derive it more fulsomely here. The idea is to retain the full phase function in the calculation of single scattering, but to use the rescaled truncated phase function for multiple scattering. In this section we shall use the caret to denote rescaled quantities. Under rescaling the phase function is rewritten as

$$P(\mathbf{n}', \mathbf{n}) = 4\pi f \delta(\mathbf{n}' - \mathbf{n}) + (1 - f) \hat{P}(\mathbf{n}', \mathbf{n}) \tag{2.142}$$

Splitting the diffuse and direct beams as usual we obtain the following equation for the diffuse radiance, I,

$$\begin{aligned}(\mathbf{n}.\nabla)I(\mathbf{n}) &= -(k^{(s)}+k^{(a)})I(\mathbf{n}) \\ &+ \frac{k^{(s)}}{4\pi}\int_\Omega I(\mathbf{n}')\left(4\pi f\delta(\mathbf{n}'-\mathbf{n})+(1-f)\hat{P}(\mathbf{n}',\mathbf{n})\right)d\omega_{\mathbf{n}'} \\ &+ \frac{k^{(s)}}{4\pi}\int_\Omega I_\odot(\mathbf{n}')P(\mathbf{n}',\mathbf{n})\,d\omega_{\mathbf{n}'}\end{aligned} \tag{2.143}$$

Notice here that $I_\odot$ refers to the true solar beam, calculated without rescaling, since we have not used a rescaled phase function for single scattering. Writing this equation in terms of the rescaled optical propeties we have

$$\mu\frac{dI}{d\hat{\tau}} = I - \frac{\hat{\omega}}{4\pi}\int_\Omega I\hat{P}\,d\omega'_{\mathbf{n}} - \frac{\hat{\omega}}{4\pi(1-f)}\int_\Omega I_\odot P\,d\omega'_{\mathbf{n}} \tag{2.144}$$

To obtain the exact approximation of Nakajima and Tanaka [1988] we replace$I$ in the first integral with $\hat{I}_T$, the truncated diffuse radiance and $\hat{P}$ with $\hat{P}_T$, the truncated rescaled phase function.

This sits very easily with the method of solution for radiances originally suggested by Kourganoff (1955), in which we regard the spherical harmonic solution as defining the source function for the diffuse radiation in the above equation, but it is actually more convenient to proceed very slightly differently from Nakajima and Tanaka [1988]. To be precise, we first solve the truncated rescaled equation using spherical harmonics to get a rescaled truncated diffuse radiance, $\hat{I}_T$, and a rescaled direct radiance, $\hat{I}_\odot$. Our first approximation to the true (unrescaled) diffuse radiance is thus

$$\tilde{I} = \hat{I}_T + \hat{I}_\odot - I_\odot, \tag{2.145}$$

allowing for the change in the definition of the direct beam when switching from rescaled to unrescaled radiances. Now, it is necessary to be very careful in the treatment of the direct terms: errors may arise either in the form of δ-functions in the solar direction, or as diffused errors at other angles. These fast methods are not accurate close to the solar direction, so in practice it turns out to be better to drop the contribution to the diffuse radiance from the change in the definition of the solar beam, which concentrates errors around the solar peak, rather than concentrating some there and diffusing others, so we take just $\hat{I}_T$ as the diffuse radiance.

Substituting this into the second term of the above equation we get

$$\mu\frac{dI}{d\hat{\tau}} = I - \frac{\hat{\omega}}{4\pi}\int_\Omega \hat{I}_T\hat{P}\,d\omega'_{\mathbf{n}} - \frac{\hat{\omega}}{4\pi}\int_\Omega I_\odot\frac{P}{(1-f)}\,d\omega'_{\mathbf{n}} \tag{2.146}$$

$\hat{I}_T$ involves only harmonics up to the order of $\hat{P}_T$, so we may use the truncated phase function when multiplying it, hence

$$\mu\frac{dI}{d\hat{\tau}} = I - \frac{\hat{\omega}}{4\pi}\int_\Omega \hat{I}_T\hat{P}_T\,d\omega'_{\mathbf{n}} - \frac{\hat{\omega}}{4\pi(1-f)}\int_\Omega I_\odot P\,d\omega'_{\mathbf{n}} \tag{2.147}$$

From the algorithmic point of view, we initially solve the rescaled problem and finally perform a separate calculation of the unrescaled solar contribution.

To develop the mathematics for this carefully, we introduce the sets of spherical orders $\mathcal{F}$ and $\mathcal{T}$, for the full set of spherical orders used in the final expression and for the truncated set used in the direct solution, which is written

$$\hat{I}_T(\mathbf{n}, \tau) = \sum_{(l,m)\in\mathcal{T}} Q_{l,m}(\tau) Y_l^m(\mathbf{n}) \tag{2.148}$$

Moreover,

$$\hat{P}_T(\mathbf{n}', \mathbf{n}) = 4\pi \sum_{(l,m)\in\mathcal{T}} \hat{g}_l Y_l^{m*}(\mathbf{n}') Y_l^m(\mathbf{n}) \tag{2.149}$$

and

$$\hat{P}(\mathbf{n}', \mathbf{n}) = 4\pi \sum_{(l,m)\in\mathcal{F}} \hat{g}_l Y_l^{m*}(\mathbf{n}') Y_l^m(\mathbf{n}) \tag{2.150}$$

$$\tag{2.151}$$

Substituting these expressions into the equation of transfer we obtain

$$\begin{aligned} \mu \frac{dI}{d\hat{\tau}} = I &- \hat{\omega}(\hat{\tau}) \sum_{\mathcal{T}} \hat{g}_l(\hat{\tau}) Q_{lm}(\hat{\tau}) Y_l^m(\mathbf{n}) \\ &- \hat{\omega}(\hat{\tau}) \hat{I}_\odot(\hat{\tau}) \sum_{\mathcal{F}} \hat{g}_l(\hat{\tau}) Y_l^{m*}(\mathbf{n}_\odot) Y_l^m(\mathbf{n}) \end{aligned} \tag{2.152}$$

Integrating with respect to optical depth between $\hat{\Delta}^-$ and $\hat{\Delta}^+$, we obtain

$$\begin{aligned} I(\mathbf{n}, \hat{\Delta}^+) = I(\mathbf{n}, \hat{\Delta}^-) & e^{(\hat{\Delta}^+/\mu - \hat{\Delta}^-/\mu)} \\ &- \frac{1}{\mu} e^{\hat{\Delta}^+/\mu} \sum_{(l,m)\in\mathcal{T}} Y_l^m(\mathbf{n}) \int_{\hat{\Delta}^-}^{\hat{\Delta}^+} \hat{\omega}(\hat{\tau}) \hat{g}_l(\hat{\tau}) Q_{l,m}(\hat{\tau}) e^{-\hat{\tau}/\mu}\, d\hat{\tau} \\ &- \frac{1}{\mu} e^{\hat{\Delta}^+/\mu} \sum_{(l,m)\in\mathcal{F}} Y_l^{m*}(\mathbf{n}_\odot) Y_l^m(\mathbf{n}) \int_{\hat{\Delta}^-}^{\hat{\Delta}^+} \hat{\omega}(\hat{\tau}) \hat{g}_l(\hat{\tau}) \hat{I}_\odot(\hat{\tau}) e^{-\hat{\tau}/\mu}\, d\hat{\tau} \end{aligned} \tag{2.153}$$

In the code the integrals on the right will be evaluated separately for each layer, in which the optical propeties will be taken as fixed, so if $\mathcal{I}$ denotes the set of those layers that contain regions of optical depth between $\hat{\Delta}^-$ and $\hat{\Delta}^+$ we may write

$$\begin{aligned} I(\mathbf{n}, \hat{\Delta}^+) = I(\mathbf{n}, \hat{\Delta}^-) & e^{(\hat{\Delta}^+/\mu - \hat{\Delta}^-/\mu)} \\ &+ \sum_{i\in\mathcal{I}} \sum_{(l,m)\in\mathcal{T}} \hat{\omega}_i \hat{g}_{li} Y_l^m(\mathbf{n}) A_{ilm} + \sum_{i\in\mathcal{I}} \sum_{l\in\mathcal{F}_L} \frac{(2l+1)}{4\pi} \hat{\omega}_i \hat{g}_{li} P_l(\mathbf{n}_\odot.\mathbf{n}) B_i \end{aligned} \tag{2.154}$$

where A_{ilm} and B_i denote the contributions from the individual layers with the obvious identifiation. In the case of B_i we have used standard results to reexpress the spherical harmonics as Legendre polynomials. Each of these contributions is evaluated separately, setting the limits of integration to $\hat{\Delta}_i^-$ and $\hat{\Delta}_i^+$ which will normally mark the edges of the layer, though not in the case of the layer containing the level where we seek the radiance may be within it. Now,

$$\begin{aligned} Q_{ilm}(\hat{\tau}) = {} & Z_{ilm} e^{-(\hat{\tau}-\hat{\Delta}_{i-1})/\mu_0} \\ & + \sum_k \Big[\; u^+_{mik} V_{ikl} e^{-(\hat{\Delta}_i - \hat{\tau})/\mu_{mik}} \\ & \qquad + u^-_{mik} V_{ikl} (-1)^{(l+m)} e^{-(\hat{\tau}-\hat{\Delta}_{i-1})/\mu_{mik}} \Big] \end{aligned} \tag{2.155}$$

so the contribution to the first integral from the ith layer is

$$\begin{aligned} A_{ilm} = {} & -\frac{1}{\mu} Z_{ilm} e^{(\hat{\Delta}_{i-1}/\mu_0 + \hat{\Delta}^+/\mu)} \int_{\hat{\Delta}_i^-}^{\hat{\Delta}_i^+} e^{-\hat{\tau}(1/\mu+1/\mu_0)} \, d\hat{\tau} \\ & - \frac{1}{\mu} \sum_k u^+_{mik} V_{ikl} e^{(\hat{\Delta}^+/\mu - \hat{\Delta}_i/\mu_{mik})} \int_{\hat{\Delta}_i^-}^{\hat{\Delta}_i^+} e^{\hat{\tau}(-1/\mu+1/\mu_{mik})} \, d\hat{\tau} \\ & - \frac{1}{\mu} \sum_k u^-_{mik} V_{ikl} (-1)^{(l+m)} e^{-(\hat{\Delta}^+/\mu + \hat{\Delta}_{i-1}/\mu_{mik})} \int_{\hat{\Delta}_i^-}^{\hat{\Delta}_i^+} e^{-\hat{\tau}(1/\mu+1/\mu_{mik})} \, d\hat{\tau} \\ = {} & Z_{ilm} \frac{\mu_0}{\mu+\mu_0} \left\{ \exp\left(\frac{\hat{\Delta}^+ - \hat{\Delta}_i^+}{\mu} + \frac{\hat{\Delta}_{i-1} - \hat{\Delta}_i^+}{\mu_0} \right) \right. \\ & \qquad \left. - \exp\left(\frac{\hat{\Delta}^+ - \hat{\Delta}_i^-}{\mu} + \frac{\hat{\Delta}_{i-1} - \hat{\Delta}_i^-}{\mu_0} \right) \right\} \\ & + \sum_k u^+_{ikm} V_{ikl} \frac{\mu_{mik}}{\mu_{mik} - \mu} \left\{ \exp\left(\frac{\hat{\Delta}^+ - \hat{\Delta}_i^+}{\mu} + \frac{\hat{\Delta}_i^+ - \hat{\Delta}_i}{\mu_{mik}} \right) \right. \\ & \qquad \left. - \exp\left(\frac{\hat{\Delta}^+ - \hat{\Delta}_i^-}{\mu} + \frac{\hat{\Delta}_i^- - \hat{\Delta}_i}{\mu_{mik}} \right) \right\} \\ & + \sum_k u^-_{ikm} (-1)^{(l+m)} V_{ikl} \frac{\mu_{mik}}{\mu_{mik} + \mu} \left\{ \exp\left(\frac{\hat{\Delta}^+ - \hat{\Delta}_i^+}{\mu} + \frac{\hat{\Delta}_{i-1} - \hat{\Delta}_i^+}{\mu_{mik}} \right) \right. \\ & \qquad \left. - \exp\left(\frac{\hat{\Delta}^+ - \hat{\Delta}_i^-}{\mu} + \frac{\hat{\Delta}_{i-1} - \hat{\Delta}_i^-}{\mu_{mik}} \right) \right\}. \end{aligned} \tag{2.156}$$

Likewise, from the second term we obtain a contribution

$$\begin{aligned} B_i = {} & -\frac{1}{\mu} \hat{I}_{\odot i-1} e^{(\hat{\Delta}_{i-1}/\mu_0 + \hat{\Delta}^+/\mu)} \int_{\hat{\Delta}_i^-}^{\hat{\Delta}_i^+} e^{-\hat{\tau}(1/\mu+1/\mu_0)} \, d\hat{\tau} \\ = {} & \hat{I}_{\odot i-1} \frac{\mu_0}{\mu+\mu_0} \left\{ \exp\left(\frac{\hat{\Delta}^+ - \hat{\Delta}_i^+}{\mu} + \frac{\hat{\Delta}_{i-1} - \hat{\Delta}_i^+}{\mu_0} \right) \right. \\ & \qquad \left. - \exp\left(\frac{\hat{\Delta}^+ - \hat{\Delta}_i^-}{\mu} + \frac{\hat{\Delta}_{i-1} - \hat{\Delta}_i^-}{\mu_0} \right) \right\} \end{aligned} \tag{2.157}$$

There is a problem with ill-conditioning when $\mu \to \mu_0$ or $\mu \to \pm\mu_{mik}$. Each geometrical factor which may produce ill-conditioning is of the form

$$\begin{aligned} G &= \frac{\tilde{\mu}}{\tilde{\mu}-\mu}\left\{e^{(-s_n+\hat{\tau}_i/\tilde{\mu}} - e^{-s_f}\right\} \\ &= \hat{\mu}e^{-s_n}\frac{e^{\hat{\tau}_i/\tilde{\mu}} - e^{\hat{\tau}_i/\mu}}{\tilde{\mu}-\mu} \end{aligned} \tag{2.158}$$

where $\tilde{\mu}$ stands generically for μ_0 or $\pm\mu_{mik}$ and s_n and s_f represent the slant depths from the observing level to the nearer and farther boundaries of the layer. As $\mu \rightarrow \tilde{\mu}$,

$$\begin{aligned} G &\rightarrow \frac{\tilde{\mu}}{\tilde{\mu}-\mu}e^{-s_n+\hat{\tau}/\tilde{\mu}}\left(1 - e^{-\hat{\tau}(1/\mu-1/\tilde{\mu})}\right) \\ &\rightarrow \frac{\hat{\tau}}{\mu}e^{-s_n+\hat{\tau}/\tilde{\mu}} \end{aligned} \tag{2.159}$$

Now reacall L'Hôpital's rule that if $\lim_{x\rightarrow 0} f(x), g(x) = 0$ then

$$\lim_{x\rightarrow 0}\frac{f(x)}{g(x)} = \lim_{x\rightarrow 0}\frac{f'(x)}{g'(x)}. \tag{2.160}$$

Consequently,

$$\lim_{x\rightarrow 0}\frac{(f(x)+\eta(x)f'(x))}{(g(x)+\eta(x)g'(x))} = \lim_{x\rightarrow 0}\frac{f(x)}{g(x)}. \tag{2.161}$$

Supposing that $g'(0) \neq 0$, it follows that if we arrange that $\eta(x)$ is small compared to $g(x)$ except in the neighbourhood of $x = 0$, we have an expression for the quotient which does not become indeterminate as $x \rightarrow 0$ and will be approximately accurate for all values of x. One possible choice for η is $\eta(x) = \epsilon/(x+\sqrt{\epsilon})$ where ϵ is the smallest number such that $1-\epsilon \neq 1$ to the computer's precision. This will introduce errors of $O(\sqrt{\epsilon})$ when $x = O(\sqrt{\epsilon})$. In the present case we define

$$\eta = \frac{\epsilon}{(\tilde{\mu}-\mu)+\operatorname{sgn}(\tilde{\mu}-\mu)\sqrt{\epsilon}} \tag{2.162}$$

and put

$$G \approx \tilde{\mu}\frac{\left(1-\frac{\eta\tau}{\mu\tilde{\mu}}\right)e^{-(s_n+\hat{\tau}/\tilde{\mu})} - e^{-s_f}}{\tilde{\mu}-\mu+\eta} \tag{2.163}$$

2.5 Fast Solution of the linear equations

This algorithm has not yet been coded into the radiance code, but represents a more efficient treatment of the core of the algorithm.

We start from the expression for the amplitude of each spherical harmonic for a fixed azimuthal order m in a layer of optical dept $\bar{\tau}$ in the form

$$I_l = \sum_{k=1}^{N} u_k^-(-1)^{l+m}V_{lk}e^{-\tau/\mu_k} + u_k^+V_{lk}e^{-(\bar{\tau}-\tau)/\mu_k} + G_l \tag{2.164}$$

where τ is the local optical depth extending from 0 at the top to $\bar{\tau}$ at the bottom. G is the source function and $2N$ polar orders are retained, starting with $l =$. Introducing the reduced index $r = l + 1 - m$, $r = 1, \ldots, 2N$, the equations may be reindexed as

$$I_r = \sum_{k=1}^{N} u_k^- (-1)^{r+1} V_{rk} e^{-\tau/\mu_k} + u_k^+ V_{rk} e^{-(\bar{\tau}-\tau)/\mu_k} + G_r. \tag{2.165}$$

Collecting alternate terms of the eigenvector, we define

$$W_{sk} = \{V_{rk} : r = 2s - 1, s = 1, \ldots, N\} \tag{2.166}$$

and

$$U_{sk} = \{V_{rk} : r = 2s, s = 1, \ldots, N\}. \tag{2.167}$$

Defining $\theta_k = e^{-\bar{\tau}/\mu_k}$, the amplitude at the top of the layer is

$$I_r = \sum_{k=1}^{N} u_k^- (-1)^{r+1} V_{rk} + u_k^+ V_{rk} \theta_k + \hat{G}_r, \tag{2.168}$$

where the hat on G denotes its evaluation at the top of the layer; while at the bottom of the layer

$$I_r = \sum_{k=1}^{N} u_k^- (-1)^{r+1} V_{rk} \theta_k + u_k^+ V_{rk} + \check{G}_r, \tag{2.169}$$

where the haček denotes a value at the bottom of the layer.

The orthogonality relations between the eigenvectors give

$$\sum_{r=1}^{2N} s_r V_{rk} V_{rk'} = \delta_{kk'} \tag{2.170}$$

and

$$\sum_{r=1}^{2N} s_r (-1)^{r+1} V_{rk} V_{rk'} = 0. \tag{2.171}$$

By taking the sum and the difference we deduce that

$$\sum_{r \text{ odd}}^{2N} s_r V_{rk} V_{rk'} = \delta_{kk'}, \tag{2.172}$$

or with the obvious identifications:

$$\sum_{s=1}^{N} \rho_s W_{sk} W_{sk'} = \delta_{kk'}. \tag{2.173}$$

Similarly, from the even terms

$$\sum_{s=1}^{N} \sigma_s U_{sk} U_{sk'} = \delta_{kk'}. \tag{2.174}$$

At the top we impose Marshak's condition, that the inner product with harmonics of odd parity, taken over the downward hemisphere, should vanish if there is no incident radiation:

$$\sum_l \int_{\Omega_-} Y_L^{m*} I_{lm} Y_l^m \, d\omega = 0 \tag{2.175}$$

where $L + m$ is odd. This gives

$$\frac{1}{2} I_l \delta_{Ll} + \sum_l \frac{1}{2} \tilde{M}_{Ll} I_l = 0 \tag{2.176}$$

where

$$\frac{1}{2} \tilde{M}_{Ll} = \int_{\Omega_-} Y_L^{m*} Y_l^m \, d\omega. \tag{2.177}$$

Defining $M_{sp} = \tilde{M}_{2s+1-m,2p-m}$ we have

$$\begin{aligned} &\sum_{k=1}^{N} \left[u_k^-(-1) U_{sk} + u_k^+ U_{sk} \theta_k \right] + \hat{\bar{G}}_s \\ &\qquad + \sum_{p=1}^{N} M_{sp} \left\{ \sum_{k=1}^{N} \left[u_k^-(-1) W_{pk} + u_k^+ W_{pk} \theta_k \right] + \hat{G}'_p \right\}, \end{aligned} \tag{2.178}$$

where $\bar{G}$ denotes even terms of G and G' odd terms.

The equations may then be cast in a block matrix form:

$$\begin{bmatrix} -U_1 + MW_1 & (U_1 + MW_1)\theta_1 & 0 & 0 & 0 & 0 & \cdots \\ W_1\theta_1 & W_1 & -W_2 & -W_2\theta_2 & 0 & 0 & \cdots \\ -U_1\theta_1 & U_1 & U_2 & -U_2\theta_2 & 0 & 0 & \cdots \\ 0 & 0 & W_2\theta_2 & W_2 & -W_3 & -W_3\theta_2 & \cdots \\ 0 & 0 & -U_2\theta_2 & U_2 & U_3 & -U_3\theta_2 & \cdots \\ \cdots & \cdots & \cdots & \cdots & \cdots & \cdots & \ddots \end{bmatrix} \begin{bmatrix} u_1^- \\ u_1^+ \\ u_2^- \\ u_2^+ \\ u_3^- \\ u_3^+ \\ \vdots \end{bmatrix} = \begin{bmatrix} g_0 \\ h_1 \\ g_1 \\ h_2 \\ g_2 \\ h_3 \\ \vdots \end{bmatrix} \tag{2.179}$$

The second and third rows refer to conditions at the bottom of the first layer and may be simplified to eliminate elements most distant from the diagonal. After premultilpying the second row by $\theta_1^{-1} W_1^T \rho_1$ and the third by $U_1\theta_1$, subtraction gives

$$\begin{bmatrix} \cdots & \cdots & \cdots & \cdots & \cdots \\ 1 & \theta_1^{-1} & -\theta_1^{-1} W_1^T \rho_1 W_2 & -\theta_1^{-1} W_1^T \rho_1 W_2 \theta_2 & \cdots \\ 0 & 2U_1 & U_2 - U_1 W_1^T \rho_1 W_2 & -(U_2 + U_1 W_1^T \rho_1 W_2)\theta_2 & \\ \cdots & \cdots & \cdots & \cdots & \cdots \end{bmatrix} \begin{bmatrix} \vdots \end{bmatrix} = \begin{bmatrix} \vdots \\ \theta_1^{-1} W_1^T \rho_1 h_1 \\ g_1 + U_1 W_1^T \rho_1 h_1 \\ \vdots \end{bmatrix} \tag{2.180}$$

Premultiplying the new form of the third row by $(1/2)U_1^T\sigma_1$ we obtain

$$\begin{bmatrix} \cdots & \cdots & \cdots & \cdots & \cdots \\ 0 & 1 & \frac{1}{2}(U_1^T\sigma_1 U_2 - W_1^T\rho_1 W_2) & -\frac{1}{2}(U_1^T\sigma_1 U_2 + W_1^T\rho_1 W_2) & \\ \cdots & \cdots & \cdots & \cdots & \cdots \end{bmatrix} \begin{bmatrix} \vdots \end{bmatrix} = \begin{bmatrix} \vdots \\ \frac{1}{2}(U_1^T\sigma_1 g_1 + W_1^T\rho_1 h_1) \\ \vdots \end{bmatrix} \tag{2.181}$$

Similarly, by eliminating the fourth entry of the original second row we obtain

$$\begin{bmatrix} \cdots & \cdots & \cdots & \cdots & \cdots \\ -\frac{1}{2}(W_2^T\rho_2 W_1 + U_2^T\sigma_2 U_1) & -\frac{1}{2}(W_2^T\rho_2 W_1 - U_2^T\sigma_2 U_1) & 1 & 0 & \\ \cdots & \cdots & \cdots & \cdots & \cdots \end{bmatrix} \begin{bmatrix} \vdots \end{bmatrix} = \begin{bmatrix} \vdots \\ -\frac{1}{2}(W_2^T\rho_2 h_1 + U_2^T\sigma_2 g_1) \\ \vdots \end{bmatrix} \tag{2.182}$$

Coding these equations in reversed order yields two rows of the form

$$\begin{bmatrix} \cdots & \cdots & \cdots & \cdots & \cdots \\ 0 & 1 & A_1 & B_1 & \\ D_1 & C_1 & 1 & 0 & \\ \cdots & \cdots & \cdots & \cdots & \cdots \end{bmatrix} \begin{bmatrix} \vdots \end{bmatrix} = \begin{bmatrix} \vdots \\ x_1 \\ y_1 \\ \vdots \end{bmatrix} \tag{2.183}$$

where

$$A_1 = \frac{1}{2}(P-Q) \qquad B_1 = -\frac{1}{2}(P+Q)\theta_2 \tag{2.184}$$

$$C_1 = \frac{1}{2}(R-S) \qquad D_1 = -\frac{1}{2}(R+S)\theta_1 \tag{2.185}$$

$$x_1 = \frac{1}{2}(U_1^T\sigma_1 g_1 + W_1^T\rho_1 h_1) \qquad y_1 = -\frac{1}{2}(W_2^T\rho_2 h_1 + U_2^T\sigma_2 g_1). \tag{2.186}$$

where in turn

$$P = U_1^T\sigma_1 U_2 \qquad Q = W_1^T\rho_1 W_2 \tag{2.187}$$

$$R = U_2^T\sigma_2 U_1 \qquad S = W_2^T\rho_2 W_1 \tag{2.188}$$

$$\tag{2.189}$$

Furthermore,

$$R = P^{-1} \qquad S = Q^{-1} \tag{2.190}$$

From the recurrence relation for the eigenvalues it may also be shown that

$$P = \text{diag}(\mu_{11}^{-1}, \mu_{21}^{-1}, \mu_{31}^{-1}, \ldots, \mu_{N1}^{-1}) S^T \text{diag}(\mu_{12}, \mu_{22}, \mu_{32}, \ldots, \mu_{N2}) \tag{2.191}$$

where the first suffix refers to the eigenvector and the second to the layer. Hence,

$$R = \text{diag}(\mu_{12}^{-1}, \mu_{22}^{-1}, \mu_{32}^{-1}, \ldots, \mu_{N2}^{-1}) S^{-T} \text{diag}(\mu_{11}, \mu_{21}, \mu_{31}, \ldots, \mu_{N1}) \tag{2.192}$$

This is efficient computationally, since the the direct evaluation of $P, \ldots, S$ would require about $4N^3$ multiplications, but using these formulae finding P and R requires $4N^2$ multiplications. Finding Q by inversion of S is about equally as expensive as direct calculation, unless further advantage can be taken of the structure of the matrices.

A recurrence representing Gaussian elimination can now be defined:

$$Z_n = C_n - D_n X_{n-1} \tag{2.193}$$

$$Y_n = (Z_n^{-1} - A_n)^{-1} \tag{2.194}$$

$$X_n = -Y_n B_n \tag{2.195}$$

$$z_n = Q_n \left[Z_n^{-1}(y_n - D_n z_{n-1}) - x_n\right] \tag{2.196}$$

starting with the definitions

$$X_0 = -(1 - U_1^T \sigma_1 M W_1)^{-1}(1 + U_1^T \sigma_1 M W_1)\theta_1 \tag{2.197}$$

$$z_0 = -(1 - U_1^T \sigma_1 M W_1)^{-1} U_1^T \sigma_1 g_0. \tag{2.198}$$

After forward elimination the equations reduce to

$$\begin{bmatrix} 1 & X_0 & \dots & \dots & \dots \\ 0 & 1 & A_1 & B_1 & \dots \\ & 0 & 1 & X_1 & \dots \\ \dots & \dots & \dots & \dots & \dots \end{bmatrix} \begin{bmatrix} u_1^- \\ u_1^+ \\ u_2^- \\ \vdots \end{bmatrix} = \begin{bmatrix} z_0 \\ x_1 \\ z_1 \\ \vdots \end{bmatrix} \tag{2.199}$$

establishing a recurrence for back substitution of the form

$$u_n^+ = x_n - A_n u_{n+1}^- - B_n u_{n+1}^+ \tag{2.200}$$

$$u_n^- = z_n - X_n x_n. \tag{2.201}$$

Direct solution of the original block matrix using a banded solver with partial pivoting on rows would have a operation count of the order of $18N^3L$, where L is the number of layers. The dominating operation count for this scheme is $6N^3L$ (comprising two matrix multiplications to find S and Q and two matrix multiplications and two inversions in the forward recurrence). Since we need keep only the matrices A, B and X at each level for backward substitution, the memory requirement is also reduced by a factor of three.

Chapter 3

The Spectral Files

3.1 Introduction and General Remarks

To cover the broad range of frequencies encountered in atmospheric radiation, discretization in frequency or wavelength must be considered carefully. The approach adopted in all codes for use in general circulation models (GCMs) is to divide the solar or infra-red spectral region into a number of bands, across which all radiative quantities, except the absorption coefficients of gases, may be considered uniform. More accurate computations can be made if more bands are used; but this comes at increased computational expense, and the balance to be struck between the two requirements will depend on the application. For operational use in GCMs only a small number of bands can be used.

The Edwards-Slingo radiation scheme was developed to meet a range of varied requirements for radiative modelling, extending beyond the demands of the Unified Model itself. To meet this need for flexibility, the discretization in frequency within this radiation code is not fixed, but is set by an external file supplied by the user when the code runs: this file is known as the *spectral file*. This flexibility facilitates assessment of the files used in the UM itself against reference data in controlled experiments.

The generation of spectral files requires a detailed knowledge of radiative transfer and judgements about efficiency for the application in question. It is therefore not envisaged that users of the code within the Unified Model in particular will generate their own files, unless they have this knowledge and are developing a specific new application. Instead, standard spectral files, appropriate for use in the Unified Model are provided in a central directory, `$UMDIR/vn$VN/ctldata/spectral`. When a new requirement arises, such as the need to model the radiative effects of a new gas, users should contact the radiation group to discuss the requirement.

The following general points should be noted.

1. A spectral file is not an ancillary file: it contains no geographical information, but refers to the discretization in frequency.

2. A spectral file released with a certain version of the Unified Model will normally be compatible with future releases (but the reverse is not generally true because of the possible addition of data to deliver new functionality). This makes upgrading to newer releases of the Model simpler than it would otherwise be. A caveat to this point is that at version 8.6 of the Unified Model the format of the spectral files was changed from a namelist to a readable text file as used by the offline Edwards-Slingo radiation code suite. Utilities are available within the offline suite to convert between namelist and text versions of the spectral files.

3. **Naming Convention**

   Although there is no formal requirement to adopt a particular naming convention, the names of shortwave spectral files begin with the string `sp_sw` and those of longwave spectral files with the string `sp_lw`. (Spectral files in namelist format as used with the UM prior to version 8.6 begin with the string `spec_` or `spec3a_`.) When a new release of the model is prepared, the UM team copy all existing spectral files from the old release to the new one without change, unless advised differently by the radiation group.

   As new functionality is developed, it is sometimes necessary to change spectral files, either by adding new material or by replacing old material. If new material is added, in such a way that the results of existing runs are unchanged at the new release, the name of the file is not changed; but if existing data are altered, a new name is used. An example may make this clearer. Suppose that at version 5.11 of the UM we have a file `spec3a_sw_orig` and that for version 5.12 a new scheme is to be added to the UM which requires the radiative modelling of volcanic ash. This would require the addition of information to the spectral file, but the new material would not change the results of any run which could be carried out at both versions 5.11 and 5.12: to allow for simple upgrading, the new material would be added to the spectral files for 5.12 without any change of name. Suppose now that for version 5.13 improvements to the modelling of ash had been made and that the data in the spectral file needed to be changed. This would represent a modification to an existing capability, so the old spectral file would be copied to the new directory for 5.13 without new data to allow existing configurations to continue, but a new spectral file with the revised data and a new name would be introduced. If the old file were revised without a change of name it would be possible to upgrade an existing experiment and get different results: that would be unacceptable.

4. **Generation of and Additions to Spectral Files**

   As noted before, the generation or alteration of spectral files requires expertise in radiative transfer. The responsibility for changes to the standard files lies with the radiation group. Most users will never need to alter a spectral file, but it is possible that some users of the portable model with expertise in radiative transfer may wish to generate files for their own specific purposes and the next paragraph is addressed to them.

   Spectral files are generated using the pre-processing suite in the off-line version of the radiation code, which is maintained by the radiation team. It is possible to generate a spectral file form scratch, but more usually, the requirement is to add to or modify an existing file. Prior to version 8.6 spectral files were read into the UM as namelists. The current UM along with the off-line code uses a more readable text format. Conversion from a namelist to the text format is carried out with the program `nml_spec` of the external suite and in the reverse direction with the program `spec_nml`.

Data on aerosols are generated in consultation with the aerosol modelling group.

3.2 The Structure of Spectral Files

The file consists of a number of blocks of data, each referring to a different physical process. The flag `l_present(i)` is set to `.TRUE.` if a block of type `i` is present: not all possible blocks are required for all calculations.

Block 0 contains the number and physical natures of gases and aerosols. There are a vast number of gases and aerosols in the atmosphere, not all of which are relevant in all applciations. In each spectral file a subset of all the gases is selected and indexed $1, \ldots, n$. This number is referred to as the indexing number and is used internally by the radiation code. There is still a need to know the physical nature of each species, and this is recorded by the *type* number. The array `TYPE_ABSORB` holds the type numbers for gaseous absorbers. The meaning of these numbers is set in the module `gas_list_pcf`. Aerosols are indexed in a similar way, the type numbers for these being recorded in `rad_pcf`.

Block 1 contains the limits of the spectral bands used as wavelengths in metres. *Note: UM standards require the use of SI units.* In a number of UM shortwave files, it will be observed that some bands have the same limits: this indicates that they are not true spectral bands, and that one should not consider the fluxes in individual bands alone, but only the sum of the fluxes in the bands which does represent the true flux across the specified region. For example, if band 1 is specified as running from 0.2–0.32 μm, but bands 2 and 3 both have limits 0.32–0.69μm, it is meaningful to consider the flux in band 1 as representing the true flux between 0.2 and 0.32 μm, but the flux in band 2 or band 3 should not be considered alone: all that can be said is that the sum of the fluxes in bands 2 and 3 can meaningfully be taken as that in the region 0.32–0.69μm.

Block 2 is required only in shortwave files and contains the fraction of the solar spectrum in each band.

Block 3 is required only in shortwave files and contains the Rayleigh scattering coefficients.

Block 4 contains the list of gaseous absorbers active in each band, listed by their indexing numbers. Note that the first gas listed must be the primary absorber in the band *i.e.* that which makes the greatest contribution to the atmospheric absorption when considered alone.

Block 5 contains the k-fits to the gaseous transmissions.

Block 6 is required only for infra-red calculations and contains the coefficients of a polynomial fit to the Planck function in each band.

Block 7 is obsolete and not present in any file used in the UM.

Block 8 contains the list of continuum absorbers in each band. In principle, there are several species of continuum absorber, but in practice the main continua are the self and foreign-broadened continua of water vapour.

Block 9 contains the continuum absorption coefficients in each band.

Block 10 contains parametrizations for the single scattering properties of droplets. The file may contain data for a number of different *types* of droplet. The term type is deliberately vague to allow for flexibility: a different type may indicate a parametrization appropriate to a different collection of droplets, say droplets in convective clouds and stratiform clouds, a different parametrization of the same data or different spectral averaging. Type numbers are supplied at runtime and must be selected for the appropriate spectral file. The details are given below. Parametrizations are generated over a range of particle sizes, so the minimum and maximum dimensions for which the parametrization is valid are recorded as well.

Block 11 contains data on aerosols. The selection of aerosols included is very varied and is described for each file listed below.

Block 12 contains parametrizations for the single scattering properties of ice crystals. The file may contain data for a number of different *types* of droplet. As for water droplets, the term type is deliberately vague to allow for flexibility: a different type may indicate a parametrization appropriate to a different collection of ice crystals, say, crystals in convective clouds and stratiform clouds, a different parametrization of the same data, a different crystal shape, or different spectral averaging. Type numbers are supplied at runtime and must be selected for the appropriate spectral file. The details are given below. Parametrizations are generated over a range of particle sizes, so the minimum and maximum dimensions for which the parametrization is valid are recorded as well.

Block 13 is only relevant in the longwave region and is obsolescent. It contains heuristic adjustments for Doppler broadening. Eventually, these will be moved to block 5.

Block 14 specifies exclusions. In the original version of the radiation code a band had to be a contiguous range of frequencies, but for use in the UM it was desirable to allow for split bands. This concept is most easily explained by an example. If we specify that band 5 extends from 8 to 12 μm and band 6 from 10–11μm, and exclude band 6 from band 5, this means that we take band 5 effectively to consist of the regions 8–10 μm and 11–12μm. In this case, the limits for band 6 will naturally be set as 10 and 11 μm, but band 5 will have limits of 8 and 12 μm. Exclusions are of importance in the generation of the spectral file, but are not of such relevance in runs in the UM. If diagnostics covering only a portion of the spectrum were defined, it would be necessary to know about any exclusions in order to weight the contributions from individual bands appropriately. Split bands are used only for reasons of efficiency.

3.3 Standard Spectral Files

Standard spectral files that have been used operationally for numerical weather prediction or climate runs are described. Spectral files with names beginning spec_ or spec3a_ are namelist files available for UM versions up to 8.5 (readable text equivalents of these files are available with the offline Edwards-Slingo code). Files with names beginning sp_ are readable text versions for use with UM versions 8.6 onwards or the offline code.

3.3.1 Global Atmosphere Configuration 9

Spectral files for the GA9 configuration are a minor update on those used for GA7. Principal changes are to the water vapour continuum and aerosol optical properties. Minor updates have also been made to the cloud optical properties including an adjustment to the optimal sampling configuration for MCICA: the mcica_data file adds 10 monochromatic calculations to the SW and 6 to the LW.

Scripts to update the ga7 spectral files to the ga9 configuration are provided in examples/sp_ga9.

Elsey-Shine water vapour continuum

An update to the CAVIAR water vapour continuum has been provided by Jon Elsey and Keith P. Shine, motivated by several advancements in understanding since the version used with GA7:

- Changes to the far-infrared continuum [Mlawer et al., 2019] as part of MT_CKD3.2 - increased continuum at 0-500 cm^{-1} with more modest changes at other wavenumbers.
- Additional near-infrared in-band measurements from Ptashnik et al. [2019], Birk et al. [2020].
- Additional window measurements in 4, 2.1 and 1.6 μm windows using Cavity Ring-Down Spectroscopy (CRDS) e.g. Mondelain et al. [2014], Ventrillard et al. [2015], Richard et al. [2017].
- Increased understanding of CAVIAR-lab measurements [Ptashnik et al., 2011], as inconsistencies in the temperature dependence were discovered when using room-temperature data (293 K). Omitting this low-temperature data in the 4 and 2.1 μm windows leads to better consistency with the various Grenoble data (although that consistency varies between near-IR windows). See Elsey et al. [2020] for more details.

Aerosols

CLASSIC aerosol optical properties have been recalculated following the recommendations of Ben T. Johnson in order to more closely match the optical properties of GLOMAP-mode aerosols:

- Change soot species refractive index to make it consistent with black carbon (BC) in GLOMAP GA7.1 [Bond and Bergstrom, 2006].

- Change soot species size distribution to make it consistent with freshly emitted size distribution for FF BC in GLOMAP-mode (diameter reduced from 80nm to 60nm, stdev reduced from 2.0 to 1.59).
- Reduce soot density from current value of 1.9g/cm^3 to value of 1.5g/cm^3 in GLOMAP-mode.
- Re-compute biomass burning aerosol refractive index based on the BC:OC mass ratio already assumed in CLASSIC but using the refractive index of Bond and Bergstrom [2006] and density of 1.5 g/cm^3 for the BC component as in GLOMAP-mode GA7.1.
- All aerosol optical properties have been recalcuated with the GA7 spectral file waveband limits (compared to GA6 and earlier the only change is that SW bands 2 and 3 are no longer identical but have been split into 0.32 - 0.505, 0.505 - 0.69 μm), using the refractive indices and size distributions above and previously documented. This has resulted in minor changes in aerosol species not listed above in both the SW and LW.

Spectral file: sp_sw_ga9

Sections are identical to sp_sw_ga7 except for changes to the water vapour continuum and aerosols (detailed above), along with cloud droplet optical properties:

Cloud droplets

The cloud droplet optical properties have been recalculated using identical methodology as previous files (first detailed for the HadGEM1 spectral files below). The only change is the band weighting, using the latest band limits for SW bands 2 and 3 (now split into 0.32 - 0.505, 0.505 - 0.69 μm) and the "lean_12" solar spectrum.

Spectral file: sp_lw_ga9

Sections are identical to sp_lw_ga7 except for changes to the water vapour continuum and aerosols (detailed above).

3.3.2 Global Atmosphere Configuration 7

Spectral file: sp_sw_ga7

Sections are identical to sp_sw_ga3_0 except for changes to the spectral bands, solar spectrum (including Rayleigh coefficients), and gaseous absorption:

Spectral bands

The six spectral bands are identical to sp_sw_ga3_0 except the combined bands 2 and 3 are now properly split into two true bands at 505nm. Band limits are now:

Band	Wavelength (nm)
1	200 - 320
2	320 - 505
3	505 - 690
4	690 - 1190
5	1190 - 2380
6	2380 - 10000

Solar spectrum

New solar spectrum (”lean_12”) taken as a mean of the spectral data from 2000-2011 from the recommendation of the SPARC/SOLARIS group (data from Judith Lean, available here: http://solarisheppa.geomar.de/ccmi). Associated updates to Rayleigh scattering coefficients.

Gaseous absorption

Newly derived gaseous absorption for all gases based on HITRAN 2012 and CAVIAR water vapour continuum. Scaling of absorption coefficients uses a look-up table of 59 pressures with 5 temperatures per pressure level based around a mid-latitude summer profile.

Addition of N2O and CH4 minor gases.

Ozone cross sections for the UV and visible come from Serdyuchenko et al. [2014] and Gorshelev et al. [2014] (with Brion-Daumont-Malicet cross-sections for the far UV) taken from this website: http://igaco-o3.fmi.fi/ACSO/cross_sections.html. In band 1, a single k-term is calculated for each 20nm sub-interval from 200 to 320nm as done for the GA3 spectral file. In band 2, a single k-term is calculated for each of the sub-intervals 320-400nm and 400-505nm. This allows the incoming solar flux to be supplied on these finer wavelength bands for experiments concerning solar spectral variability.

Absorption due to Sulphur dioxide (SO2, principally in the UV, plus near-IR) and Carbonyl sulphide (OCS, near-IR) is included based on HITRAN 2012 (only used for particular experimental configurations).

Total of 41 major gas k-terms.

Spectral file: sp_lw_ga7

Sections are identical to sp_lw_ga3_0 except for changes to gaseous absorption, thermal emission:

Spectral bands

The nine spectral bands are identical to sp_lw_ga3_0. Band limits are:

Band	Wavenumber (cm^{-1})	Wavelength (μm)
1	1 - 400	25 - 10000
2	400 - 550	18.18 - 25
3	550 - 590 and 750 - 800	12.5 - 13.33 and 16.95 - 18.18
4	590 - 750	13.33 - 16.95
5	800 - 990 and 1120 - 1200	8.33 - 8.93 and 10.10 - 12.5
6	990 - 1120	8.93 - 10.10
7	1200 - 1330	7.52 - 8.33
8	1330 - 1500	6.67 - 7.52
9	1500 - 2995	3.34 - 6.67

Gaseous absorption

Newly derived gaseous absorption for all gases (except CO2 in band 4) based on HITRAN 2012 and CAVIAR water vapour continuum. Scaling of absorption coefficients uses a look-up table of 59 pressures with 5 temperatures per pressure level based around a mid-latitude summer profile.

The improved representation of CO2 in the window region (more minor gas k-terms in bands 5 and 6) provides a better forcing response to increases in CO2 (tested up to x32 present day).

Greenhouse gases included: H2O, CO2, O3, N2O, CH4, CFC11, CFC12, CFC113, HCFC22 and HFC134a.

Absorption due to Sulphur dioxide (SO2) and Carbonyl sulphide (OCS) is included based on HITRAN 2012 (only used for particular experimental configurations).

Total of 81 major gas k-terms. The new method of "hybrid" scattering may be used with this spectral file. This will run the full scattering solver for 27 of the major gas k-terms (where their nominal optical depth is less than 10 in a mid-latitude summer atmosphere). The remaining 54 k-terms (optical depth > 10) will use a much cheaper non-scattering solver.

Thermal emission

The Planckian function in each band is represented by a quartic fit in the temperature, generated by a least squares fit over the range 160 to 330 K. This increases the lower bound of the fit from 150K used with sp_lw_ga3_0 and slightly improves the fit over the important temperature range for the Earth's atmosphere.

3.3.3 Global Atmosphere Configuration 3

Spectral file: sp_sw_ga3_0 / spec_sw_ga3_0

Sections are identical to spec3a_sw_hadgem1_5o_rlfx except for changes to the solar spectrum (including Rayleigh coefficients), gaseous absorption, aerosols, and ice crystals:

Solar spectrum

The Lean (2000, updated) spectrum [Lean, 2000] is based on satellite observations at wavelengths shorter than 735nm with the Kurucz spectrum at longer wavelengths. The satellite observations provided monthly data which have been meaned over the last 2 solar cycles (between 1983 and 2004 inclusive).

Gaseous absorption

Changes to O3 k-terms in bands 1-3. The revision was made in order to improve ozone heating rate calculations and better incorporate solar variability. Briefly, the first UV band is divided into six relatively narrow sub-bands, each of which has only one ozone absorption coefficient so that, although the total number of bands is increased, the computational demands are similar to the previous k-distribution method for the UV band. Each new sub-band has physically realistic band limits and the ozone absorption coefficients are obtained from mean transmission functions calculated with high resolution (1 cm^{-1}) and using a fitting procedures similar to that described by Chou and Lee [1996]. Ozone cross-sections used in the calculations are a combination of Hitran2004 (0.24 - 0.34 μm), Molina and Molina [1986] (0.2 - 0.24 μm) and Voigt et al. [2001] (above 0.34 μm). This new broad-band model has greater accuracy due to the higher number of bands within the UV. It also provides an easier vehicle for experiments in which variations in the solar irradiance spectrum may be imposed because the k-distribution of lines is restricted to the narrower bands.

For more information see Zhong et al. [2008].

Aerosols

Addition of 4 aerosol species: Fresh and Aged OCFF (Organic Carbon Fossil Fuel), ‘delta’ aerosol, and nitrate aerosol. The optical properties of the 6 divisions of mineral dust have been revised using the set of refractive indices from Balkanski et al. [2007]. This makes mineral dust less absorbing in the SW and more absorbing in the LW.

Ice crystals

A new parametrisation for the optical properties of ice crystals has been developed by Anthony Baran based on the latest observed particle size distributions (from Paul Field) and an ensemble model of ice crystal type and orientation. The optical properties are linked directly to temperature and ice water content with no intermediate dependence on ice-crystal size. This parametrisation is added as type 9.

Spectral file: sp_lw_ga3_0 / spec_lw_ga3_0

spec_lw_ga3_0 is used for climate configurations and is favoured to spec_lw_ga3_1 principally where a more accurate treatment of the stratosphere is required. Sections are identical to spec3a_lw_hadgem1_5C except for changes to gaseous absorption, thermal emission, aerosols, and ice crystals (also note that obsolete coefficients for the continuum in band 9 have been removed):

Gaseous absorption

New k-terms have been provided by Wenyi Zhong for CO2 in band 4 and O3 in band 6. This increases the total number of k-terms by 14 (with a corresponding increase in computational cost) but allows for a more accurate treatment of stratospheric absorption. The k-terms for CO2 and O3 have been taken from a spectral file developed by Wenyi Zhong for the "Met Office Middle Atmosphere" model based on HadCM3 [Zhong and Haigh, 2000].

Thermal emission

The Planckian function in each band is represented by a quartic fit in the temperature, generated by a least squares fit over the range 150 to 330 K. The previous fit (using the range of 180 to 330 K) for spec3a_lw_hadgem1_5C could give negative emission for the very cold temperatures sometimes seen at the top of the model.

Aerosols

Addition of 4 aerosol species: Fresh and Aged OCFF (Organic Carbon Fossil Fuel), 'delta' aerosol, and nitrate aerosol. The optical properties of the 6 divisions of mineral dust have been revised using the set of refractive indices from Balkanski et al. [2007]. This makes mineral dust less absorbing in the SW and more absorbing in the LW. Aerosol Optical Depth coefficients have been altered accordingly.

Ice crystals

A new parametrisation (type 9) has been added to be used in conjunction with the new SW ice properties. These are based on the near-IR properties from spec_sw_ga3_0 as the full LW properties have not yet been modelled.

Spectral file: sp_lw_ga3_1 / spec_lw_ga3_1

spec_lw_ga3_1 is used for forecast configurations and is favoured to spec_lw_ga3_0 where speed of computation and more accurate treatment of the troposphere is required. Sections are identical to spec3a_lw_hadgem1_5C except for changes to aerosols and ice crystals (also note that obsolete coefficients for the continuum in band 9 have been removed):

Aerosols

Addition of 4 aerosol species: Fresh and Aged OCFF (Organic Carbon Fossil Fuel), 'delta' aerosol, and nitrate aerosol. The optical properties of the 6 divisions of mineral dust have been revised using the set of refractive indices from Balkanski et al. [2007]. This makes mineral dust less absorbing in the SW and more absorbing in the LW. Aerosol Optical Depth coefficients have been altered accordingly.

Ice crystals

A new parametrisation (type 9) has been added to be used in conjunction with the new SW ice properties. These are based on the near-IR properties from spec_sw_ga3_0 as the full LW properties have not yet been modelled.

Spectral files: sp_sw_cloud3_0 & sp_lw_cloud3_0

These are simple spectral files designed specifically for use with the "incremental radiative time-stepping" scheme for improved sampling of cloud. They represent regions of high transmissivity in the SW and LW in order to capture the radiative effects of changes in low cloud. A full description of these files is available in Manners et al. [2009]. (Namelist versions starting spec_ are also available.)

3.3.4 HadGEM2

Spectral file: spec3a_sw_hadgem1_5o_rlfx

spec3a_sw_hadgem1_5o_rlfx is used in the HadGEM2-A model and the global forecast model from PS20. All sections are identical to spec3a_sw_hadgem1_3 except for changes to aerosols and Rayleigh scattering:

Rayleigh scattering bug-fix

Rayleigh scattering coefficients in spec3a_sw_hadgem1_3 were found to be in error by approximately 20% due to a bug in the generating code. These are corrected here. Further information on this error and its impact in the global model is available in Haywood et al. [2008].

Aerosols

Mie scattering calculations have provided the optical properties for 7 additional aerosols: 6 size bins (also termed divisions) for mineral dust, and 1 mode representing biogenic aerosols from terpene emissions. The biogenic aerosol size distribution is lognormal, with a modal radius of 0.095 microns and a standard deviation of 1.5. Its density is 1300 kg/m3. Biogenic aerosols experience hygroscopic growth. In addition, parametrisations of Aitken Sulphate, Fresh Biomass (mode 1), and Aged Biomass (mode 2) have been changed. Aitken sulphate lognormal size distribution has now a modal radius of 0.0065 microns with a standard deviation of 1.3. Biomass aerosols are now hygroscopic following aircraft measurements. Their size distributions now use a modal radius of 0.1 and 0.12 microns for fresh and aged biomass, respectively, with a standard deviation of 1.3. Biomass aerosol density is now 1350 kg/m3.

Spectral file: spec3a_lw_hadgem1_5C

spec3a_lw_hadgem1_5C is used in the HadGEM2-A model and the global forecast model from PS20. All sections are identical to spec3a_lw_hadgem1_3 except for changes to aerosols:

Aerosols

Mie scattering calculations have provided the optical properties for 7 additional aerosols: 6 size bins (also termed divisions) for mineral dust, and 1 mode representing biogenic aerosols from terpene emissions. The biogenic aerosol size distribution is lognormal, with a modal radius of 0.095 microns and a standard deviation of 1.5. Its density is 1300 kg/m3. Biogenic aerosols experience hygroscopic growth. In addition, parametrisations of Aitken Sulphate, Fresh Biomass (mode 1), and Aged Biomass (mode 2) have been changed. Aitken sulphate lognormal size distribution has now a modal radius of 0.0065 microns with a standard deviation of 1.3. Biomass aerosols are now hygroscopic following aircraft measurements. Their size distributions now use a modal radius of 0.1 and 0.12 microns for fresh and aged biomass, respectively, with a standard deviation of 1.3. Biomass aerosol density is now 1350 kg/m3.

In addition, a new block, number 15, is introduced. It contains the specific absorption and scattering coefficients of each aerosol mode (in the same order as in the aerosol block 11). In contrast to the content of block 11, which are averaged across spectral bands, block-15 coefficients are monochromatic (given at specific wavelengths). They are used by the model to compute the aerosol optical depth at these wavelengths. There are 6 wavelengths, in the order: 0.38, 0.44, 0.55, 0.67, 0.87, 1.02 microns. As in the aerosol block 11, those aerosols which are hygroscopic have relative-humidity-dependent coefficients.

3.3.5 HadGEM1

Spectral file: spec3a_sw_hadgem1_3

spec3a_sw_hadgem1_3 is the standard SW spectral file for HadGEM1.

The spectrum is divided into six bands, the second and third of which are not true bands, as discussed above under the remarks on block 1.

The solar spectrum is based on that published by Kurucz [1995], and this is used in the frequency weighting of Rayleigh scattering coefficients.

Gaseous absorption

Gaseous absorption by water vapour, ozone, carbon dioxide and oxygen is included. Version 2.4 of the CKD continuum is included. The foreign component is combined with the line data and fitted as one entity. The self-broadened continuum is represented explicitly. The spectroscopic data used in generating the absorption data come from HITRAN2000, with the published corrections, augmented by theoretical weak lines and extra observations from ESA (see Zhong et al. [2001] for an introduction to this matter and further references). The data for gases other than water vapour are identical to those used in HadCM3, as described in Cusack et al. [1999].

Aerosols

Aerosols included comprise the five aerosols of the standard climatology (Cusack et al. [1998]) and two modes each for sulphate, black carbon, sea-salt and biomass aerosols and six divisions of dust aerosol. The properties of aerosols depend on their nature and the size distribution. Size distributions and optical properties for the climatological aerosols are specified as in the standard WMO report (see Cusack et al. [1998] for details). The single scattering parameters for aerosols are generated by running a Mie scattering code and averaging over the assumed size distribution. The climatology is specified in terms of an optical depth, but densities for the aerosols are not required or specified. However, the radiation code works in terms of mass extinction coefficients, so a density must be assumed. Provided that the same density is used in the code and in the generation of the spectral file, its value is irrelevant and a conventional density of 1000 kgm^{-3} has been assumed. If spectral data for the climatological aerosols are combined with mass-loadings specified other than through the climatology, it is necessary to consider whether this density is appropriate. Note that climatological aerosols will not be a part of the final standard version of HadGEM1, having been superceded by prognostics aerosols

Sulphate aerosols are hygroscopic, so their optical properties depend on the relative humidity. The nature of this dependence is a matter for aerosol modellers. From the point of view of generating radiative data, a size distribution of the dry aerosol must be assumed. Two distinct modes of aerosol are included in this file: the Aitken and accumulation modes. For each of these modes, a log-normal size distribution is assumed. For the Aitken mode, the modal radius, $\hat{r} = 24$ nm and the standard deviation $\sigma = 1.45$. In the case of the accumulation mode $\hat{r} = 95$ nm and $\sigma = 1.4$. The density of dry aerosol is taken as 1769 kgm^{-2}.

Black carbon aerosols not not hygroscopic. They are represented as fresh and aged aerosols, each obeying a log-normal distribution. In this case $\hat{r} = 40$ nm and $\sigma = 2.0$ for both modes. The density is taken as 1000 kgm^{-2}. (Note that these size distributions differ from those used in `spec3a_sw_3_asol2c_hadcm3`).

Film and jet modes of sea-salt aerosol are included. Data were generated using log-normal size distributions with $\hat{r} = 0.1$ μm and $\sigma = 2.0$ for the film mode and $\hat{r} = 1.0$ μm and $\sigma = 2.0$ for the jet mode.

Prognostic dust aerosols are modelled using six size classes with limits as follows: 6.32456E-8 – 2.0E-7 (m), 2.0E-7 – 6.32456E-7, 6.32456E-7 – 2.0E-6, 2.0E-6 – 6.32456E-6, 6.32456E-6 – 2.0E-5 and 2.0E-5 – 6.32456E-5. The size distribution is taken as uniform within each bin. The density of dust is taken as 2650 kgm^{-3}. Data were generated using a Mie scattering code, taking the refractive indices given by Deepak and Gerber [1983].

Two modes of biomass smoke are included. For the fresh smoke (biomass 1), a log-normal distribution with $\hat{r} = 69$ μm and $\sigma = 1.65$ is assumed. For the aged smoke (biomass 2), $\hat{r} = 200$ μm and $\sigma = 1.58$.

For further details about aerosols, the documentation on this area should be consulted.

Cloud droplets

Data for water droplets were generated using a Mie scattering code. Whilst a single size distribution may be assumed for each species of aerosol individually, size distributions for droplets vary widely, depending on the location and moisture content of the atmosphere. Some appropriate but variable measure of the size of droplet is required. For radiative purposes, the appropriate measure of size is the effective radius, r_e. r_e may be parametrized or imposed (see section 1). The numbers in the spectral file represent coefficients in a parametrization. They are generated by running a Mie scattering code for a number of different size distributions at a range of wavelengths, averaging the single scattering properties across the spectral bands, weighting with an appropriate function of frequency and then fitting using some appropriate function of the effective radius. This may clearly be done in many different ways, and to allow general freedom, the concept of a *type* of droplet is introduced. In the current file, four types are available, namely 2, 3, 4 and 5. In all cases the size distributions specified by Rockel et al. [1991] with effective radii in the range 1.5 – 50 microns were used as the basis of the Mie calculations. In particular, this uses a modified gamma distribution of this form:

$$\frac{\mathrm{d}n}{\mathrm{d}r} = \frac{N\beta\left(\frac{r}{r_m}\right)^{\alpha-1} e^{-\left(\frac{r}{r_m}\right)^{\beta}}}{r_m \Gamma\frac{\alpha}{\beta}} \tag{3.1}$$

with parameters: $\alpha = (1/N_e) - 2$, $\beta = 1$, $r_m = N_e R_e$ 1.0E-6. Where the distribution variance (N_e) takes a number of values: $N_e = 0.01, 0.1, 0.175, 0.25$.

Calculations are done for each N_e value at a number of different effective radii (R_e) and then a fit is made for each of the optical properties (extinction, single scattering albedo, asymmetry) against effective radius.

Weighting was carried out using the solar spectrum of Labs and Neckel [1970]. In the case of types 2 and 4, the method of thin averaging (Edwards and Slingo [1996]) was used, whereas for types 3 and 5, the method of thick averaging was used. Types 2 and 3 have in fact been retained for historical consistency with HadAM3 and are based on the linear fits of the functional form of Slingo and Schrecker [1982]. Simple linear fits do not allow the use of a wide range of particles sizes, as was required for use with the wider range of studies of the indirect effects of sulphate envisaged with HadAM4. To meet this need, new Padé fits were developed, and their use is recommended. Type 4 corresponds to thin averaging and type 5 to thick averaging. The use of type 5 is preferred for both convective and large-scale clouds.

Ice crystals

The generation of single-scattering data for ice crystals is more complicated than for water clouds, because issues of crystal shape must be addressed. When HadAM3 was defined, methods for generating single-scattering data for non-spherical particles were not available, so data for ice particles were generated analogously to the approach for water droplets, using the size distributions for ice particles given by Rockel et al. [1991] with effective radii in the range 24 – 80 microns, weighting with the solar spectrum of Labs and Neckel [1970] and using thin averaging for type 2 and thick averaging for type 3. In this case, because large-scale ice cloud is often thin, we recommend the use of type 2 for large-scale cloud, but type 3 for convective cloud. Since the definition of HadAM3, progress has been made with the treatment of non-spherical particles. Type 7 invokes a treatment of ice crystals as planar polycrystals, based on the anomalous diffraction approximation (see Kristjánsson et al. [1999] and Kristjánsson et al. [2000]). In this case, the parameters represent a fit in terms of the mean maximum dimension of the crystals. The mean maximum dimension is predicted in the model. At releases up to 5.5, the use of this ice scheme automatically selects this method of specifying the crystal size. A new parametrization [Edwards et al., 2007] was introduced for ice crystals at 5.5. This is based on the representation of ice aggregates introduced by Baran et al. [2001]. The data were generated from the aggregate database (A. J. Baran pres. comm.) using 83 representative size distributions measured during CEPEX and fitted using the appropriate functional form. Thin averaging was performed. Note that this fit is provided in terms of the effective dimension. It may be selected by choosing type 8 for ice crystals.

Thickly averaged data are not available for ice crystals. (*Technical Note: Kristjánsson et al. [2000] use tenth-order polynomial fits to the optical properties, but the parametrization in this file is based on two splined quartic fits. The two fits are to the same data, but the tenth order scheme was used in the paper for the convenience of running a common scheme in CCM3 and the UM: the splined quartic fit had already become part of HadAM4 when the tenth-order fit was developed.*)

Spectral file: spec3a_lw_hadgem1_3

spec3a_lw_hadgem1_3 is the standard longwave spectral file for HadGEM1. The spectrum is divided into nine bands, the third and fifth of which are split, as discussed above under the remarks on block 14.

The Planckian function in each band is represented by a quartic fit in the temperature, generated by a least squares fit over the range 180 to 330 K.

Gaseous absorption

Gaseous absorption by water vapour, ozone, carbon dioxide, methane, nitrous oxide, CFC11, CFC12, CFC113, HCFC22, HFC125 and HFC134a is included. The spectroscopic data used in generating the absorption coefficients for gases other than the halocarbons and water vapour come from HITRAN92: for further details see Cusack et al. [1999]. Absorption cross-sections for the halocarbons were based on data supplied by K. Shine (pers. comm.). Data for absorption by water vapour were generated from HITRAN2000. The water vapour continuum is represented using version 2.4 of the CKD model. The self-broadened continuum is represented explicitly, while the foreign broadened continuum is combined with the line absorption, the combined absorption being fitted as if it were line data.

Aerosols

Aerosols included comprise the five aerosols of the standard climatology (Cusack et al. [1998]), two modes each for sulphate, black carbon, sea-salt and biomass aerosols and six divisions of dust aerosol. The properties of aerosols depend on their nature and the size distribution. Size distributions and optical properties for the climatological aerosols are specified as in the standard WMO report (see Cusack et al. [1998] for details). The single scattering parameters for aerosols are generated by running a Mie scattering code and averaging over the assumed size distribution. The climatology is specified in terms of an optical depth, but densities for the aerosols are not required or specified. However, the radiation code works in terms of mass extinction coefficients, so a density must be assumed. Provided that the same density is used in the code and in the generation of the spectral file, its value is irrelevant and a conventional density of 1000 kgm^{-3} has been assumed. If spectral data for the climatological aerosols are combined with mass-loadings specified other than through the climatology, it is necessary to consider whether this density is appropriate. Note that climatological aerosols are not included in the standard version of HadGEM1, being replaced by prognostic aerosols.

Sulphate aerosols are hygroscopic, so their optical properties depend on the relative humidity. The nature of this dependence is a matter for aerosol modellers. From the point of view of generating radiative data, a size distribution of the dry aerosol must be assumed. Two distinct modes of aerosol are included in this file: the Aitken and accumulation modes. For each of these modes, a log-normal size distribution is assumed. For the Aitken mode, the modal radius, $\hat{r}$ = 24 nm and the standard deviation $\sigma = 1.45$. In the case of the accumulation mode $\hat{r} = 95$ nm and $\sigma = 1.4$. The density of dry aerosol is taken as 1769 kgm^{-2}.

Black carbon aerosols not not hygroscopic. They are represented as fresh and aged aerosols, each obeying a log-normal distribution. In this case $\hat{r} = 40$ nm and $\sigma = 2.0$ for the both the fresh and modes.

Film and jet modes of sea-salt aerosol are included. Data were generated for log-normal size distributions with $\hat{r} = 0.1$ μm and $\sigma = 2.0$ for the film mode and $\hat{r} = 1.0$ μm and $\sigma = 2.0$ for the jet mode.

Prognostic dust aerosols are modelled using six size classes with limits as follows: 6.32456E-8 – 2.0E-7 (m), 2.0E-7 – 6.32456E-7, 6.32456E-7 – 2.0E-6, 2.0E-6 – 6.32456E-6, 6.32456E-6 – 2.0E-5 and 2.0E-5 – 6.32456E-5. The size distribution is taken as uniform within each bin. The density of dust is taken as 2650 kgm^{-3}. Data were generated using a Mie scattering code, taking the refractive indices given by Deepak and Gerber [1983].

Two modes of biomass smoke are included. For the fresh smoke (biomass 1), a log-normal distribution with $\hat{r} = 69$ μm and $\sigma = 1.65$ is assumed. For the aged smoke (biomass 2), $\hat{r} = 200$ μm and $\sigma = 1.58$.

For further details about aerosols, the documentation on this area should be consulted.

Cloud droplets

Data for water droplets were generated using a Mie scattering code. Whilst a single size distribution may be assumed for each species of aerosol individually, size distributions for droplets vary widely, depending on the location and moisture content of the atmosphere. Some appropriate but variable measure of the size of droplet is required. For radiative purposes, the appropriate measure of size is the effective radius, r_e. r_e may be parametrized or imposed (see section 1). The numbers in the spectral file represent coefficients in a parametrization. They are generated by running a Mie scattering code for a number of different size distributions at a range of wavelengths, averaging the single scattering properties across the spectral bands, weighting with an appropriate function of frequency and then fitting using some appropriate function of the effective radius. This may clearly be done in many different ways, and to allow general freedom, the concept of a *type* of droplet is introduced. Data for type 1 were obtained by using the size distributions specified by Rockel et al. [1991] with effective radii in the range 1.5 – 50 microns as the basis of the Mie calculations. Weighting was carried out using a Planckian function at a temperature of 250 K, and spectral averaging was carried out using the method of thin averaging (Edwards and Slingo [1996]) and the functional form of Slingo and Schrecker [1982] was used for fitting. These data are retained for historical consistency and the use of the Padé fits of types 4 and 5, which are valid over a wider range of effective radii is now recommended. These data were generated from the same sources as type 1, but differ in the fitting used. Type 4 was generated using thin averaging and type 5 with thick averaging.

Ice crystals

The generation of single-scattering data for ice crystals is more complicated than for water clouds, because issues of crystal shape must be addressed. When HadAM3 was defined, methods for generating single-scattering data for non-spherical particles were not available, so data for ice particles were generated analogously to the approach for water droplets, using the size distributions for ice particles given by Rockel et al. [1991] with effective radii in the range 24 – 80 microns, weighting with the a Planckian function at 250 K and using thin averaging. The functional form of Slingo and Schrecker [1982] was used again: only data for type 1 were initially available. Since the definition of HadAM3, progress has been made with the treatment of non-spherical particles. Type 7 invokes a treatment of ice crystals as planar polycrystals, based on the anomalous diffraction approximation (see Kristjánsson et al. [1999] and Kristjánsson et al. [2000]). In this case, the parameters represent a fit in terms of the mean maximum dimension of the crystals. The mean maximum dimension is predicted in the model. At releases up to 5.5, the use of this ice scheme automatically selects this method of specifying the crystal size. A new parametrization [Edwards et al., 2007] was introduced for ice crystals at 5.5. This is based on the representation of ice aggregates introduced by Baran [2003]. The data were generated from the aggregate database (A. J. Baran pres. comm.) using 83 representative size distributions measured during CEPEX and fitted using the appropriate functional form. Thin averaging was performed. Note that this fit is provided in terms of the effective dimension. It may be selected by choosing type 8 for ice crystals. Thickly averaged data are not available for non-spherical ice crystals. (*Technical Note: Kristjánsson et al. [2000] use tenth-order polynomial fits to the optical properties, but the parametrization in this file is based on two splined quartic fits. The two fits are to the same data, but the tenth order scheme was used in the paper for the convenience of running a common scheme in CCM3 and the UM: the splined quartic fit had already become part of HadAM4 when the tenth-order fit was developed.*)

3.3.6 Older spectral files

1. `spec3a_sw_3_asol2c_hadcm3` is the standard shortwave spectral file used in HadCM3 runs. The spectrum is divided into six bands, the second and third of which are not true bands, as discussed above under the remarks on block 1.

   The solar spectrum is based on that published by Labs and Neckel [1970], and this is used in the frequency weighting of Rayleigh scattering coefficients.

   Gaseous absorption by water vapour (without the continuum), ozone, carbon dioxide and oxygen is included. The spectroscopic data used in generating the absorption data come from HITRAN92, except for the data on ozone which were generated from LOWTRAN7: for further details see Cusack et al. [1999].

   Aerosols included comprise the five aerosols of the standard climatology (Cusack et al. [1998]), two modes of sulphate aerosol and two modes of black carbon aerosol. The properties of aerosols depend on their nature and the size distribution. Size distributions and optical properties for the climatological aerosols are specified as in the standard WMO report (see Cusack et al. [1998] for details). The single scattering parameters for aerosols are generated by running a Mie scattering code and averaging over the assumed size distribution. The climatology is specified in terms of an optical depth, but densities for the aerosols are not required or specified. However, the radiation code works in terms of mass extinction coefficients, so a density must be assumed. Provided that the same density is used in the code and in the generation of the spectral file, its value is irrelevant and a conventional density of 1000 kgm^{-3} has been assumed. If spectral data for the climatological aerosols are combined with mass-loadings specified other than through the climatology, it is necessary to consider whether this density is appropriate.

Sulphate aerosols are hygroscopic, so their optical properties depend on the relative humidity. The nature of this dependence is a matter for aerosol modellers. From the point of view of generating radiative data, a size distribution of the dry aerosol must be assumed. Two distinct modes of aerosol are included in this file: the Aitken and accumulation modes. For each of these modes, a log-normal size distribution is assumed. For the Aitken mode, the modal radius, $\hat{r} = 24$ nm and the standard deviation $\sigma = 1.45$. In the case of the accumulation mode $\hat{r} = 95$ nm and $\sigma = 1.4$. The density of dry aerosol is taken as 1769 kgm^{-2}.

Black carbon aerosols not not hygroscopic. They are represented as fresh and aged aerosols, each obeying a log-normal distribution. In this case $\hat{r} = 20$ nm and $\sigma = 2.0$ for the fresh modes, but $\hat{r} = 100$ nm and $\sigma = 2.0$ for the aged mode. The density is taken as 1000 kgm^{-2}.

Data for water droplets were generated using a Mie scattering code. Whilst a single size distribution may be assumed for each species of aerosol individually, size distributions for droplets vary widely, depending on the location and moisture content of the atmosphere. Some appropriate but variable measure of the size of droplet is required. For radiative purposes, the appropriate measure of size is the effective radius, r_e. r_e may be parametrized or imposed (see section 1). The numbers in the spectral file represent coefficients in a parametrization. They are generated by running a Mie scattering code for a number of different size distributions at a range of wavelengths, averaging the single scattering properties across the spectral bands, weighting with an appropriate function of frequency and then fitting using some appropriate function of the effective radius. This may clearly be done in many different ways, and to allow general freedom, the concept of a *type* of droplet is introduced. In the current file, two types are available, namely 2 and 3. In both cases the size distributions specified by Rockel et al. [1991] with effective radii in the range 1.5 – 50 microns were used as the basis of the Mie calculations. Weighting was carried out using the solar spectrum of Labs and Neckel [1970]. In the case of type 2, the method of thin averaging (Edwards and Slingo [1996]) was used, whereas for type 3, the method of thick averaging was used. In both cases the functional form of Slingo and Schrecker [1982] was used. Tests against more highly spectrally resolved data suggest that thick averaging is more representative for water clouds, and the use of type 3 for both large-scale and convective clouds is recommended.

The generation of single-scattering data for ice crystals is more complicated than for water clouds, because issues of crystal shape must be addressed. When HadAM3 was defined, methods for generating single-scattering data for non-spherical particles were not available, so data for ice particles were generated analogously to the approach for water droplets, using the size distributions for ice particles given by Rockel et al. [1991] with effective radii in the range $24-80$ microns, weighting with the solar spectrum of Labs and Neckel [1970] and using thin averaging for type 2 and thick averaging for type 3. In this case, because large-scale ice cloud is often thin, we recommend the use of type 2 for large-scale cloud, but type 3 for convective cloud. Since the definition of HadAM3, progress has been made with the treatment of non-spherical particles. Type 7 invokes a treatment of ice crystals as planar polycrystals, based on the anomalous diffraction approximation (see Kristjánsson et al. [1999] and Kristjánsson et al. [2000]). In this case, the parameters represent a fit in terms of the mean maximum dimension of the crystals. The mean maximum dimension is predicted in the model. At releases up to 5.5, the use of this ice scheme automatically selects this method of specifying the crystal size. Thickly averaged data are not available for non-spherical ice crystals. (*Technical Note: Kristjánsson et al. [2000] use tenth-order polynomial fits to the optical properties, but the parametrization in this file is based on two splined quartic fits. The two fits are to the same data, but the tenth order scheme was used in the paper for the convenience of running a common scheme in CCM3 and the UM: the splined quartic fit had already become part of HadAM4 when the tenth-order fit was developed.*)

2. `spec3a_sw_hadcm4` is the standard shortwave spectral file used in HadAM4 runs. The spectrum is divided into six bands, the second and third of which are not true bands, as discussed above under the remarks on block 1.

   The solar spectrum is based on that published by Labs and Neckel [1970], and this is used in the frequency weighting of Rayleigh scattering coefficients.

   Gaseous absorption by water vapour, ozone, carbon dioxide and oxygen is included. Version 2.1 of the CKD continuum is included. The foreign component is combined with the line data and fitted as one entity. The self-broadened continuum is represented explicitly. The spectroscopic data used in generating the absorption data come from HITRAN92. Absorption by water vapour in the near infra-red has been improved relative to the treatment in `spec3a_sw_asol2c_hadcm4`, as used in HadCM3, by the addition of an extra k-term in the fourth band. The data for gases other than water vapour are identical to those used in HadCM3, as described in Cusack et al. [1999].

   Aerosols included comprise the five aerosols of the standard climatology (Cusack et al. [1998]), and two modes of sulphate aerosols. The properties of aerosols depend on their nature and the size distribution. Size distributions and optical properties for the climatological aerosols are specified as in the standard WMO report (see Cusack et al. [1998] for details). The single scattering parameters for aerosols are generated by running a Mie scattering code and averaging over the assumed size distribution. The climatology is specified in terms of an optical depth, but densities for the aerosols are not required or specified. However, the radiation code works in terms of mass extinction coefficients, so a density must be assumed. Provided that the same density is used in the code and in the generation of the spectral file, its value is irrelevant and a conventional density of 1000 kgm^{-3} has been assumed. If spectral data for the climatological aerosols are combined with mass-loadings specified other than through the climatology, it is necessary to consider whether this density is appropriate.

Sulphate aerosols are hygroscopic, so their optical properties depend on the relative humidity. The nature of this dependence is a matter for aerosol modellers. From the point of view of generating radiative data, a size distribution of the dry aerosol must be assumed. Two distinct modes of aerosol are included in this file: the Aitken and accumulation modes. For each of these modes, a log-normal size distribution is assumed. For the Aitken mode, the modal radius, $\hat{r} = 24$ nm and the standard deviation $\sigma = 1.45$. In the case of the accumulation mode $\hat{r} = 95$ nm and $\sigma = 1.4$. The density of dry aerosol is taken as 1769 kgm^{-2}.

Data for water droplets were generated using a Mie scattering code. Whilst a single size distribution may be assumed for each species of aerosol individually, size distributions for droplets vary widely, depending on the location and moisture content of the atmosphere. Some appropriate but variable measure of the size of droplet is required. For radiative purposes, the appropriate measure of size is the effective radius, r_e. r_e may be parametrized or imposed (see section 1). The numbers in the spectral file represent coefficients in a parametrization. They are generated by running a Mie scattering code for a number of different size distributions at a range of wavelengths, averaging the single scattering properties across the spectral bands, weighting with an appropriate function of frequency and then fitting using some appropriate function of the effective radius. This may clearly be done in many different ways, and to allow general freedom, the concept of a *type* of droplet is introduced. In the current file, four types are available, namely 2, 3, 4 and 5. In all cases the size distributions specified by Rockel et al. [1991] with effective radii in the range 1.5 – 50 microns were used as the basis of the Mie calculations. Weighting was carried out using the solar spectrum of Labs and Neckel [1970]. In the case of types 2 and 4, the method of thin averaging (Edwards and Slingo [1996]) was used, whereas for types 3 and 5, the method of thick averaging was used. Types 2 and 3 have in fact been retained for historical consistency with HadAM3 and are based on the linear fits of the functional form of Slingo and Schrecker [1982]. Simple linear fits do not allow the use of a wide range of particles sizes, as was required for use with the wider range of studies of the indirect effects of sulphate envisaged with HadAM4. To meet this need, new Padé fits were developed, and their use is recommended. Type 4 corresponds to thin averaging and type 5 to thick averaging. The use of type 5 is preferred for both convective and large-scale clouds.

The generation of single-scattering data for ice crystals is more complicated than for water clouds, because issues of crystal shape must be addressed. When HadAM3 was defined, methods for generating single-scattering data for non-spherical particles were not available, so data for ice particles were generated analogously to the approach for water droplets, using the size distributions for ice particles given by Rockel et al. [1991] with effective radii in the range 24 – 80 microns, weighting with the solar spectrum of Labs and Neckel [1970] and using thin averaging for type 2 and thick averaging for type 3. In this case, because large-scale ice cloud is often thin, we recommend the use of type 2 for large-scale cloud, but type 3 for convective cloud. Since the definition of HadAM3, progress has been made with the treatment of non-spherical particles. Type 7 invokes a treatment of ice crystals as planar polycrystals, based on the anomalous diffraction approximation (see Kristjánsson et al. [1999] and Kristjánsson et al. [2000]). In this case, the parameters represent a fit in terms of the mean maximum dimension of the crystals. The mean maximum dimension is predicted in the model. At releases up to 5.5, the use of this ice scheme automatically selects this method of specifying the crystal size. Thickly averaged data are not available for ice crystals. (*Technical Note: Kristjánsson et al. [2000] use tenth-order polynomial fits to the optical properties, but the parametrization in this file is based on two splined quartic fits. The two fits are to the same data, but the tenth order scheme was used in the paper for the convenience of running a common scheme in CCM3 and the UM: the splined quartic fit had already become part of HadAM4 when the tenth-order fit was developed.*)

3. `spec3a_sw_h4_meso2` is a spectral file designed for use with the mesoscale mode. *Important Note: This file has been developed for use where speed of execution is critical and the balance between speed and accuracy is very much toward speed, with minimal numbers of k-terms being used for each gas. It is used operationally only for mesoscale runs out to 36 hours and not for global or climate runs. Its use for off-line radiation calculations is not encouraged.*

   The shortwave spectral region is divided into five bands. The solar spectrum is based on that published by Labs and Neckel [1970], and this is used in the frequency weighting of Rayleigh scattering coefficients.

   Gaseous absorption by water vapour, ozone and carbon dioxide is included. Version 2.1 of the CKD continuum is included: here the self and foreign components of the continuum are treated separately. The spectroscopic data used in generating the absorption data come from HITRAN92.

   Aerosols included comprise the five aerosols of the standard climatology (Cusack et al. [1998]). The properties of aerosols depend on their nature and the size distribution. Size distributions and optical properties for the climatological aerosols are specified as in the standard WMO report (see Cusack et al. [1998] for details). The single scattering parameters for aerosols are generated by running a Mie scattering code and averaging over the assumed size distribution. The climatology is specified in terms of an optical depth, but densities for the aerosols are not required or specified. However, the radiation code works in terms of mass extinction coefficients, so a density must be assumed. Provided that the same density is used in the code and in the generation of the spectral file, its value is irrelevant and a conventional density of 1000 kgm^{-3} has been assumed. If spectral data for the climatological aerosols are combined with mass-loadings specified other than through the climatology, it is necessary to consider whether this density is appropriate.

   Data for water droplets were generated using a Mie scattering code. Whilst a single size distribution may be assumed for each species of aerosol individually, size distributions for droplets vary widely, depending on the location and moisture content of the atmosphere. Some appropriate but variable measure of the size of droplet is required. For radiative purposes, the appropriate measure of size is the effective radius, r_e. r_e may be parametrized or imposed (see section 1). The numbers in the spectral file represent coefficients in a parametrization. They are generated by running a Mie scattering code for a number of different size distributions at a range of wavelengths, averaging the single scattering properties across the spectral bands, weighting with an appropriate function of frequency and then fitting using some appropriate function of the effective radius. This may clearly be done in many different ways, and to allow general freedom, the concept of a *type* of droplet is introduced. In the current file, four types are available, namely 2, 3, 4 and 5. In all cases the size distributions specified by Rockel et al. [1991] were used as the basis of the Mie calculations. Weighting was carried out using the solar spectrum of Labs and Neckel [1970]. In the case of types 2 and 4, the method of thin averaging (Edwards and Slingo [1996]) was used, whereas for types 3 and 5, the method of thick averaging was used. Types 2 and 3 have in fact been retained for historical consistency with HadAM3 and are based on the linear fits of the functional form of Slingo and Schrecker [1982]. Simple linear fits do not allow the use of a wide range of particles sizes, as was required for use with the wider range of studies of the indirect effects of sulphate envisaged with HadAM4. To meet this need, new Padé fits were developed, and their use is recommended. Type 4 corresponds to thin averaging and type 5 to thick averaging. The use of type 5 is preferred for both convective and large-scale clouds.

The generation of single-scattering data for ice crystals is more complicated than for water clouds, because issues of crystal shape must be addressed. When HadAM3 was defined, methods for generating single-scattering data for non-spherical particles were not available, so data for ice particles were generated analogously to the approach for water droplets, using the size distributions for ice particles given by Rockel et al. [1991] with effective radii in the range 24 − 80 microns, weighting with the solar spectrum of Labs and Neckel [1970] and using thin averaging for type 2 and thick averaging for type 3. In this case, because large-scale ice cloud is often thin, we recommend the use of type 2 for large-scale cloud, but type 3 for convective cloud. Since the definition of HadAM3, progress has been made with the treatment of non-spherical particles. Type 7 invokes a treatment of ice crystals as planar polycrystals, based on the anomalous diffraction approximation (see Kristjánsson et al. [1999] and Kristjánsson et al. [2000]). In this case, the parameters represent a fit in terms of the mean maximum dimension of the crystals. The mean maximum dimension is predicted in the model. At releases up to 5.5, the use of this ice scheme automatically selects this method of specifying the crystal size. Thickly averaged data are not available for ice crystals. (*Technical Note: Kristjánsson et al. [2000] use tenth-order polynomial fits to the optical properties, but the parametrization in this file is based on two splined quartic fits. The two fits are to the same data, but the tenth order scheme was used in the paper for the convenience of running a common scheme in CCM3 and the UM: the splined quartic fit had already become part of HadAM4 when the tenth-order fit was developed.*)

4. `spec3a_lw_3_asol2c_hadcm3` is the standard longwave spectral file used in HadCM3 runs. The spectrum is divided into eight bands, the third and fifth of which are split, as discussed above under the remarks on block 14.

   The Planckian function in each band is represented by a quartic fit in the temperature, generated by a least squares fit over the range 200 to 300 K.

Gaseous absorption by water vapour, ozone, carbon dioxide, methane, nitrous oxide, CFC11, CFC12, CFC113, HCFC22, HFC125 and HFC134a is included. The spectroscopic data used in generating the absorption parametrizations for gases other than halocarbons come from HITRAN92: for further details see Cusack et al. [1999]. Data for CFC11 and CFC12 are taken from Varanasi and Chudamani [1988], while cross-sectional data for other gases were supplied by K. Shine (pers. comm.). (*Note in respect of potential revision of these data: Cross-sectional data are now included in the HITRAN database and the use of this source of data is recommended for future work.*) The water vapour continuum is represented using version 2.1 of the CKD model. The self-broadened continuum is represented explicitly, while the foreign broadened continuum is combined with the line absorption, the combined absorption being fitted as if it were line data.

Aerosols included comprise the five aerosols of the standard climatology (Cusack et al. [1998]), two modes of sulphate aerosol and two modes of black carbon aerosol. The properties of aerosols depend on their nature and the size distribution. Size distributions and optical properties for the climatological aerosols are specified as in the standard WMO report (see Cusack et al. [1998] for details). The single scattering parameters for aerosols are generated by running a Mie scattering code and averaging over the assumed size distribution. The climatology is specified in terms of an optical depth, but densities for the aerosols are not required or specified. However, the radiation code works in terms of mass extinction coefficients, so a density must be assumed. Provided that the same density is used in the code and in the generation of the spectral file, its value is irrelevant and a conventional density of 1000 kgm^{-3} has been assumed. If spectral data for the climatological aerosols are combined with mass-loadings specified other than through the climatology, it is necessary to consider whether this density is appropriate.

Sulphate aerosols are hygroscopic, so their optical properties depend on the relative humidity. The nature of this dependence is a matter for aerosol modellers. From the point of view of generating radiative data, a size distribution of the dry aerosol must be assumed. Two distinct modes of aerosol are included in this file: the Aitken and accumulation modes. For each of these modes, a log-normal size distribution is assumed. For the Aitken mode, the modal radius, $\hat{r} = 24$ nm and the standard deviation $\sigma = 1.45$. In the case of the accumulation mode $\hat{r} = 95$ nm and $\sigma = 1.4$. The density of dry aerosol is taken as 1769 kgm^{-2}.

Black carbon aerosols not not hygroscopic. They are represented as fresh and aged aerosols, each obeying a log-normal distribution. In this case $\hat{r} = 20$ nm and $\sigma = 2.0$ for the fresh modes, but $\hat{r} = 100$ nm and $\sigma = 2.0$ for the aged mode. The density is taken as 1000 kgm^{-2}.

Data for water droplets were generated using a Mie scattering code. Whilst a single size distribution may be assumed for each species of aerosol individually, size distributions for droplets vary widely, depending on the location and moisture content of the atmosphere. Some appropriate but variable measure of the size of droplet is required. For radiative purposes, the appropriate measure of size is the effective radius, r_e. r_e may be parametrized or imposed (see section 1). The numbers in the spectral file represent coefficients in a parametrization. They are generated by running a Mie scattering code for a number of different size distributions at a range of wavelengths, averaging the single scattering properties across the spectral bands, weighting with an appropriate function of frequency and then fitting using some appropriate function of the effective radius. This may clearly be done in many different ways, and to allow general freedom, the concept of a *type* of droplet is introduced. In this file, only one type is available, type 1. The size distributions specified by Rockel et al. [1991] with effective radii in the range 1.5 – 50 microns were used as the basis of the Mie calculations. Weighting was carried out using a Planckian function at a temperature of 250 K, and spectral averaging was carries out using the method of thin averaging (Edwards and Slingo [1996]). The functional form of Slingo and Schrecker [1982] was used for fitting.

The generation of single-scattering data for ice crystals is more complicated than for water clouds, because issues of crystal shape must be addressed. When HadAM3 was defined, methods for generating single-scattering data for non-spherical particles were not available, so data for ice particles were generated analogously to the approach for water droplets, using the size distributions for ice particles given by Rockel et al. [1991] with effective radii in the range 24 – 80 microns, weighting with the a Planckian function at 250 K and using thin averaging. The functional form of Slingo and Schrecker [1982] was used again: only data for type 1 were initially available. Since the definition of HadAM3, progress has been made with the treatment of non-spherical particles. Type 7 invokes a treatment of ice crystals as planar polycrystals, based on the anomalous diffraction approximation (see Kristjánsson et al. [1999] and Kristjánsson et al. [2000]). In this case, the parameters represent a fit in terms of the mean maximum dimension of the crystals. The mean maximum dimension is predicted in the model. At releases up to 5.5, the use of this ice scheme automatically selects this method of specifying the crystal size. Thickly averaged data are not available for non-spherical ice crystals. (*Technical Note: Kristjánsson et al. [2000] use tenth-order polynomial fits to the optical properties, but the parametrization in this file is based on two splined quartic fits. The two fits are to the same data, but the tenth order scheme was used in the paper for the convenience of running a common scheme in CCM3 and the UM: the splined quartic fit had already become part of HadAM4 when the tenth-order fit was developed.*)

5. `spec3a_lw_hadcm4_N` is the standard longwave spectral file used in HadAM4 runs. The spectrum is divided into nine bands, the third and fifth of which are split, as discussed above under the remarks on block 14. This nine-band configuration was developed from that used in HadAM3. In order to improve the treatment of the spectral overlap between absorption by methane and nitrous oxide in the region 1200 – 1500 cm^{-1}, it was decided to split the original seventh spectral band, but as tuning of HadAM4 was well advenced at that stage, it was desired not to alter the spectral characteristics of absorption by water vapour. Consequently, the seventh and eighth bands are not true spectral bands (see the general discussion of block 1 above).

   The Planckian function in each band is represented by a quartic fit in the temperature, generated by a least squares fit over the range 200 to 300 K, but the fits for bands 7 and 8 are a partitioning of the fit for the region 1200 – 1500 cm^{-1} for the reasons discussed above.

Gaseous absorption by water vapour, ozone, carbon dioxide, methane, nitrous oxide, CFC11, CFC12, CFC113, HCFC22, HFC125 and HFC134a is included. The spectroscopic data used in generating the absorption coefficients for gases other than the halocarbons come from HITRAN92: for further details see Cusack et al. [1999]. Absorption cross-sections for the halocarbons were based on data supplied by K. Shine (pers. comm.). The water vapour continuum is represented using version 2.1 of the CKD model. The self-broadened continuum is represented explicitly, while the foreign broadened continuum is combined with the line absorption, the combined absorption being fitted as if it were line data.

Aerosols included comprise the five aerosols of the standard climatology (Cusack et al. [1998]) and two modes of sulphate aerosol. The properties of aerosols depend on their nature and the size distribution. Size distributions and optical properties for the climatological aerosols are specified as in the standard WMO report (see Cusack et al. [1998] for details). The single scattering parameters for aerosols are generated by running a Mie scattering code and averaging over the assumed size distribution. The climatology is specified in terms of an optical depth, but densities for the aerosols are not required or specified. However, the radiation code works in terms of mass extinction coefficients, so a density must be assumed. Provided that the same density is used in the code and in the generation of the spectral file, its value is irrelevant and a conventional density of 1000 kgm^{-3} has been assumed. If spectral data for the climatological aerosols are combined with mass-loadings specified other than through the climatology, it is necessary to consider whether this density is appropriate.

Sulphate aerosols are hygroscopic, so their optical properties depend on the relative humidity. The nature of this dependence is a matter for aerosol modellers. From the point of view of generating radiative data, a size distribution of the dry aerosol must be assumed. Two distinct modes of aerosol are included in this file: the Aitken and accumulation modes. For each of these modes, a log-normal size distribution is assumed. For the Aitken mode, the modal radius, $\hat{r} = 24$ nm and the standard deviation $\sigma = 1.45$. In the case of the accumulation mode $\hat{r} = 95$ nm and $\sigma = 1.4$. The density of dry aerosol is taken as 1769 kgm^{-2}.

Data for water droplets were generated using a Mie scattering code. Whilst a single size distribution may be assumed for each species of aerosol individually, size distributions for droplets vary widely, depending on the location and moisture content of the atmosphere. Some appropriate but variable measure of the size of droplet is required. For radiative purposes, the appropriate measure of size is the effective radius, r_e. r_e may be parametrized or imposed (see section 1). The numbers in the spectral file represent coefficients in a parametrization. They are generated by running a Mie scattering code for a number of different size distributions at a range of wavelengths, averaging the single scattering properties across the spectral bands, weighting with an appropriate function of frequency and then fitting using some appropriate function of the effective radius. This may clearly be done in many different ways, and to allow general freedom, the concept of a *type* of droplet is introduced. Data for type 1 were obtained by using the size distributions specified by Rockel et al. [1991] with effective radii in the range 1.5 – 50 microns as the basis of the Mie calculations. Weighting was carried out using a Planckian function at a temperature of 250 K, and spectral averaging was carried out using the method of thin averaging (Edwards and Slingo [1996]) and the functional form of Slingo and Schrecker [1982] was used for fitting. These data are retained for historical consistency and the use of the Padé fits of types 4 and 5, which are valid over a wider range of effective radii is now recommended. These data were generated from the same sources as type 1, but differ in the fitting used. Type 4 was generated using thin averaging and type 5 with thick averaging.

The generation of single-scattering data for ice crystals is more complicated than for water clouds, because issues of crystal shape must be addressed. When HadAM3 was defined, methods for generating single-scattering data for non-spherical particles were not available, so data for ice particles were generated analogously to the approach for water droplets, using the size distributions for ice particles given by Rockel et al. [1991] with effective radii in the range 24 – 80 microns, weighting with the a Planckian function at 250 K and using thin averaging. The functional form of Slingo and Schrecker [1982] was used again: only data for type 1 were initially available. Since the definition of HadAM3, progress has been made with the treatment of non-spherical particles. Type 7 invokes a treatment of ice crystals as planar polycrystals, based on the anomalous diffraction approximation (see Kristjánsson et al. [1999] and Kristjánsson et al. [2000]). In this case, the parameters represent a fit in terms of the mean maximum dimension of the crystals. The mean maximum dimension is predicted in the model. At releases up to 5.5, the use of this ice scheme automatically selects this method of specifying the crystal size. Thickly averaged data are not available for non-spherical ice crystals. (*Technical Note: Kristjánsson et al. [2000] use tenth-order polynomial fits to the optical properties, but the parametrization in this file is based on two splined quartic fits. The two fits are to the same data, but the tenth order scheme was used in the paper for the convenience of running a common scheme in CCM3 and the UM: the splined quartic fit had already become part of HadAM4 when the tenth-order fit was developed.*)

6. `spec3a_lw_h4_meso2` is a spectral file designed for use with the mesoscale mode. *Important Note: This file has been developed for use where speed of execution is critical and the balance between speed and accuracy is very much toward speed, with minimal numbers of k-terms being used for each gas. It is used operationally only for mesoscale runs out to 36 hours and not for global or climate runs. Its use for off-line radiation calculations is not encouraged.*

   The longwave spectral region is divided into five bands. The Planckian function in each band is represented by a quartic fit in the temperature, generated by a least squares fit over the range 190 to 310 K.

   Gaseous absorption by water vapour, ozone and carbon dioxide and nitrous oxide is included. Version 2.1 of the CKD continuum is included. The self-broadened component is represented explicitly, but the foreign-broadened component has been added to the line data for water vapour and the k-terms represent a fit to the combined entity. The spectroscopic data used in generating the absorption data come from HITRAN92.

Aerosols included comprise the five aerosols of the standard climatology (Cusack et al. [1998]). The properties of aerosols depend on their nature and the size distribution. Size distributions and optical properties for the climatological aerosols are specified as in the standard WMO report (see Cusack et al. [1998] for details). The single scattering parameters for aerosols are generated by running a Mie scattering code and averaging over the assumed size distribution. The climatology is specified in terms of an optical depth, but densities for the aerosols are not required or specified. However, the radiation code works in terms of mass extinction coefficients, so a density must be assumed. Provided that the same density is used in the code and in the generation of the spectral file, its value is irrelevant and a conventional density of 1000 kgm^{-3} has been assumed. If spectral data for the climatological aerosols are combined with mass-loadings specified other than through the climatology, it is necessary to consider whether this density is appropriate.

Data for water droplets were generated using a Mie scattering code. Whilst a single size distribution may be assumed for each species of aerosol individually, size distributions for droplets vary widely, depending on the location and moisture content of the atmosphere. Some appropriate but variable measure of the size of droplet is required. For radiative purposes, the appropriate measure of size is the effective radius, r_e. r_e may be parametrized or imposed (see section 1). The numbers in the spectral file represent coefficients in a parametrization. They are generated by running a Mie scattering code for a number of different size distributions at a range of wavelengths, averaging the single scattering properties across the spectral bands, weighting with an appropriate function of frequency and then fitting using some appropriate function of the effective radius. This may clearly be done in many different ways, and to allow general freedom, the concept of a *type* of droplet is introduced. Data for type 1 were obtained by using the size distributions specified by Rockel et al. [1991] as the basis of the Mie calculations. Weighting was carried out using a Planckian function at a temperature of 250 K, and spectral averaging was carried out using the method of thin averaging (Edwards and Slingo [1996]) and the functional form of Slingo and Schrecker [1982] was used for fitting. Data for ice crystals have been generted analogously, using the size distributions given by Rockel et al. [1991] as a basis and treating ice crystals as spheres of ice. Fits were generated using a similar functional form. *Note: In the generation of this file, the full range of size distributions given by Rockel et al. [1991] was used, including data for small particles. In the longwave region, this encompasses a range of sizes much below those for which geometrical optics applies, in some instances giving an increase in the extinction with particle size.*

Chapter 4

Interface to the calling model

The interface to the core radiation code is designed to present a clear and logical structure to the input and output fields. This is done by wrapping related variables into defined types. All arguments passed to the routine radiance_calc are contained within 8 defined types:

control: control options initially read in via a namelist

dimen: dimensions for arrays

spectrum: spectral discretisation and optical properties read in from the spectral file

atm: grid discretisation and atmospheric profiles of thermodynamic quantities and gas amounts

cld: cloud fields (fractions, mixing ratios and sub-grid structure)

aer: aerosol fields (mixing ratios for CLASSIC aerosols, optical properties for GLOMAP-MODE aerosols)

bound: boundary conditions at top-of-atmosphere and surface (input fluxes, albedo/emissivity etc)

radout: all output variables (fluxes and other diagnostics)

The first 7 defined types are INTENT(IN) and radout is INTENT(OUT). All variables required or output by the code are contained within these types: modules are only used to pass parameters, constants and type definitions.

The structure of the interface from the calling model (such as the UM) should look like this:

```
CALL read_control -- sets up control (elements that are not time-step dependent)
CALL read_spectrum -- sets up spectrum by reading from a standard spectral file

--- Begin loop over time-steps / calls to radiation -->
```

```
    CALL set_control -- sets control for this call

    --- Begin loop over OpenMP segments -->

        CALL set_dimen -- sets dimen for segment
        CALL set_atm   --> CALL allocate_atm(atm, dimen), set atm
        CALL set_cld   --> CALL allocate_cld(cld, dimen), set cld
        CALL set_aer   --> CALL allocate_aer(aer, dimen), set aer
        CALL set_bound --> CALL allocate_bound(bound, dimen), set bound

        CALL radiance_calc(control, dimen, spectrum, atm, cld, aer, bound, radout)
                       --> CALL allocate_out(radout, dimen), calculate radout

        --> Assign required variables from radout onto full model grid

        DEALLOCATE(atm, cld, aer, bound, radout)

    <-- End loop over OpenMP segments ---

<-- End loop over time-steps / calls to radiation ---
```

This structure is repeated for the SW and LW radiation calls.

The core radiation code will contain the interface definition comprising the routines:

read_spectrum: a standard routine to read in spectral files that can then be used interchangeably between models

def_spectrum, def_control, def_dimen, def_atm, def_cld, def_aer, def_bound, def_out: type definitions including associated allocate/deallocate routines (and netCDF read/write routines in the future)

radiance_calc and called routines: the core radiation code itself

The calling model will contain the routines to set the input variables:

set_control, set_dimen, set_atm, set_cld, set_aer, set_bound: these will USE the def_ modules from the core code.

Chapter 5

The Stellar Illumination Code

A scheme to calculate the stellar illumination for a given point on a planet's surface is available through the *socrates_illuminate* interface. Once given the orbital parameters and stellar constant this will provide the stellar irradiance, zenith and azimuthal angles for a given time, latitude and longitude.

5.1 Calculation of Incoming Insolation

The following discussion of positional astronomy is abbreviated from Smart [1944], where greater detail may be found, particularly in chapters II, V and VI. Let time t be measured from the beginning of the calendar year and perihelion (the planet's closest approach to the star) occur at time τ . The mean anomaly M is defined:

$$M = \frac{2\pi(t-\tau)}{T_Y} \tag{5.1}$$

where T_Y is the length of the year. The true anomaly v, the angular distance of the planet round its orbit from perihelion, can be calculated from M for a Keplerian orbit, as an expansion called the equation of the centre. We use the third-order approximation (Smart, pp119-120):

$$v = M + (2e - e^3/4)\sin M + \frac{5}{4}e^2 \sin 2M + \frac{13}{12}e^3 \sin 3M \tag{5.2}$$

where e is the eccentricity of the planet's orbit (a geometric quantity which quantifies how non-circular an ellipse is). The normally directed incoming stellar radiation at the top of the atmosphere is given by the inverse-square law:

$$S(t) = S_0 \frac{r_{au}^2}{r(t)^2} \tag{5.3}$$

where S_0 is the "stellar constant", the incoming stellar radiation on unit area exposed normally at a distance of 1 astronomical unit r_{au}, and $r(t)$ is the actual star-planet distance. From Kepler's Second Law:

$$S(t) = S_0 \left(\frac{1 + e\cos v}{a(1-e^2)} \right)^2 \tag{5.4}$$

where a is the semi-major axis of the planet's orbit in astronomical units.

One other global quantity has to be found, the stellar declination δ, the latitude where the star is vertically overhead. This depends on the planet's rotation, which defines latitude, as well as its position in its orbit:

$$\sin\delta = \sin\epsilon\sin\theta \tag{5.5}$$

where ϵ is the obliquity of the ecliptic (the angle between the axes of the planet's rotation and of its orbit) and θ is the angular distance the planet has travelled round its orbit since the vernal equinox, the point in the planet's orbit (reached around 21st March for the Earth) where δ is zero (the star is overhead at the equator) and increasing (moving towards Northern summer). This is obviously equal to:

$$\sin\delta = \sin\epsilon\sin(v - \lambda) \tag{5.6}$$

where λ is the angle from perihelion to the vernal equinox (the quantity $\pi - \lambda$ is called the longitude of perihelion).

For user supplied orbital elements the above calculations are carried out for the middle of the supplied timestep. Where the fixed or secularly varying orbital elements for the Earth are used the above calculations are carried out with t for 1200 GMT on the current day. This conveniently makes daily mean incoming sunlight a function of latitude only, and introduces negligible error.

5.1.1 Calculation of stellar zenith angle

Calculating the incoming radiation perpendicular to the local vertical at some point requires the stellar zenith angle ζ there, i.e. the angle between the star and the local vertical. At latitude (north) ϕ, longitude (east) λ and time t (now measured from prime meridian stellar midnight), geometry gives:

$$\cos\zeta = \cos\phi\cos\delta\cos\Omega + \sin\phi\sin\delta \tag{5.7}$$

where

$$\Omega = \lambda + \pi(2t/T_D - 1) \tag{5.8}$$

is the hour angle of the star (the angle through which the planet has rotated since local stellar noon) and T_D is the length of the day (e.g. Paltridge and Platt [1976]).

In order to correct for the difference between prime meridian stellar time and universal time (or model time) we employ the "Equation of Time". The varying angular velocity of the planet in its orbit causes variation in the length of the stellar day (the time for the star to return to the same apparent position in the sky, consisting of one complete rotation of the planet plus as much extra rotation as is needed to catch up with the change in the planet/star angle as it goes round the star). For the Earth, these are of order 10 seconds and accumulate to give differences between solar and mean time of up to 17 minutes. The *Equation of Time* may be calculated from the equations for the planet's orbit. The original formulation of Smart [1944] is generally used for the Earth. A second formulation (Mueller [1995]) is available which contains higher order terms and may be necessary for more eccentric orbits.

The stellar zenith angle is calculated as a mean value over the portion of the timestep that the star is above the horizon. Integrating (5.7) gives the mean $\cos\zeta$ between hour angles Ω_1 and Ω_2 :

$$\langle\cos\zeta\rangle = \frac{\cos\phi\cos\delta(\sin\Omega_2 - \sin\Omega_1) + \sin\phi\sin\delta(\Omega_2 - \Omega_1)}{\Omega_2 - \Omega_1} \tag{5.9}$$

This must be calculated only for the part of the timestep (if any) when $\cos\zeta$ is positive, i.e. the star is up. Where $\tan\phi\tan\delta > 1$ there is perpetual day and where $\tan\phi\tan\delta < -1$ perpetual night. At other latitudes the hour angles for sunset (Ω_S) and sunrise (Ω_R) are:

$$\Omega_S = \cos^{-1}(-\tan\phi\tan\delta) \tag{5.10}$$

$$\Omega_R = -\Omega_S \tag{5.11}$$

Thus, for example, at a point where the star sets but does not rise within the timestep, $\cos\zeta$ is given by:

$$\langle\cos\zeta\rangle = \frac{\cos\phi\cos\delta(\sin\Omega_S - \sin\Omega_B)}{\Omega_S - \Omega_B} + \sin\phi\sin\delta \tag{5.12}$$

where Ω_B is the hour angle for that point at the beginning of the timestep. Two separate periods of daylight need to be accounted for if the star sets and then rises during a timestep.

The incoming stellar radiation for the timestep at any location is then $S(t)$ times $\langle\cos\zeta\rangle$ times the fraction of the timestep that the star is up at that point.

5.1.2 Calculation of stellar azimuth angle

For certain applications the stellar azimuth angle is also required, such as when dealing with shadows from surface terrain. Here a mean hour angle $\overline{\Omega}$ is determined for the middle of the period where the star is above the (horizontal) horizon. If the star sets and rises during the timestep then the mean hour angle is arbitrarily taken as the middle of the timestep.

The solar azimuth angle (α) measured clockwise from north, is then calculated using the formulation from Manners et al. [2012]:

$$\alpha = \mathrm{atan2}\left(-\cos\delta\sin\overline{\Omega},\ \sin\delta\cos\phi - \cos\delta\cos\overline{\Omega}\sin\phi\right) \tag{5.13}$$

5.1.3 Specification of orbital elements

The following parameters for the planet's orbit may be user-defined:

Epoch [Julian days]

The Julian day number on which the specified orbital elements apply. The increments are then the change in these orbital elements per Julian day from the given epoch.

The J2000 epoch is specified by the Julian day number 2451545.0 which equates to midday on the 1st January 2000.

Orbital Eccentricity [unitless]

The orbital eccentricity determines the amount by which the orbit deviates from a perfect circle. A value of 0 is a circular orbit, values between 0 and 1 form an elliptic orbit, 1 is a parabolic escape orbit, and greater than 1 is a hyperbola. (The latter two cases are not available in this formulation.)

Increment to eccentricity per Julian day from epoch [/day]

Argument of periapsis [radians]

The angle between the ascending node and the periapsis (anticlockwise).

The ascending node in this context is the point in the orbit where the planet passes through its autumn equinox for the northern hemisphere. The direction from the star to planet at this point in the orbit is the zero of the reference frame used here for the orbital elements. This direction is also where the host star appears in the sky as viewed from the planet at its northern hemisphere spring equinox. For the Earth this is known as the First Point of Aries. (Note, for a planet with zero obliquity, this zero direction is arbitrarily defined.)

The periapsis is the point of closest approach in the planet's elliptical orbit. For a circular orbit it is undefined (can be set to zero.)

As we are using the ascending node as the zero point for the reference frame here, then by definition, the longitude of the ascending node is zero, and the argument of periapsis is equal to the longitude of periapsis. For a planet around the sun this is known as the longitude of perihelion.

Increment to the argument of periapsis per Julian day from epoch [radians/day]

Obliquity of the orbit [radians]

The angle between the rotational axis of the planet and the orbital axis, where the direction is defined so the rotation is in the same sense (i.e. anticlockwise).

Increment to obliquity of the orbit per Julian day from epoch [radians/day]

Semi-major axis [AU]

One half of the major axis of the orbit, equivalent to the average between the orbital distance at periapsis and apoapsis (perihelion and aphelion for orbits around the Sun). For the Earth this was originally defined as 1 AU (astronomical unit), but 1 AU is now defined as exactly 149597870700 metres.

Increment to semi-major axis per Julian day from epoch [AU/day]

Mean anomaly at epoch [radians]

The fraction of the orbital period since passage through periapsis expressed as a fraction of a circle in radians. If the orbit were completely circular then this would describe the actual angular position of the planet in the orbit (the true anomaly).

This is the mean anomaly at the time of the given epoch.

Increment to mean anomaly per Julian day from epoch [radians/day]
This setting defines the orbital period. It equates to 2π over the orbital period in Julian days.

Hour angle at epoch [radians]
The fraction of the planet's day since the host star was over the planet's prime meridian expressed as a fraction of a circle in radians. For the Earth, this is the angle the Sun has moved westwards since solar noon.

This is the hour angle at the time of the given epoch.

Increment to hour angle per Julian day from epoch [radians/day]
This setting defines the mean length of the planet's day. It equates to 2π times the length of the planet's day over the length of a Julian day.

The actual day length will vary slightly over an eccentric orbit which will be accounted for by the *Equation of Time.*

The mean hour angle increment should be consistent with the planetary angular rotation rate ω [radians/second]. If ω is predefined within a GCM, then hour_angle_inc can be determined as follows:

$$\text{hour\_angle\_inc} = 86400\omega - \text{mean\_anomaly\_inc} - \text{arg\_periapsis\_inc}$$

In reality this might not be exactly true if the position of the ascending node is changing with time (i.e. our reference frame itself is moving).

5.1.4 Special cases for length of day

In the general case the length of the day is defined by setting the hour angle increment as described above. The following special cases are also available:

Tidally locked planet
When the hour_angle_inc is set to zero the planet will be tidally locked with one side always facing the star. For this case it is not necessary to calculate a mean value of the stellar zenith angle and equation 5.7 can be used directly.

The longitude at which the star is overhead will still vary with the *equation of time* to allow for an eccentric orbit and a constant rotation rate, and the stellar declination will vary with the orbital parameters.

Earth day
A preset is available to use an Earth day with hour_angle_inc set to exactly 2π. This avoids any numerical drift due to an inexact user setting of 2π.

Fixed sun

The position of the sun in the sky is fixed to the same value for all points. The solar zenith and azimuth angles are user supplied.

5.1.5 Orbital elements for the Earth

Presets are available to define the orbital elements of the Earth:

Earth: Fixed

A standard Earth orbit that does not vary from one year to the next. The day number of the passage through perihelion is set to a mean value for the years 1995-2005.

As the orbit is reset at the beginning of each year there will be a slight discontinuity in the orbital position. The epoch used is therefore always midday on the first day of the current year. The orbital elements used are taken from JPL and the Astronomical Almanac (1984) and equivalent to:

eccentricity = 1.6710222E-02
eccentricity_inc = 0.0
arg_periapsis = 1.796767421
arg_periapsis_inc = 0.0
obliquity = 0.409092804
obliquity_inc = 0.0
semimajor_axis = 1.0
semimajor_axis_inc = 0.0
mean_anomaly = -0.037278428
mean_anomaly_inc = 0.01720278179
hour_angle = 0.0

Earth: Secular variation

An Earth orbit with secular variations of the orbital elements described by Berger [1978]. These use higher order terms than the simple linear increments available with the user defined orbital elements.

Option to use a 360 day calendar

It has been common practice to run Earth climate models with an artifical year of 360 days. When using this option, the distortions of the seasonal cycle of insolation thus introduced are minimised by altering the date of perihelion:

$$\tau_{360} = \tau_{365\frac{1}{4}} = \frac{360}{365\frac{1}{4}} + 0.71 \tag{5.14}$$

where the constant 0.71 is derived from the lengths of the months in the two calendars. This changes the current mean value of τ from 2.5 days to 3.2 days for the *Earth:Fixed* preset. The actual value varies from year to year (more because of the effects of the moon and the other planets on the earth's orbit than because of the variation in the length of the calendar year) but in the model the only variation is that forecast mode leap years have a slightly different distribution of insolation from other years.

5.1.6 Orbital elements for solar system planets

A fortran utility is available called *orb_elem* that can generate the user defined orbital elements for solar system planets in the required reference frame of the planet's orbit.

Orbital elements available in the literature are generally given in the Earth's reference frame so require some coordinate transformation.

The fortran code in *src/aux/orb_elem.f90* should be modified directly in order to output the elements for a given planet.

Chapter 6

The Non-LTE Radiation Code

6.1 Introduction to the non-LTE Radiation Code

The NLTE (non-Local Thermodynamic Equalibrium) radiation scheme is an adjustment to heating rates and fluxes to account for NLTE effects in the radiation scheme. These effects become important above 70 km, and should allow the UM to be extended to above 85 km.

The code was written following the papers by Dr Victor Fomichev: the relevant papers are listed below:

1. Fomichev, V. I., Blanchet J.-P., and Turner D. S. (1998), Matrix parameterization of the 15 μm CO_2 band cooling in the middle and upper atmosphere for variable CO_2 concentration, J. Geophys. Res., 103, No. D10, 11505 - 11528

2. Fomichev, V. I., and Blanchet J.-P. (1995), Development of the new CCC/GCM radiation model for extension into the Middle Atmosphere, Atmosphere-Ocean, 33, No. 3, 513-529.

3. Ogibalov V. P., and V. I. Fomichev (2003), Parameterization of solar heating by the near IR CO2 bands in the mesosphere, Adv. Space Res., 32, No. 5, 759-764.

4. Fomichev V. I., V. P. Ogibalov, and S. R. Beagley (2004), Solar heating by the near-IR CO2 bands in the mesosphere, Geophys. Res. Lett., 31, L21102, doi:10.1029/2004GL020324.

Reference 1 (Fomichev et al., 1988) is for the CO_2 cooling code. Reference 2 (Fomichev and Blanchet, 1995) includes O_3 cooling with the CO_2 code. References 3 and 4 (Ogibalov and Fomichev, 2003; Fomichev et al., 2004) describe a scheme for CO_2 heating in the near-IR (near-Infra-Red) bands, which is most important in the mesosphere, and require an NLTE treatment.

The NLTE code lives in the SOCRATES code under `srcs/nlte/`. `nlte_heating_mod.f90` is the LW (longwave) correction and `sw_nlte_heating_mod.f90` is the SW (shortwave) correction.

The UM calls the LW NLTE heating rate correction from
`src/atmosphere/radiation_control/lw_rad.f90`.
The SW code `src/atmosphere/radiation_control/sw_rad.f90` calls a series of three subroutines: the NLTE heating rate correction is done in the last of these:
`src/atmosphere/radiation_control/socrates_postproc.f90`.

6.2 LW Schemes

Here, x is a dimensionless vertical scale height.

Fomichev's 1998 scheme for CO$_2$

0. $x \leq 2$
   Existing radiation scheme used.

1. $2 < x \leq 10$
   CO$_2$ volume mixing ratio (c_{CO_2}) independent of height.
   Cooling only proportional to T and c_{CO_2}.
   A matrix parameterisation is used for this LTE layer.

2. $10 < x \leq 12.5$
   CO$_2$ volume mixing ratio independent of height.
   There is no significant influence from atomic O$_2$, the matrix parametisation is used with the coefficients corrected.

3. $12.5 \leq x < 14$
   CO$_2$ volume mixing ratio proportional to scale height x.
   The recurrence formula is used, corrected such that the escape function is corrected to account for radiative heat exchange with the atmosphere and contribution of other bands other than the fundamental band.

4. $14 \leq x \leq 16.5$
   CO$_2$ volume mixing ratio proportional to scale height.
   The fundamental CO$_2$ isotope dominates the radiative cooling. The recurrence formula is used for the NLTE layer.

5. $x > 16.5$
   Smooth transition to cooling-to-space approximation, without any parameterisation.

Fomichev's 1995 scheme for O$_3$

0. $x \leq 2$
   Existing radiation scheme used.

1. $2 < x \leq 10.5$
   Matrix parameterisation used with corrected components.

2. $x > 10.5$
   No contribution.

6.3 Full LW code outline

6.3.1 Set up vertical scale height (x) and corresponding pressure levels

$x = \ln \frac{100000}{p_x}$

Outputs

1. x: Dimensionless scale height, set in code from $0 \leq x \leq 17.5$ with steps of $\Delta x = 0.25$ (bottom of atmosphere to top)
2. p_x: Pressure corresponding to the x-levels x (Pa)

References

- Equation - Fomichev 98 eq 1 and Fomichev 95 eq 1 (but differ in terms of log vs ln)
- Scale height should be ln not log - `http://scienceworld.wolfram.com/physics/PressureScaleHeight.html`
- Δx intervals - Fomichev 98 section 2

6.3.2 Interpolate the UM temperatures and gas mix ratios to x

Inputs

1. p: Pressure levels, from the UM (top of atmosphere to bottom) (Pa)
2. T: Temperatures corresponding to the pressure levels, from the UM (top of atmosphere to bottom) (K)
3. g_q: Mass mixing ratio at different pressure levels and for different gases q, from the UM (top of atmosphere to bottom) (parts per million, ppm)

Outputs

1. T_x: Temperatures corresponding to the dimensionless scale x, (bottom of atmosphere to top) (K)
2. $g_{x,q}$: Mass mixing ratios for different gases q corresponding to the dimensionless scale x (bottom of atmosphere to top) (ppm)

Requirements

- Spline interpolation code - using `interpolate_p` in SOCRATES.

6.3.3 Convert mass mixing ratios to volume mixing ratios over scale required

$c_{x,q} = \frac{\mu_x}{M_q} g_{x,q}$

Inputs

1. $g_{x,q}$: Mass mixing ratio (ppm)
2. μ_x: Molar mass of dry air per scale height (kg mol^{-1})
3. M_q: Molar mass of required atmospheric species (kg mol^{-1})

Outputs

1. $c_{x,q}$: Volume mixing ratios for different gases q corresponding to the dimensionless scale x (parts per million volume, ppmv)

Data

- Currently there are no mass mixing ratios for O_2, N_2 and O in the UM, and these are taken from Fomichev's code. These profiles should be replaced with something that can be referenced. The Air Force Geophysics Laboratory paper (see below) has O_2 data only. Fomichev lists his O_2, N_2 and O data as all being in ppmv, but he then converts O_2 and N_2 data as though it was in ppm. Is this a bug, or are these all in ppm? I assume Fomichev's data is in ppmv as labelled and do not convert.

- Molar mass of dry air per scale height currently taken from Fomichev's code, need proper data from somewhere that can be referenced. (This doesn't seem to be defined in atm as defined in `def_atm.f90` - this only has atm%mass which is column mass per layer).

- For molar masses of required atmospheric species, the best reference would be *General Inorganic Chemistry* by J. A. Duffy (1970), Longmans (as used in the Edwards-Slingo radiation code). Couldn't get hold of this, so currently using values from `https://environmentalchemistry.com/yogi/reference/molar.html`)

References

- Method - Fomichev 98, section 6, paragraph 1.

- For conversion of mass mixing ratio to volume mixing ratio see e.g. `https://software.ecmwf.int/wiki/pages/viewpage.action?pageId=61121586`

- Possible O_2 volume mixing ratio data - AFGL Atmospheric Constituent Profiles (0-120km), AFGL-TR-86-0110, Environmental Research Papers No. 954

Notes

- The use in the Fomichev code of M_O to calculate c_{x,O_2} instead of M_{O_2} is probably just a bug according to Omar.

- Fomichev uses the info that the mass mixing ratio of CO_2 is near constant below $x = 12.5$, but I have currently used the mmr of CO_2 directly from the UM code.

- Another possible bug in the Fomichev code, `o2_conv` is calculated as `am_in(ii)` in the $x = 51, 67$ range which appears to be the wrong airmass.

6.3.4 Calculate the exponential part of the Planck function for CO2 and O3

$\phi_{x,q} = \exp(-hc_s V_q / kT_x)$

Inputs

1. h: Planck's constant (J s)

2. c_s: Speed of light (m s^{-1})

3. V_{CO_2}, V_{O_3}: Frequencies of the main vibrational transitions of the main isotopes of CO_2 and O_3 (m^{-1})

4. k: Boltzmann's constant (J K^{-1})

5. T_x: Temperature per scale height x (K)

Outputs

1. $\phi_{x,CO_2}, \phi_{x,O_3}$: Exponential parts of the Planck function for CO_2 and O_3 respectively (dimensionless)

Data

- Currently using data for the main vibrational transitions of the main isotopes of CO_2 and O_3 directly from Fomichev's code - could not find a proper reference for these.

References

- Equation - Fomichev 98 equation 6 (shows T-dependence only). The exponent constant is $hc_s V_{CO_2}/k$, but I don't have a reference for this. There is a small difference in the value of the exponent calculated from the constants and that given in the paper.

6.3.5 Calculate the CO2 coefficients for the matrix parameterisation 2 $<x$ <12.5 for the particular concentration of CO2

- For each given scale height x, height level j and concentration c, the parameters $a_{j,x}$ and $b_{j,x}$ are found by interpolating over c between sets of values $a_{c,j,x}$ and $b_{c,j,x}$.

- For those sets of parameters where $a_{c,j,x}$ or $b_{c,j,x}$ have the same sign across all c, linear interpolation of $\log[a_{c,j,x}/c_{x,q}]$ or $\log[b_{c,j,x}/c_{x,q}]$ is recommended. Otherwise a second-order interpolation of $a_{c,j,x}$ or $b_{c,j,x}$ should be used.

Note that Fomichev calculates heat capacity in units of $\mathrm{cm}^2\mathrm{s}^{-3}$, which is equivalent to $10^4\mathrm{Jkg}^{-1}\mathrm{s}^{-1}$. I leave the coefficients in these units but need to convert the heat capacity to standard units of $\mathrm{Jkg}^{-1}\mathrm{s}^{-1}$ once calculated.

Inputs

1. $a_{c,j,x}$, $b_{c,j,x}$: Tables of matrix coefficients for CO_2 versus given volume mixing ratios of CO_2
2. $c_{x<12.5,CO_2}$: Volume mixing ratio of CO_2 for x<12.5 (ppmv)

Outputs

1. $a_{j,x}$, $b_{j,x}$: Matrix coefficients interpolated to the required CO_2 concentration

Requirements

- Requires linear and third-order spline interpolation.

References

- Fomichev 98, section 6, end paragraph 2 for notes on how to interpolate
- Fomichev 98, tables 2-9 for CO_2 coefficient tables. The tables in Fomichev 98 differ from the code by a smallish but significant amount.
- Fomichev 98, section 3.1 paragraph 3 suggests 360ppm is used for the concentration of CO_2, but this is outdated.
  `http://ds.data.jma.go.jp/gmd/wdcgg/pub/products/summary/sum41/10_03co2.pdf`
  for the CO_2 concentration below $x = 12.5$. 2015 had 400.0ppmv of CO_2, with +2.1ppmv each year, i.e. 406.3ppmv in 2018. (Note that this paper refers to mole fraction, which is equivalent to volume mixing ratio.)

Issues

- Fomichev suggests a CO_2 concentration of 360ppm in his paper, but in his code he uses 0.72e-3. His paper is also unclear on whether the coefficients correspond to volume or mass mixing ratios - he refers to volume mixing ratios, but gives the units ppm. I suspect they are all supposed to be volume mixing ratios.
- Is `interp_p` okay to use?
- Note that all matrix constants must be divided by their reference CO_2 concentration and multiplied by the CO_2 concentration below $x = 12.5$, this isn't 100% clear from the paper.

6.3.6 Calculation of heating rates using matrix approach

$$\epsilon_x = \sum_{j=-5}^{3} [a_{j,x} + b_{j,x}\phi_{x,CO_2}]\phi_{j,CO_2} + \sum_{j=-3}^{2} c_{O_3} c_{j,x}\phi_{j,O_3}$$

where:

Dimensionless height steps for CO_2:

j	Δx_j
-5	-6.25
-4	-3.0
-3	-1.75
-2	-0.75
-1	-0.25
0	0
1	0.25
2	0.75
3	1.5

Dimensionless height steps for O_3:

j	Δx_j
-3	-4.0
-2	-1.25
-1	-0.25
0	0
1	0.25
2	1.75

- This applies from $2 < x < 10.5$ (CO_2 and O_3) and $10.75 < x \leq 12.5$ (CO_2 only)

Inputs

1. $a_{j,x}$, $b_{j,x}$, $c_{j,x}$: Matrix coefficients
2. ϕ_{x,CO_2}, ϕ_{x,O_3}: Exponential part of Planck function for CO_2 and O_3 (dimensionless)
3. Δx_j versus j: dimensionless height steps and indices of levels used to calculate heat exchange

Outputs

1. ϵ_x: Heating rates up to $x \leq 12.5$ (J kg^{-1} s^{-1})

References

- Fomichev 98 equation 5 and Fomichev 95 equation 2, for the summing equation
- Fomichev 98 section 4.1 final paragraph for notes on the parameterised grid
- Fomichev 98 table 1 and Fomichev 95 table 1 for the parameterised grid steps

6.3.7 Calculate the CO2 column amount for 12.5 $<x<$16.5

The integral over the depth of the atmosphere defines the *atmospheric column* of CO_2 (or another gas species x) as

$$u_{x,\mathrm{CO_2}} = \int n_{x,\mathrm{CO_2}} dx,$$

where x is the dimensionless scale height and $n_{x,\mathrm{CO_2}}$ is the number density of CO_2 (molecules cm^{-3}). The number density $n_{x,\mathrm{CO_2}}$ and the volume mixing ratio $c_{x,\mathrm{CO_2}}$ are related by the number density of air $n_{x,a}$ as follows:

$$n_{x,\mathrm{CO_2}} = c_{x,\mathrm{CO_2}} n_{x,a}.$$

The number density of air $n_{x,a}$ is related to the number of moles of air N and the volume V by Avogadro's constant $A_v = 6.023 \times 10^{23}\,\mathrm{molecules\,mol^{-1}}$:

$$n_{x,a} = \frac{A_v N}{V}.$$

The ideal gas law may be expressed as $pV = NRT$, which can be used to obtain the following expression for the number density of air:

$$n_{x,a} = \frac{A_v p}{RT}$$

From the ideal gas law, it can also be obtained that $\rho_{x,a} = p\mu_x/RT$, where μ_x is the molar mass of dry air per scale height ($\mathrm{kg\,mol^{-1}}$). By assuming hydrostatic balance, $\frac{dp}{dx} = -\rho_{x,a}\, g$, together these give:

$$dx = \frac{RT}{p\mu_x\, g} dp.$$

With these expressions, the following equation for the CO_2 column amount can be obtained:

$$\begin{aligned} u_{x,\mathrm{CO_2}} &= \int n_{x,\mathrm{CO_2}}\, dx \\ &= \int c_{x,\mathrm{CO_2}}\, n_{x,a}\, dx \\ &= \int c_{x,\mathrm{CO_2}} \frac{A_v p}{RT} \frac{RT}{p\, m_{\mathrm{air}}\, g} dp \\ &= \frac{A_v}{g} \int \frac{c_{x,\mathrm{CO_2}}}{\mu_x}\, dp. \end{aligned}$$

Next, differentiate this expression with respect to the dimensionless scale height x. Note that $p_x = 10^5 e^{-x}$, and so $dp = -10^5 e^{-x}$. Then:

$$\begin{aligned}
\frac{du_{x,\mathrm{CO_2}}}{dx} &= \frac{A_v}{g}\frac{d}{dx}\left(\int \frac{c_{x,\mathrm{CO_2}}}{\mu_x} dp\right) \\
&= \frac{A_v}{g}\frac{d}{dx}\left[\int \frac{c_{x,\mathrm{CO_2}}}{\mu_x}(-10^5 e^{-x})\, dx\right] \\
&= -\frac{10^5 A_v}{g}\frac{c_{x,\mathrm{CO_2}}\, e^{-x}}{\mu_x}.
\end{aligned} \tag{6.1}$$

To evaluate the expression for Δu_x: the difference between u_x at x_i and x_{i-1}, we need the average value of e^{-x} evaluated at x_i and x_{i-1}, so $e^{-x}|_{i-1/2} = \frac{1}{2}(e^{-x_i} + e^{-x_{i-1}})$. Note that $\Delta x = 0.25$. Then the expression for the derivative of the column amount may be expressed as:

$$\begin{aligned}
\Delta u_{x,\mathrm{CO_2}}|_{i-1/2} &= -\frac{10^5 A_v}{g}\left(\frac{c_{x,\mathrm{CO_2}}}{\mu_x} e^{-x}\Delta x\right)_{i-1/2} \\
&= \frac{0.25 \times 10^5 A_v}{g}\left(\frac{c_{x_i,\mathrm{CO_2}} e^{-x_i}}{\mu_{x_i}} + \frac{c_{x_{i-1},\mathrm{CO_2}} e^{-x_{i-1}}}{\mu_{x_{i-1}}}\right).
\end{aligned}$$

Now let $Y = 0.25 \times 10^5 A_v / 2g$ and rearrange this to obtain:

$$u_{x_{i-1}} = u_{x_i} + Y\left(\frac{c_{x_i,\mathrm{CO_2}} e^{-x_i}}{\mu_{x_i}} + \frac{c_{x_{i-1},\mathrm{CO_2}} e^{-x_{i-1}}}{\mu_{x_{i-1}}}\right)$$

This formulation is then identical to what is used in Fomichev's stand-alone code.

The column amount above $x = 16.5$, $u_{x=16.5,CO_2}$, is used as a boundary condition to generate the array of u_{x,CO_2} for $12.5 < x < 16.5$.

Inputs

1. A_v: Avogadro's constant (mol^{-1})
2. μ_x: Molar mass of dry air per scale height (kg mol^{-1})
3. g: Acceleration due to gravity (ms^{-1})
4. c_{x,CO_2}: Volume mixing ratio for $\mathrm{CO_2}$ (ppmv)
5. x: Dimensionless scale height (dimensionless)
6. $u_{x>16.5,CO_2}$: $\mathrm{CO_2}$ column amount above $x = 16.5$ (cm^{-2})

Outputs

1. u_{x,CO_2}: Column amount, or number of molecules of $\mathrm{CO_2}$ per unit area (cm^{-2})

References

- Fomichev 98 section 6 paragraph 4 states the CO_2 column amount is used, but not how it is calculated or what the value is.
- 'Introduction to Atmospheric Chemistry', Daniel J. Jacob, Princeton University Press, 1999. Available at `http://acmg.seas.harvard.edu/people/faculty/djj/book/`. This is used to derive the equation for the CO_2 column amount.

Issues

- Where does the CO_2 column amount above $x = 16.5$ come from? No value seems to be given in the paper. Set in code, but not explained, just with a note that says "does this need changing?" (written by Omar)
- Are SI units correct in column calc, e.g. p in Pa?

6.3.8 Calculate the coefficients dj for the recurrence formula for 12.5 $<x$ $<$16.5

$d_x = \alpha_{u,x} L_u$ for $12.5 \leq x \leq 13.75$

$d_x = L_u$ for $x >= 14.0$

where
L_u is the escape function
$\alpha_{u,x}$ is the correction to the escape function

- L_u for x is found by linear interpolation of $\log L_u$ over u_x.
- α_x for x is found by linear interpolation of $\log \alpha_{u,x}$ over u_x, where a different $\log \alpha_{u,x} - u_x$ association is available for each x.
- Note that Tables 10 and 11 in Fomichev 98 have $\log(u)$ rather than u, so these have been converted.
- For the range $12.5 \leq x \leq 13.75$, $\log L_u + \log \alpha_{u,x}$ is calculated before the exponential is taken to obtain d_x

Inputs

1. u_x: CO_2 column amount (cm^{-2})
2. L_u: Escape function for CO_2 column amount u_x
3. $\alpha_{u,x}$: Correction to escape function for CO_2 column amount u_x and scale height x

Outputs

1. d_x: Coefficients for the recurrence formula (dimensionless)

Requirements

- Linear interpolation.

References

- Fomichev 98 table 10 - Escape function L_u for CO_2 column amount u_x
- Fomichev 98 table 11 - Correction to escape function $\alpha_{u,x}$ for CO_2 column amount u_x and for x
- Fomichev 98 section 6 paragraph 4 for interpolation methods.

Issues

- Fomichev 98 tables 10 and 11 are not identical to the code - for a start, the code has u rather than log(u) and α rather than $\log\alpha$.

6.3.9 Calculate number density

$\rho_x = \frac{p_x}{kT_x}$

Use

$x = \ln\frac{1000}{p_x}$

where p_x is in mbar (and 1 mbar = 100 Pa = 100 kg m^{-1} s^{-2}) to get

$\rho_x = 10^5\frac{e^{-x}}{kT_x}$

Inputs

1. x: Dimensionless scale height (dimensionless)
2. k: Boltzmann Constant in (J K^{-1})
3. T_x: Temperature at scale height x (K)

Outputs

1. ρ_x: Number density at scale height x (m^3)

6.3.10 Calculate parameter lambda for use in the recurrence formula

$\lambda_x = A_{CO_2}/\{A_{CO_2} + \rho_x[c_{x,N_2}k_{N_2} + c_{x,O_2}k_{O_2} + c_{x,O}k_o]\}$

where the collisional deactivation rate constants in m^3s^{-1} are

$k_{N_2} = 5.5 \times 10^{-17}\sqrt{T_x} + 6.7 \times 10^{-10}\exp(-83.8T_x^{-1/3})$
$k_{O_2} = 10^{-15}\exp(23.37 - 230.9T_x^{-1/3} + 564T_x^{-2/3})$
$k_O = 3 \times 10^{-12}$

and where

A_{CO_2} is the Einstein A coefficient for CO_2 in s^{-1}

ρ_x is the number density in m^{-3} of the background atmosphere

Inputs

1. A_{CO_2}: Einstein A coefficient for the fundamental band for the main isotope of CO_2 (s^{-1})
2. x: Dimensionless scale height (dimensionless)
3. k: Boltzmann Constant (J K^{-1})
4. T_x: Temperature at scale height x (K)
5. k_{N_2}, k_{O_2}, k_O: Collisional deactivation rate constants (m^3 s^{-1})
6. c_{x,N_2}, c_{x,O_2}, $c_{x,O}$: Volume mixing ratios (ppmv)

Outputs

1. λ_x: Recurrence formula parameter (dimensionless)

References

- Fomichev 98 equation 8
- Fomichev 98 section 2.2 for the collisional deactivation rate constants (taken from Shved et al, 1998)

Issues

- The only place this constant is referred to as Einstein's A coefficient is in the code, not the paper. Is this actually this coeff, or is it a paper town?
- Where can I find Einstein's coefficient for the fundamental band for CO_2 main isotope?

6.3.11 Calculation of the boundary condition at x=12.5 for the recurrence formula

$$\gamma_{x=12.5} = \frac{\epsilon_{x=12.5}\mu_{x=12.5}}{Kc_{x=12.5,CO_2}[1 - \lambda_{x=12.5}]}$$

where

$K = N_a h c_s V_{CO_2} A_{CO_2} W$ in mol^{-1}m^{2}kgs^{-3}

where W is the ratio of the statistical weights for the fundamental transition.

Inputs

1. N_a: Avogadro's Constant (mol^{-1})
2. h: Planck Constant (m^2 kg s^{-1})
3. c_s: Speed of light (m s^{-2})
4. V_{CO_2}: Frequency of the main vibrational transition of CO$_2$ (m^{-1})
5. A_{CO_2} : Einstein A coefficient for the fundamental band for the main isotope of CO_2 (s^{-1})
6. W: Ratio of the statistical weights for the fundamental transition (dimensionless)
7. $\mu_{x<12.5}$: Molar mass of dry air per scale height (kg mol^{-1})
8. $\epsilon_{x=12.5}$: Heating rate at x=12.5 calculated from the matrix method (J kg^{-1} s^{-1})
9. c_{x,CO_2}: Volume mixing ratio of CO$_2$ (ppmv)
10. λ: Recurrence formula parameter (dimensionless)

Outputs

1. $\gamma_{x=12.5}$: Boundary condition for the recurrence formula at $x = 12.5$ (dimensionless)

References

- Fomichev 98 equation 10
- Fomichev 98 section 4.1 paragraph 5 for frequency of the main transition 01^{1}0-00^{0}0 of the ^{12}C^{16}O$_2$ isotope, 667.3799 cm^{-1}

Issues

- Where can I find Einstein's coefficient for the fundamental band for CO$_2$ main isotope?
- The constant for Fomichev equation 10 does not match the 1/constb in the code, which it corresponds to. There is a note in the code about how to calculate this constant which does not seem to be in the paper.

6.3.12 Solve the recurrence formula for the heating rate correction, and calculate the heating rate for 12.5 $<x$ <16.5

Use

$[1 - \lambda_x(1 - D_x)]\gamma_x = [1 - \lambda_{x-1}(1 - D_{x-1})]\gamma_{x-1} + D_{x-1}\phi_{x-1} - D_x\phi_x$

where

$D_x = \frac{1}{4}(d_{x-1} + 3d_x)$ $D_{x-1} = \frac{1}{4}(3d_{x-1} + d_x)$

to find the γ_x, using the boundary condition value $\gamma_{x=12.5}$. Then

$\epsilon_x = \frac{Kc_{x,CO_2}(1-\lambda_x)}{\mu_x}\gamma_x$

Inputs

1. d_x: Coefficients for the recurrence formula (dimensionless)
2. λ_x: Recurrence formula parameter (dimensionless)
3. $\gamma_{x=12.5}$: Boundary condition for the recurrence formula at $x = 12.5$ (dimensionless)
4. K: Constant defined as before (mol^{-1} m^2 kg s^{-3})
5. c_{x,CO_2}: Volume mixing ratio of CO_2 (dimensionless)
6. μ_x: Molar mass of dry air per scale height (kg mol^{-1})

Outputs

1. ϵ_x: Heating rate (J kg^{-1} s^{-1})

References

- Fomichev 98 equation 9
- Fomichev 98 equation 11
- Fomichev 98 equation 7

Issues

- The constant for Fomichev equation 7 does not exactly match the const in the code which it corresponds to. There is a note in the code about how to calculate this constant which does not seem to be in the paper - I need a reference for this.

6.3.13 Calculation of the heating rate above *x*=16.5

$\epsilon_{x>16.5} = \frac{Kc_{x,CO_2}(1-\lambda_x)}{\mu_x}[F_{x=16.5} - \phi_{x,CO_2}]$

where

F is the upward flux, with $F_{x=16.5}$ defined by the boundary condition

$F_{x=16.5} = \gamma_{x=16.5} + \phi_{x=16.5,CO_2}$

Inputs

1. K: Constant defined as before (mol^{-1} m^2 kg s^{-3})
2. c_{x,CO_2}: Volume mixing ratio of CO_2 (ppmv)
3. λ_x: Recurrence formula parameter (dimensionless)
4. μ_x: Molar mass of dry air per scale height (kg mol^{-1})
5. $\gamma_{x=16.5}$: Boundary condition for the recurrence formula at $x = 16.5$ (dimensionless)
6. ϕ_{x,CO_2}: Exponential part of the Planck function for CO_2 (dimensionless)

Outputs

1. ϵ_x: Heating rate for $x > 16.5$ (J kg^{-1} s^{-1})

References

- Fomichev 98 equation 13
- Fomichev 98 equation 14

6.3.14 Convert heating rates into K/day using the specific heat capacity

$\epsilon_x = \frac{nC_P\Delta T_x}{m_{total}}$

where
ϵ_x is the heating rate in J s^{-1} kg^{-1}
C_P is the specific heat capacity in J mol^{-1} K^{-1}
n is the number of moles in mol
ΔT_x is the temperature change in K s^{-1}
m_{total} is the total mass of gas in kg

Using $n = \frac{m_{total}}{\mu_x}$:

$\Delta T_x = \frac{\epsilon_x \mu_x}{C_P}$.

For a monatomic ideal gas

$C_P = \frac{5}{2}R$.

For diatomic and polyatomic ideal gases

$C_P = \frac{7}{2}R$.

where R is the gas constant.

For $x \leq 10.25$ there is assumed not to be any significant concentration of monatonic gas.

$C_P = \frac{7}{2}R$

For $x \geq 10.25$ it is assumed that atomic oxygen makes a significant contribution.

$C_P = R[\frac{7}{2}(1 - c_{x,O}) + \frac{5}{2}c_{x,O}]$.

Finally convert from units of K s^{-1} to K day^{-1}.

Inputs

1. ϵ_x: Heating rate (J s^{-1} kg^{-1})
2. μ_x: Molar mass of dry air per scale height (kg mol^{-1})
3. R: Gas constant (J mol^{-1} K^{-1})
4. c_O: Volume mixing ratio for O (absolute units, not ppmv)

Outputs

1. ΔT_x in (K day^{-1})

References

- None in papers. See e.g. `http://physics.bu.edu/~redner/211-sp06/class24/class24_heatcap.html`

Issues

- What is a decent reference for the calculation of the heat capacity?
- Where is the reference that the O concentration should only be considered at $x >= 10.5$? Is this simply from looking at the O profile?

6.3.15 Heating rates interpolated to the original pressure levels

Inputs

1. ϵ_x: Heating rates corresponding to the dimensionless scale height x (J kg^{-1} s^{-1})
2. p_x: Pressure corresponding to the x-levels x (converted to top of atmosphere to bottom) (Pa)
3. p: Pressure levels, from the UM (top of atmosphere to bottom) (Pa)

Outputs

1. ϵ_p: Heating rates corresponding to the original pressure levels in the UM (top of atmosphere to bottom) (J kg^{-1} s^{-1})

Requirements

- 3rd order spline interpolation

6.3.16 Heating rates blended with the LTE rates

For $p < 0.1$, $\epsilon = \epsilon_p$
For $p >= 0.1$, $\epsilon = \epsilon_{p,LTE}$

Inputs

1. ϵ_p: Heating rates corresponding to the original pressure levels in the UM (top of atmosphere to bottom) (J kg^{-1} s^{-1})

2. $\epsilon_{p,LTE}$: Heating rates from the UM with no NLTE correction applied (top of atmosphere to bottom) (J kg^{-1} s^{-1})

3. p: Pressure levels, from the UM (top of atmosphere to bottom) (Pa)

Ouputs

1. $\epsilon_{p,NLTE}$: Blended heating rates with NLTE correction applied (top of atmosphere to bottom) (J kg^{-1} s^{-1})

Issues

- Is there a reference for the level at which the heating rates are blended?

6.3.17 Misc

I use NIST values for Physical constants:
`https://physics.nist.gov/cuu/Constants/`
CO_2 fundamental vibrational frequency -
`https://webbook.nist.gov/cgi/cbook.cgi?ID=B4000020&Mask=800`
O_3 fundamental vibrational frequency -
`https://webbook.nist.gov/cgi/formula?ID=B4000064&Mask=800`

O2 and N2 profiles are taken from the United States Standard Atmosphere USSA-76 model (Chamberlain and Hunten 1987).

Might possibly be a useful reference on statistical weights -
`https://www.cfa.harvard.edu/atmosphere/publications/2006-EinsteinA-JQSRT-98.pdf`

James has confirmed that I need to loop over n_profile (number of atmospheric profiles for radiation calculations) in the code, but can feel free to ignore n_channel (number of output channels for diagnostics)

Tables 1-4 in Fomichev 95 for $a_{O_3,j,x}$ and $b_{O_3,,j,x}$ differ from those in the code - the tables in the paper are for 6 points in the atmosphere, the ones in the code for 9 points.

6.3.18 Outstanding Issues

1. Some of the data is taken from the Fomichev code directly, and therefore doesn't have a good reference that can be given. Ideally this should be replaced with referenceable data.
2. In nlte_heating_mod.F90, the gases to pick from the gas list sp_lw_ga7 are referenced directly by hardcoding the gas_list_index. This should work with the data files so as not to be hardcoded.
3. Still issues calculating the CO_2 column constant.

6.4 SW Schemes

Fomichev and Ogibalov's 2003/2004 scheme for CO$_2$

0. $x \leq 2$
   Existing radiation scheme used.
1. $2 < x \leq 14$
   Parameterisation scheme used which sets heating adjustment according to CO$_2$ volume mixing ratio (c) and solar zenith angle.

6.5 Full code outline SW

6.5.1 Notes

1. This is stated in Ogibalov and Fomichev to be a daytime correction to the CO$_2$ cooling previously only parameterised for nighttime conditions. Do I need to apply only partially?
2. The heating rate is blended to only $x = 15.5$, should I do this? (Probably, there is no parameterisation data about $x = 14$)

6.5.2 Scale CO2 column amount by the tropospheric CO2 volume mixing ratio

Scale the CO$_2$ column amount per dimensionless scale height from the parameterisation data by the ratio of the tropospheric CO$_2$ volume mixing ratio in the model, and that in the parameterisation data set.

$$u_{CO_2,x} = u_{CO_2,x,ref} \times \frac{c_{CO_2,x=trop}}{c_{CO_2,x=trop,ref}}$$

Inputs

1. $u_{CO_2,x,ref}$: CO$_2$ column amount by dimensionless scale height parameterisation data
2. $c_{CO_2,x=trop,ref}$: Tropospheric value of CO$_2$ volume mixing ratio from parameterisation data
3. $c_{CO_2,x=trop}$: Tropospheric value of CO$_2$ volume mixing ratio from model

Outputs

1. $u_{CO_2,x}$: CO_2 column amount by dimensionless scale height data scaled by volume mixing ratio of tropospheric CO_2

6.5.3 Calculate the amount of CO2 along the zenith path

Mean effective pathlength factor

$P = \frac{35}{\sqrt{1224 \cos\theta_z^2 + 1}}$

Scale the CO_2 column amount by the mean effective pathlength factor

$u_{CO_2,x,z} = u_{CO_2,x} \times P$

Inputs

1. $u_{CO_2,x}$: CO_2 column amount by dimensionless scale height data scaled by volume mixing ratio of tropospheric CO_2
2. $\cos\theta_z$: Cosine of the solar zenith angle

Outputs

1. $u_{CO_2,x,z}$: CO_2 column amount by dimensionless scale height data along the zenith path scaled by volume mixing ratio of tropospheric CO_2

References

- Rodgers C. D., 1967, The radiative heat budget of the troposphere and lower stratosphere
- Other refs, e.g. Li & Shibata, 2006, On the Effective Solar Pathlength, `https://journals.ametsoc.org/doi/pdf/10.1175/JAS3682.1`

6.5.4 User parameterisation to find heating rate

Interpolate the log of the CO_2 path amount linearly to find the heating rate from the parameterisation.

For values outside the range for which interpolation data is available:
If $\log u_{CO_2,x,z} < \log u_{param,CO_2,x}(1)$, set $q_{CO_2} = q_{param,CO_2,x}(1)$
If $\log u_{CO_2,x,z} > \log u_{param,CO_2,x}(10)$, set $q_{CO_2} = 0$

Inputs

1. $\log u_{CO_2,x,z}$: log CO_2 column amount along zenith path
2. $\log u_{param,CO_2,x}$: Parameterisation reference data CO_2 column amounts, ten values at each scale height
3. $q_{param,CO_2,x}$: Parameterisation reference data heating rates, ten values at each scale height corresponding to different CO_2 column amounts

Outputs

1. $q_{CO_2,unscl}$: CO_2 heating rate in K/s corresponding to zenith path

Requirements

- Spline interpolation code - is it okay to use interpolate_p?

6.5.5 Scale the heating rate

In the UM:

- The UM converts fluxes to increments, and then multiplies by $\frac{pts}{C_P}$ where pts is the timestep factor, and C_P the layer heat capacity which appears to be per pressure (looking at the subroutine set_thermodynamic).
- Before passing this heating rate into the NLTE correction code, it is multiplied by $\frac{s/day}{pts}$. This converts the heating rate into the form $\frac{Q(inK/day)}{C_P}$.

In the correction code:

- In the NLTE correction code, the heating rate found from the parameterisation is in units $\frac{Q(inK/s)}{C_V c_{CO_2}}$.
- This is multipled by $(s/day)c_{CO_2}(C_V/C_P)$ to convert to the same form as the UM heating rates.

For an ideal gas

$C_P = C_V + nR$

For a monotonic gas

$C_V = \frac{3}{2}nR$ so $C_P = \frac{5}{2}nR$ and $C_V/C_P = \frac{3}{5}$

For a polyatomic gas

$C_V = \frac{5}{2}nR$ so $C_P = \frac{7}{2}nR$ and $C_V/C_P = \frac{5}{7}$

These two cases are blended above $x \geq 10.5$ where atomic oxygen makes a difference, as with the heat capacity for the LW NLTE correction. So
For $x < 10.5$:

$C_V/C_P = \frac{5}{7}$

For $x >= 10.5$:

$C_V/C_P = \frac{5}{7}(1 - vmr_{o,x}) + \frac{3}{5}vmr_{o,x}$

The scaled volume mixing ratio is calculated according to the tropospheric values as

$c_{CO_2,x,scl} = c_{CO_2,x} \times \frac{c_{CO_2,x=trop}}{c_{CO_2,x=trop,ref}}$

And the overall scaling

$q_{CO_2} = q_{CO_2,unscl} \times c_{CO_2,x,scl}(C_V/C_P)(s/day)$

Inputs

1. $c_{CO_2,x}$: CO_2 volume mixing ratio
2. $c_{CO_2,x=trop,ref}$: Tropospheric value of CO_2 volume mixing ratio from parameterisation data
3. $vmr_{o,x}$: Volume mixing ratio of atomic oxygen per scale height
4. $q_{CO_2,unscl}$: CO_2 heating rate in K/s corresponding to zenith path

Outputs

1. q_{CO_2}: CO_2 heating rate in K/day corresponding to zenith path

6.5.6 Outstanding Issues

1. The cos of the solar zenith angle used was not the correct version - the spherical geometry version is needed, but trying to put this in makes things crash!
2. Need to finish calculating the O_3 NLTE profile to add to the CO_2 NLTE profile. This needs using the per-band flux up and down rates to separate out band 1 heating rate (this can be used for the Hartley band, which takes the NLTE efficiency correction) and bands 2-4 can be used as a proxy for the Huggins and Chappuis O_3 heating rates.
3. The O_3 Hartley efficiency function has a rough part which needs a bit of interpolation over.

Bibliography

S. A. Ackerman and G. L. Stephens. The absorption of solar radiation by cloud droplets: An application of anomalous diffraction theory. *J. Atm. Sci.*, 44:1,574–1,588, 1987.

Y. Balkanski, M. Schulz, T. Claquin, and S. Guibert. Reevaluation of mineral aerosol radiative forcings suggests a better agreement with satellite and aeronet data. *Atmos. Chem. Phys.*, 7:81–95, 2007.

A. J. Baran. Simulation of infrared scattering from ice aggregates using a size-shape distribution of circular ice cylinders. *Appl. Optics-LP*, 42:2811–2818, 2003.

A. J. Baran, P. N. Francis, L.-C. Labonnote, and M. Doutriaux-Boucher. A scattering phase function for ice cloud: Tests of applicability using aircraft and satellite multi-angle multi-wavelength radiance measurements of cirrus. *Q. J. Roy. Meteorol. Soc.*, 127:2395–2416, 2001.

Anthony J. Baran. From the single-scattering properties of ice crystals to climate prediction: A way forward. *Atmospheric Research*, 112(0):45–69, 2012. doi: 10.1016/j.atmosres.2012.04.010.

Anthony J. Baran, P.J. Connolly, and C. Lee. Testing an ensemble model of cirrus ice crystals using midlatitude in situ estimates of ice water content, volume extinction coefficient and the total solar optical depth. *Journal of Quantitative Spectroscopy and Radiative Transfer*, 110(14-16):1579–1598, 2009. doi: 10.1016/j.jqsrt.2009.02.021.

Anthony J. Baran, Paul Field, Kali Furtado, James Manners, and Andrew Smith. A new high- and low-frequency scattering parameterization for cirrus and its impact on a high-resolution numerical weather prediction model. *AIP Conf. Proc*, 1531:716–719, 2013. doi: 10.1063/1.4804870.

Anthony J. Baran, Peter Hill, Kalli Furtado, Paul Field, and James Manners. A Coupled Cloud Physics-Radiation Parameterization of the Bulk Optical Properties of Cirrus and its Impact on the Met Office Unified Model Global Atmosphere 5.0 Configuration. *J. Climate*, 27:7725–7752, 2014. doi: 10.1175/JCLI-D-13-00700.1.

H. W. Barker, G. L. Stephens, and Q. Fu. The sensitivity of domain-averaged solar fluxes to assumptions about cloud geometry. *Q. J. Roy. Meteorol. Soc.*, 125:2127–2152, 1999.

M. Benassi, R. D. M. Garcia, A. H. Karp, and C. E. Siewert. A high-order spherical harmonics solution to the standard problem in radiative transfer. *Astrophys. J.*, 280:853–864, 1984.

A. L. Berger. long-term variations of daily insolation and quaternary climate change. *J. Atmos. Sci.*, 35:2362–2367, 1978.

M. Birk, G. Wagner, J. Loos, and K.P. Shine. 3 μm Water vapor self- and foreign-continuum: New method for determination and new insights into the self-continuum. *Journal of Quantitative Spectroscopy and Radiative Transfer*, 253:107134, 2020. ISSN 0022-4073. doi: https://doi.org/10.1016/j.jqsrt.2020.107134.

Tami C. Bond and Robert W. Bergstrom. Light absorption by carbonaceous particles: An investigative review. *Aerosol Science and Technology*, 40(1):27–67, 2006. doi: 10.1080/02786820500421521.

I. A. Boutle, S. J. Abel, P. G. Hill, and C. J. Morcrette. Spatial variability of liquid cloud and rain: observations and microphysical effects. *Q. J. Roy. Meteorol. Soc.*, 2013. doi: 10.1002/qj.2140.

D. M. Brink and G. R. Satchler. *Angular Momentum.* Clarendon Press, 1968.

J. B. Burkholder, S. P. Sander, J. Abbatt, J. R. Barker, R. E. Huie, C. E. Kolb, M. J. Kurylo, V. L. Orkin, D. M. Wilmouth, and P. H. Wine. Chemical kinetics and photochemical data for use in atmospheric studies, evaluation no. 18. JPL Publication 15-10, Jet Propulsion Laboratory, Pasadena, 2015. URL `http://jpldataeval.jpl.nasa.gov`. last access: October 2015.

M.-D. Chou and K. T. Lee. Parameterizations for the absorption of solar radiation by water vapor and ozone. *J. Atm Sci.*, 53:1,203–1,208, 1996.

S. A. Clough, F. X. Kneizys, and R. W. Davies. Line shape and the water vapor continuum. *Atmos. Res.*, 23:229–241, 1989.

S. Cusack, A. Slingo, J. M. Edwards, and M. Wild. The radiative impact of a simple aerosol climatology on the Hadley Centre atmospheric GCM. *Q. J. Roy. Meteorol. Soc.*, 124:2517–2526, 1998.

S. Cusack, J. M. Edwards, and J. M. Crowther. Investigating k distribution methods for parameterizing gaseous absorption in the Hadley centre climate model. *J. Geophys. Res.*, 104:2051–2057, 1999.

A. Deepak and H. E. Gerber. Report of the experts' meeting on aerosols and their climatic effects. WCP 55, World Climate Programme, 1983.

J. M. Edwards. Efficient calculation of infra-red fluxes and cooling rates using the two-stream equations. *J. Atm. Sci.*, 53:1921–1932, 1996.

J. M. Edwards and A. Slingo. Studies with a flexible new radiation code. I: Choosing a configuration for a large-scale model. *Q. J. Roy. Meteorol. Soc.*, 122:689–719, 1996.

J. M. Edwards, S. Havemann, J.-C. Thelen, and A. J. Baran. A new parametrization for the radiative properties of ice crystals: Comparison with existing schemes and impact in a GCM. *J. Atmos. Res.*, 83:19–35, 2007.

J. Elsey, M. D. Coleman, T. D. Gardiner, K. P. Menang, and K. P. Shine. Atmospheric observations of the water vapour continuum in the near-infrared windows between 2500 and 6600 cm^{-1}. *Atmospheric Measurement Techniques*, 13(5):2335–2361, 2020. doi: 10.5194/amt-13-2335-2020.

J.A. Fennelly and D.G. Torr. Photoionization and photoabsorption cross sections of o, n2, o2, and n for aeronomic calculations. *Atomic Data and Nuclear Data Tables*, 51(2):321 – 363, 1992. ISSN 0092-640X. doi: https://doi.org/10.1016/0092-640X(92)90004-2. URL `http://www.sciencedirect.com/science/article/pii/0092640X92900042`.

Q. Fu. An accurate parametrization of the solar radiative properties of cirrus clouds for climate models. *J. Clim.*, 9:2,058–2,082, 1996.

Q. Fu, Ping Yang, and W. B. Sun. An accurate parametrization of the infrared radiative properties of cirrus clouds of climate models. *J. Clim.*, 11:2,223–2,237, 1998.

J. F. Geleyn and A. Hollingsworth. An economical analytical method for the computation of the interaction between scattering and line absorption of radiation. *Beiträge Phys. Atmosph.*, 52:1–16, 1979.

V. Gorshelev, A. Serdyuchenko, M. Weber, W. Chehade, and J. P. Burrows. High spectral resolution ozone absorption cross-sections - Part 1: Measurements, data analysis and comparison with previous measurements around 293 k. *Atmospheric Measurement Techniques*, 7(2):609–624, 2014. doi: 10.5194/amt-7-609-2014. URL `http://www.atmos-meas-tech.net/7/609/2014/`.

J. Haywood, N. Bellouin, J. M. Edwards, S. Havemann, B. Johnson, and J-C. Thelen. Identification/impact/rectification of a bug in radiation code pre-processing and spectral files. Technical report, Met Office, UK, 2008. URL `http://www.met.reading.ac.uk/~lem/large_models/esrad/docs/Rayleigh_scattering_error.pdf`.

B.L. Henke, E.M. Gullikson, and J.C. Davis. X-ray interactions: Photoabsorption, scattering, transmission, and reflection at e = 50-30,000 ev, z = 1-92. *Atomic Data and Nuclear Data Tables*, 54(2):181 – 342, 1993. ISSN 0092-640X. doi: https://doi.org/10.1006/adnd.1993.1013. URL `http://www.sciencedirect.com/science/article/pii/S0092640X83710132`.

P. G. Hill, J. Manners, and J. C. Petch. Reducing noise associated with the Monte Carlo Independent Column Approximation for weather forecasting models. *Q. J. Roy. Meteorol. Soc.*, 137:219–228, 2011. doi: 10.1002/qj.732.

P. G. Hill, R. J. Hogan, J. Manners, and J. C. Petch. Parametrizing the horizontal inhomogeneity of ice water content using CloudSat data products. *Q. J. Roy. Meteorol. Soc.*, 138(668):1784–1793, 2012. doi: 10.1002/qj.1893.

R. J. Hogan and A. J. Illingworth. Deriving cloud overlap statistics from radar. *Q. J. Roy. Meteorol. Soc.*, 126:1–7, 2000.

Y. X. Hu and K. Stamnes. An accurate parametrization of the radiative properties of waterr clouds suitable for use in climate models. *J. Climate*, 6:728–742, 1993.

J. H. Joseph, W. J. Wiscombe, and J. A. Weinman. The delta-Eddington approximation for radiative flux transfer. *J. Atm. Sci.*, 33:2,452–2,459, 1976.

J. E. Kristjánsson, J. M. Edwards, and D. L. Mitchell. A new parameterization scheme for the optical properties of ice crystals for use in general circulation models of the atmosphere. *Phys. Chem. Earth (B)*, 24:231–236, 1999.

J. E. Kristjánsson, J. M. Edwards, and D. L. Mitchell. The impact of a new scheme for the optical properties of ice crystals on the climates of two GCMs. *J. Geophys. Res.*, 105:10,063–10,079, 2000.

R. L. Kurucz. CD-ROM 23. *Harvard Smithsonian Center for Astrophysics*, 1995.

D. Labs and H. Neckel. Transformation of the absolute solar radiation data into the international practical temperature scale of 1968. *Solar Physics*, 15:79–87, 1970.

J. Lacoursière, S. A. Meyer, G. W. Faris, T. G. Slanger, B. R. Lewis, and S. T. Gibson. The o(1d) yield from o2 photodissociation near h lyman-α(121.6 nm). *The Journal of Chemical Physics*, 110 (4):1949–1958, 1999. doi: 10.1063/1.477852. URL `https://doi.org/10.1063/1.477852`.

J. Lean. Evolution of the sun's spectral irradiance since the maunder minimum. *Geophys. Res. Lett.*, 27:2425–2428, 2000.

J. Manners, J.-C. Thelen, J. Petch, P. Hill, and J. M. Edwards. Two fast radiative transfer methods to improve the temporal sampling of clouds in numerical weather prediction and climate models. *Q. J. R. Meteorol. Soc.*, 135:457–468, 2009.

J. Manners, S. B. Vosper, and N. Roberts. Radiative transfer over resolved topographic features for high-resolution weather prediction. *Q. J. Roy. Meteorol. Soc.*, 138(664):720–733, 2012. doi: 10.1002/qj.956.

K. Matthes, B. Funke, M. E. Andersson, L. Barnard, J. Beer, P. Charbonneau, M. A. Clilverd, T. Dudok de Wit, M. Haberreiter, A. Hendry, C. H. Jackman, M. Kretzschmar, T. Kruschke, M. Kunze, U. Langematz, D. R. Marsh, A. C. Maycock, S. Misios, C. J. Rodger, A. A. Scaife, A. Seppälä, M. Shangguan, M. Sinnhuber, K. Tourpali, I. Usoskin, M. van de Kamp, P. T. Verronen, and S. Versick. Solar forcing for cmip6 (v3.2). *Geoscientific Model Development*, 10(6):2247–2302, 2017. doi: 10.5194/gmd-10-2247-2017. URL `https://gmd.copernicus.org/articles/10/2247/2017/`.

D. L. Mitchell. Effective diameter in radiation transfer: General definition, applications and limitations. *J. Atm. Sci.*, 59:2330–2346, 2002.

D. L. Mitchell, A. Macke, and Y. Liu. Modeling cirrus clouds. Part ii: Treatment of radiative properties. *J. Atm. Sci.*, 53:2967–2988, 1996.

E. J. Mlawer, D. D. Turner, S. N. Paine, L. Palchetti, G. Bianchini, V. H. Payne, K. E. Cady-Pereira, R. L. Pernak, M. J. Alvarado, D. Gombos, J. S. Delamere, M. G. Mlynczak, and J. C. Mast. Analysis of water vapor absorption in the far-infrared and submillimeter regions using surface radiometric measurements from extremely dry locations. *Journal of Geophysical Research: Atmospheres*, 124 (14):8134–8160, 2019. doi: https://doi.org/10.1029/2018JD029508.

C. D. Mobley. *Light and Water.* Academic Press, first edition, 1994.

L. T. Molina and M. J. Molina. Absolute absorption cross section of ozone in the 185 to 350 nm wavelength range. *J. Geophys. Res.*, 91:14,501–14,508, 1986.

D. Mondelain, S. Manigand, S. Kassi, and A. Campargue. Temperature dependence of the water vapor self-continuum by cavity ring-down spectroscopy in the 1.6 μm transparency window. *Journal of Geophysical Research: Atmospheres*, 119(9):5625–5639, 2014. doi: https://doi.org/10.1002/2013JD021319.

A. Morel. Light and marine photosynthesis: a spectral model with geochemical and climatological implications. *Prog. Oceanogr.*, 26:263, 1991.

A. Morel and B. Gentili. Diffuse reflectance of oceanic waters. II. bidirectional aspects. *Appl. Optics*, 32:6,864–6,879, 1993.

A. Morel, K. J. Voss, and Bernard Gentili. Bidirectional reflectance of oceanic waters: A comparison of modeled and measured upward radiance fields. *J. Geophys. Res.*, 100(C7):13143–13150, 1995.

Markus Mueller. Equation of Time – Problem in Astronomy. II International Competition (1993/94) “First Step to Nobel Prize in Physics”. *Acta Physica Polonica A*, 88 Supplement(S-49), 1995. URL `http://info.ifpan.edu.pl/firststep/aw-works/fsII/mul/mueller.html`.

T. Nakajima and M. Tanaka. Algorithms for radiative intensity calculations in moderately thick atmospheres using a truncation approximation. *J. Quant. Spectrosc. Radiative Transfer*, 40:51–69, 1988.

G. W. Paltridge and C. M. R. Platt. *Radiative processes in meteorology and climatology*, volume 5 of *Developments in Atmospheric Science.* Elsevier, 1976.

T. J. Petzold. Volume scattering functions for selected ocean waters. Technical Report SIO Ref.72-78, Scripps Inst. of Oceanogr., La Jolla, 1972.

R. Pincus, H. W. Barker., and J.-J. Morcrette. A fast, flexible, approximate technique for computing radiative transfer in inhomogeneous cloud fields. *J. Geophys. Res.*, 108(D13):4376, July 2003. doi: 10.1029/2002JD003322.

L. Prieur and S. Sathyendranath. An optical classification of coastal and oceanic waters based on the specific spectral absorption curves of phytoplankton pigments, dissolved organic matter, and other particulate materials. *Limnol. Oceanogr.*, 26(4):671–689, 1981.

Igor V. Ptashnik, Robert A. McPheat, Keith P. Shine, Kevin M. Smith, and R. Gary Williams. Water vapor self-continuum absorption in near-infrared windows derived from laboratory measurements. *Journal of Geophysical Research: Atmospheres*, 116(D16), 2011. doi: https://doi.org/10.1029/2011JD015603.

Igor V. Ptashnik, Tatyana E. Klimeshina, Alexander A. Solodov, and Andrey A. Vigasin. Spectral composition of the water vapour self-continuum absorption within 2.7 and 6.25 μm bands. *Journal of Quantitative Spectroscopy and Radiative Transfer*, 228:97–105, 2019. ISSN 0022-4073. doi: https://doi.org/10.1016/j.jqsrt.2019.02.024.

P. Räisänen, H. W. Barker, M. F. Khairoutdinov, J. Li, and D. A. Randall. Stochastic generation of subgrid-scale cloudy columns for large-scale models. *Q. J. Roy. Meteorol. Soc.*, 130:2047–2067, 2004. doi: 10.1256/qj.03.99.

L. Richard, S. Vasilchenko, D. Mondelain, I. Ventrillard, D. Romanini, and A. Campargue. Water vapor self-continuum absorption measurements in the 4.0 and 2.1μm transparency windows. *Journal of Quantitative Spectroscopy and Radiative Transfer*, 201:171–179, 2017. ISSN 0022-4073. doi: https://doi.org/10.1016/j.jqsrt.2017.06.037.

B. Ritter and J.-F. Geleyn. A comprehensive radiation scheme for numerical weather prediction models with potential applications in climate simulations. *Mon. Wea. Rev.*, 120:303–325, 1992.

R. G. Roble, E. C. Ridley, and R. E. Dickinson. On the global mean structure of the thermosphere. *Journal of Geophysical Research: Space Physics*, 92(A8):8745–8758, 1987. doi: https://doi.org/10.1029/JA092iA08p08745. URL `https://agupubs.onlinelibrary.wiley.com/doi/abs/10.1029/JA092iA08p08745`.

B. Rockel, E. Raschke, and B. Weyres. A parametrization of broad band radiative transfer properties of water, ice and mixed clouds. *Beiträge Phys. Atmosph.*, 64:1–12, 1991.

J.-L. Roujean, M. Leroy, and P.-Y. Deschamps. A bidirectional reflectance model of the earth's surface for the correction of remote sensing data. *J. Geophys. Res.*, 97:20455–20468, 1992.

A. Serdyuchenko, V. Gorshelev, M. Weber, W. Chehade, and J. P. Burrows. High spectral resolution ozone absorption cross-sections - Part 2: Temperature dependence. *Atmospheric Measurement Techniques*, 7(2):625–636, 2014. doi: 10.5194/amt-7-625-2014. URL `http://www.atmos-meas-tech.net/7/625/2014/`.

A. Slingo and H. M. Schrecker. On the shortwave radiative properties of stratiform water clouds. *Q. J. R. Meteorol. Soc.*, 108:407–426, 1982.

W. M. Smart. *Textbook on Spherical Astronomy.* Cambridge University Press, fourth edition, 1944.

Stanley C. Solomon and Liying Qian. Solar extreme-ultraviolet irradiance for general circulation models. *Journal of Geophysical Research: Space Physics*, 110(A10), 2005. doi: 10.1029/2005JA011160. URL `https://agupubs.onlinelibrary.wiley.com/doi/abs/10.1029/2005JA011160`.

Z. Sun, J. Li, G. Shi, J. Manners, and Jiandong Li. Determination of direct normal irradiance including circumsolar radiation in climate/NWP models Part II: phase function scaling approach. *Under revision for further submission*, 2018.

P. Varanasi and S. Chudamani. Infrared intensities of some chloroflourocarbons capable of perturbing the global climate. *J. Geophys. Res.*, 93:1,666–1,668, 1988.

I. Ventrillard, D. Romanini, D. Mondelain, and A. Campargue. Accurate measurements and temperature dependence of the water vapor self-continuum absorption in the 2.1 μm atmospheric window. *The Journal of Chemical Physics*, 143(13):134304, 2015. doi: 10.1063/1.4931811.

S. Voigt, J. Orphal, K. Bogumil, and J. P. Burrows. The temperature dependence (203-293 k) of the absorption cross-sections of o3 in the 230-850 nm region measured by fourier-transform spectroscopy. *J. Photochem. Photobiol. A*, 143:1–9, 2001.

D. Walters, A. J. Baran, I. Boutle, M. Brooks, P. Earnshaw, J. Edwards, K. Furtado, P. Hill, A. Lock, J. Manners, C. Morcrette, J. Mulcahy, C. Sanchez, C. Smith, R. Stratton, W. Tennant, L. Tomassini, K. Van Weverberg, S. Vosper, M. Willett, J. Browse, A. Bushell, K. Carslaw, M. Dalvi, R. Essery, N. Gedney, S. Hardiman, B. Johnson, C. Johnson, A. Jones, C. Jones, G. Mann, S. Milton, H. Rumbold, A. Sellar, M. Ujiie, M. Whitall, K. Williams, and M. Zerroukat. The met office unified model global atmosphere 7.0/7.1 and jules global land 7.0 configurations. *Geoscientific Model Development*, 12(5):1909–1963, 2019. doi: 10.5194/gmd-12-1909-2019. URL `https://www.geosci-model-dev.net/12/1909/2019/`.

H. Yang and H. R. Gordon. Remote sensing of ocean color: assessment of water-leaving radiance bidirectional effects on atmospheric diffuse transmittance. *Appl. Optics*, 36:7887–7897, 1997.

W. G. Zdunkowski and G. J. Korb. Numerische Methoden zur Lösung der Strahlungsübertragungsgleichung. *Promet*, 2/3:26–39, 1985.

W. G. Zdunkowski, R. M. Welch, and G. Korb. An investigation of the structure of typical two-stream methods for the calculation of solar fluxes and heating rates in clouds. *Beiträge Phys. Atmosph.*, 53:147–166, 1980.

W. G. Zdunkowski, W-G. Panhans, R. M. Welch, and G. J. Korb. A radiation scheme for circulation and climate models. *Beiträge Phys. Atmosph.*, 55:215–238, 1982.

W. Zhong and J. D. Haigh. An efficient and accurate correlated-k parametrization of infrared radiative transfer for troposphere–stratosphere–mesosphere gcms. *Atmospheric Science Letters*, 1(2):125–135, 2000. ISSN 1530-261X. doi: 10.1006/asle.2000.0014. URL `http://dx.doi.org/10.1006/asle.2000.0014`.

W. Zhong, J. D. Haigh, D. Belmiloud, R. Schermaul, and J. Tennyson. The impact of new water vapour spectral line parameters on the calculation of atmospheric absorption. *Q. J. Roy. Meteorol. Soc.*, 127:1,615–1,626, 2001.

W. Zhong, S. M. Osprey, L. J. Gray, and J. D. Haigh. Influence of the prescribed solar spectrum on calculations of atmospheric temperature. *Geophysical Research Letters*, 35(L22813), 2008.